Smac mimetic and combination immunotherapy for the treatment of urothelial cell carcinoma

Tarun Sanda

A thesis submitted in partial fulfilment of the requirements for the Doctoral degree in Microbiology and Immunology

Department of Biochemistry, Microbiology, and Immunology

Faculty of Medicine

University of Ottawa

ABSTRACT

The inhibitors of apoptosis (IAP) proteins regulate cell death signaling cascades. Smac mimetic (SM) compounds are antagonists of these proteins and are being evaluated for their anti-cancer efficacy and immunomodulatory effects. Here, I adopted an orthotopic murine model of urothelial carcinoma (MB49) resistant to prominent immune-stimulating therapies BCG mycobacterium and PD-1/PD-L1 checkpoint blockade. I found treatment with a monovalent SM, LCL161, generated T lymphocyte-dependent cures of MB49, retaining potent anti-tumour immune memory and significantly improving overall survival benefit. Separately, I report SM treatment modulates multiple components comprising the cellular adaptive immune response. Specifically, I found SM promoting the expansion of antigen-presenting cells (APCs) in vitro and enabling T lymphocyte priming in vivo. I evaluated SM in combination with concurrent immune checkpoint blockade. The combination of SM with a monoclonal antibody targeting cytotoxic T lymphocyte -associated protein 4 (CTLA-4, 9h10 clone) potentiated anticancer immunity, curing all tested subjects of MB49. I verified Fc receptor-dependent intratumoural regulatory T cell depletion as a required mechanism for enhancing survival probability with the combination of SM and anti-CTLA-4. The further evaluation of mechanisms responsible for SMs stimulating immunity will promote their clinical application for cancer therapy.

TABLE OF CONTENTS

LIST OF FIGURES

LIST OF ABBREVIATIONS

ACT – Adoptive Cell Transfer

ACK – ammonium-chloride-potassium

ACVS – Animal Care and Veterinary Service

ADCC – Antibody-dependent cell-mediated cytotoxicity

ADCP – Antibody-dependent cell-mediated phagocytosis

APC – Antigen-Presenting Cell

AST – Aspartate Aminotransferase

ALT – Alanine Aminotransferase

BCG – Bacillus Calmette-Guerin mycobacterium

BIRC – Baculovirus IAP-Repeat

BMDC – Bone Marrow-Derived Dendritic Cell

BMDM – Bone Marrow-Derived Macrophage

cDC – Conventional Dendritic Cell

CD – Cluster of Differentiation

CHEO – Children's Hospital of Eastern Ontario

cIAP1 – Cellular Inhibitor of Apoptosis Protein 1

cIAP2 – Cellular Inhibitor of Apoptosis Protein 2

CpG -ODN – CpG-containing oligodeoxynucleotides

CSF1R – colony stimulating factor 1 receptor

CTLA-4 – Cytotoxic T Lymphocyte-Associated Protein 4

DC – Dendritic Cell

DIABLO – Direct IAP-Binding protein with Low isoelectric point

DMEM – Dulbecco's Modified Eagle Medium

DMSO – Dimethyl Sulfoxide

ELISA – Enzyme-Linked Immunosorbent Assay

Fab – Fragment antigen-binding

FBS – Fetal bovine serum

FC – Fragment Crystallizable

FoxP3 – Forkhead box P 3 Transcription Factor

GFP – Green Fluorescent Protein

GITR – Glucocorticoid-inducible TNF-Related Protein

GMCSF – Granulocytic macrophage colony stimulating factor

HIV – Human Immunodeficiency Virus

IAP – Inhibitor of Apoptosis Protein

IFN – Interferon

IL-2 – Interleukin 2

IL-4 Interleukin 4

IP – intraperitoneal

IV- intravenous

IFNy – interferon gamma

LAK – Lymphokine-Associated Killer

LPS - lipopolysaccharide

LT – Lymphotoxin

LUBAC – Linear Ubiquitin Assembly Complex

Luc – firefly luciferase

MB49 – Mouse bladder 49 cell line

MLKL – Mixed Lineage Kinase Domain Like Pseudokinase

mM - millimolar

NFkB – Nuclear Factor kappa B

NIK – Nuclear Factor kappa B Inducible Kinase

NK – Natural Killer

NK1.1 – Killer cell lectin-like receptor subfamily B (KLRB1)

NLR – Nod-Like Receptor

nM - nanomolar

NMIBC – Non-Muscle Invasive Bladder Cancer

OT-1 – C57BL.6-Tg(TCRaTCRb)1100Mjb/J transgenic mouse

OVA – Ovalbumin

pDC – Plasmacytoid Dendritic Cell

PD-1 – Programmed Cell Death Protein - 1

PD-L1 – Programmed Cell Death Ligand – 1

PBMCs – Peripheral Blood Mononuclear Cells

PHA – Phtohaemagglutinin P

PMA – Phorbol 12-myristate 13-acetate

Poly (I:C) – polyinosinic:polycytidylic acid

PRR – Pathogen Recognition Receptor

RIPK – Receptor-Inducible Protein Kinase

Rm – recombinant murine

RPMI – Roswell Park Memorial Institute

SC – subcutaneous

Smac – second mitochondrial activator of caspases

SM – Smac Mimetic

TB - Tuberculosis

TCR – T Cell Receptor

TGF – Tumour Growth Factor

Th – T helper cell

TLR – Toll-Like Receptor

TNF – Tumour Necrosis Factor

TNFR – TNF receptor

TNFSF9 – 41BB, Tumour Necrosis Factor Superfamily member 9

TRAF – TNFR associated factor

TRAIL – TNF-related apoptosis inducing ligand

Tregs – regulatory T cells

VC – Vehicle Control

VSV – Vesicular Stomatitis Virus

WT – wildtype

XAF – XIAP-Associated Factor

XIAP – X-linked Inhibitor of Apoptosis Protein

Zbtb46 – Zinc finger and BTB domain containing 46

μg - microgram

μM – micromolar

ACKNOWLEDGEMENTS

I extend my deepest gratitude and sincerely thank Dr. Robert Korneluk for allowing me to be part of his lab, along with the endless support and encouragement throughout my studies. I thank Dr. Shawn Beug for guiding me with how to build a cohesive story, presenting me with the examples to learn from and build on. I thank Dr. Eric LaCasse for advocating my work and always being open for discussions. The mentorship from each of you has helped me develop into the researcher I am, for which I will always be grateful.

I extend my gratitude to Janelle Holbrook and Nathalie Earl for helping me navigate the surgical experiments. I could not have completed my work without help from both of you. I further recognize other members of the CHEO RI staff for ensuring the workplace remain a pleasant environment.

A special thanks to my friends for helping me enjoy my time, reminding me life is about BIRC7 more than BIRC5.

Lastly, I thank my mother and father for always being there, believing in me and supporting me throughout this journey.

1.0 INTRODUCTION

My project aims toward promoting the clinical translation of Smac mimetics (SMs), pharmacological antagonists of the inhibitor of apoptosis proteins (IAPs), against cancer. I sought to improve efficacy and parse possible mechanism-of-action within pre-clinical models by administering SM in conjunction with prominent immunotherapies.

1.0 An overview of the IAPs and Smac Mimetics

1.0.1 Apoptosis & the IAPs

Cell death is triggered upon engagement of specific cytokines, exposure to toxic elements, physical trauma, or infection. Apoptosis, colloquially programmed cell death, is a protracted process characterized by the quiescent circularization then fragmentation of cellular constituents. This phenomenon outlines events required for the removal of dying cells by professional phagocytes or adjacent cells. The morphological similarities between dying cells irrespective of initial stimulus suggests a hierarchal system persists to resolve or preclude pathological conditions. This conserved ability is required for the maintenance of adult tissue, wound repair, and replacement of defective cells. Accordingly, apoptosis occurs in a variety of physiological settings in both healthy and disease states throughout life [Hockenbury, 1995].

The inhibitor of apoptosis protein (IAP) family is identified by the presence of one to three zinc-finger baculovirus IAP repeat (BIR) domains (Figure 1). BIR domains enable IAP proteins to induce caspase activity directly or indirectly [Mace et al., 2010]. Caspases are a family of cysteine proteases and primary effectors of apoptosis. Sequestered as inactive zymogens, these enzymes are activated by dimerization or cleavage to hydrolyze peptide

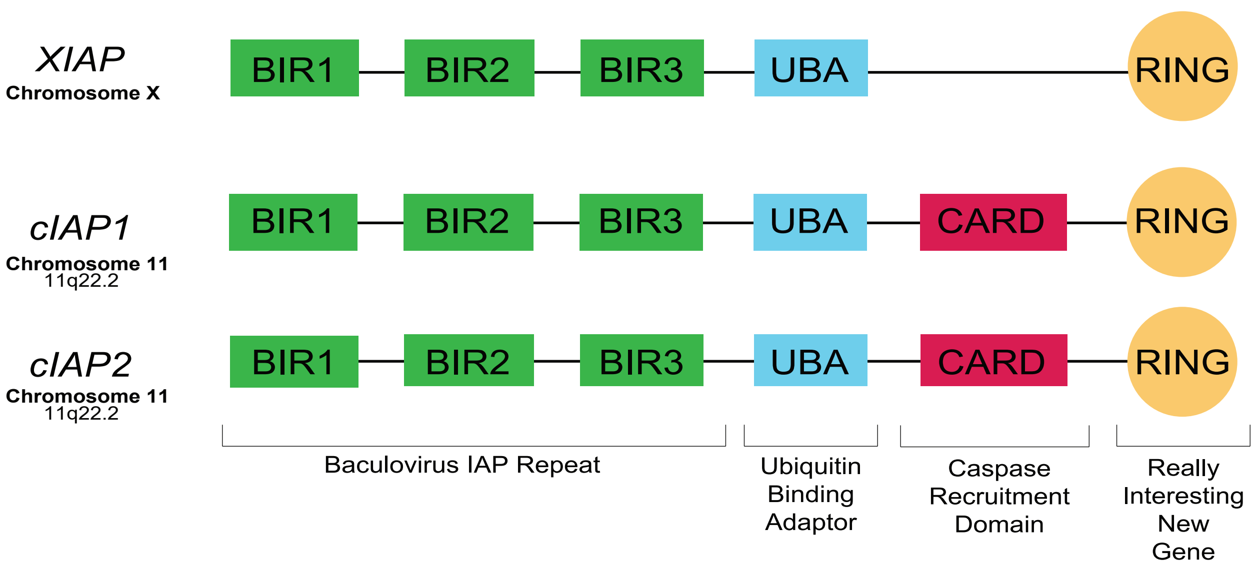

XIAP
Chromosome X
BIR1
BIR2
BIR3
UBA
RING
cIAP1
Chromosome 11
11q22.2
BIR1
BIR2
BIR3
UBA
CARD
RING
cIAP2
Chromosome 11
11q22.2
BIR1
BIR2
BIR3
UBA
CARD
RING
Baculovirus IAP Repeat
Ubiquitin Binding Adaptor
Caspase Recruitment Domain
Really Interesting New Gene

Figure 1. The inhibitors of apoptosis

Amongst the 8 mammalian members of the IAP family shown are the IAP proteins XIAP, cIAP1, and cIAP2. IAPs are characterized by the presence of one or more baculovirus IAP repeat (BIR) domains. XIAP, cIAP1, and cIAP2 further possess a ubiquitin binding adaptor (UBA) domain that enables binding of ubiquitin chains, along with a Really Interesting New Gene (RING) domain mediating E3 ubiquitin ligase activity. Distinctly, cIAP1 and cIAP2 possess a caspase recruitment domain (CARD) mediating suppression of E3 ubiquitin ligase activity.

bonds, dismantling cellular structures [Mcllwain et al., 2013]. Caspases are generally subdivided into either initiator (caspase-2, -8. -9, -10) or executioner (caspase-3, -6, -7) caspases. Initiator caspases complex to activate executioner caspases, enabling a cascade amplifying apoptotic signaling, triggering nuclear collapse and DNA fragmentation [Fan et al., 2005].

Distinct from XIAP, cIAP1 and cIAP2 each contain a caspase recruitment domain (CARD). Although the precise function is currently unknown, the presence of CARD domains likely enable interaction with other CARD-containing proteins found in the mitochondria or cytosol to form larger protein complexes [Jiang et al., 2012].

The presence of a carboxy-terminal Really Interesting New Gene (RING) domain within cellular-IAP1 (cIAP1, *Birc2*), cellular-IAP2 (cIAP2, *Birc3*), and X-linked-IAP (XIAP, *Birc4*) provides these proteins with E3 ubiquitin ligating activity, regulating trans- or auto-ubiquitination [Cheung et al., 2008]. Ubiquitination elicits pleiotropic molecular interactions facilitating myriad biological processes involved in cell trafficking and protein degradation [Soltes et al., 2011]. E3-ubiquitin ligating enzymes facilitate the thermodynamically stable transfer of omnipresent ubiquitin, an evolutionarily stagnant protein under extreme conservation across all life forms [Allan et al., 2017]. RING-domain IAPs are known to form K(Lysine)63 or K48 ubiquitin chains. Generally, K63 linkage facilitates protein signal transduction, whereas K48 linkage promotes proteasomal degradation [Akutsu et al., 2016].

XIAP is the most characterized member of the IAP family, governing the self-renewal, differentiation, maintenance, and death of numerous non-hematopoietic cell lineages [Mudde et al., 2021]. XIAP-XAF1 (XIAP Associated Factor-1) trans-regulate apoptotic cascades by sequestering initiator caspase-9, precluding cytochrome C-Apoptotic protease activating factor-1 (Apaf-1)- caspase-9 complex formation [Bratton et al., 2002]. The BIR3 domain on XIAP precludes the dimerization of caspase-9, thereby sequestering downstream executioner caspase-3 in pro-caspase form [Srinivasula et al., 2001]. XIAP has also been shown to directly bind executioner caspase-3 and -7 (Scott et al., 2005). The BIR2 domain on XIAP directly binds to caspase-3 and caspase-7, structurally blocking its active sites from access to and concomitant cleavage of substrates [Riedl et al., 2001] [Chai et al., 2001]. Collectively, the presence of XIAP prevents caspase activity at initiator and executioner stages, both directly and indirectly. This enclosed system constitutes a feedback loop insulating the primary death cascade triggered upon radiation-induced cellular damage. Notably, XIAP deficiency fosters the development of X-linked lympho-proliferative syndrome type-2 (XLP-2), despite XIAP deficiency enhancing lymphocyte vulnerability to undergo apoptosis [Rigaud et al., 2006].

Nuclear-derived cIAP1 in tandem with native cytosolic cIAP2 dynamically diversify genetic output by regulating the temporal fate of nuclear factor kappa-light-chain-enhancer of B cells (NFκB) subunits [Gyrd-Hansen & Meier, 2010]. The trans-ubiquitination control of cIAP2-NIK (NFκB inducible kinase) by cIAP1 elicits a thermodynamically stable transfer of omnipresent ubiquitin, perpetuating survival signals in cells of hematopoietic and non-hematopoietic lineage [Beug et al., 2012]. Although cIAP1 and cIAP2 may also bind caspase-3 and caspase-7 like XIAP, amino acid substitutions in their BIR domains preclude their ability to directly inhibit proteolytic function [Choi et al., 2009]. In turn, the caspases are ubiquitinated, facilitating their proteasomal degradation.

Amongst orthologues, the other members of the IAP family play a diverse role in biological responses. NAIP (BIRC1) is involved in mediating inflammasome responses and neuroprotectivity. Survivin (BIRC5) and BRUCE (BIRC6) are involved in mitosis, and Livin

(BIRC7) plays a role in development. The expression of IAP-like protein 2 (ILP2, BIRC8) is restricted to the testis, likely playing a role in spermatogenesis [Richter et al., 2001].

1.0.2 TNF and NFκB signaling modulation

The tumour necrosis factor (TNF) family contains an extensive group of structurally, genetically, and functionally similar cytokines that have likely diversified to enable specialized effector responses [Aggarwal, 2003]. TNF-alpha is an acute-phase cytokine responsible for a localized inflammatory response, thereby constituting critical functions in both the innate and adaptive immune responses. TNF-alpha signal transduction increases vasodilation and vascular permeability, leading to increased entry of inflammatory immune cells and associated metabolites to localized tissue, in addition to increased drainage of peripheral lymphatics. This cascade enables removal of damaged biological material, whilst occluding the dissemination of septic factors. In conjunction with other acute-phase proteins such as IL-1beta and IL-6, TNF-alpha stimulates the hypothalamus to raise body temperature, a physiological adjustment necessary to decrease viral or bacterial replication and promote a pathogen-specific cytotoxic immune response.

TNF-alpha signals via TNF-receptor 1 or 2 (TNFR1/2). The recruitment of cIAP1/2 to TNFR1 is mediated by TNF receptor-associated factor 2 (TRAF2) and TNF-receptor-1-associated death domain (TRADD). Receptor interacting protein kinase 1 (RIPK1), also recruited by TRADD to TNFR1, is polyubiquitinated by cIAP1/2 with a K63 (Lysine-63)-linkage ubiquitin chain. This process will allow for recruitment of the linear ubiquitin chain assembly complex (LUBAC), a complex of ring finger protein 31 (RNF31/HOIP), RanBPtype and C3HC4-type zinc finger containing 1 (RBCK1/HOIL-1) and SHANK-associated RH domain interacting protein (SIPL1/SHARPIN). This complex will modify the RIPK1 complex with M1-linked chains to allow for the efficient recruitment of downstream subunits [Peltzer et al., 2016]. This facilitates the recruitment of tumour growth factor-beta (TGF-beta)-activated kinase (TAK1) and MAP3K7 (mitogen-activated protein kinase kinase kinase 7) binding protein 2 (TAB2). Inhibitor of NFκB kinase subunit B (IKKB) is phosphorylated by TAK1, enabling activation of the IKK complex consisting of: IKK-alpha, IKK-beta, and NFκB -essential modulator (NEMO). This complex will phosphorylate the inhibitor of kB (IkB) complex, facilitating its proteasomal degradation thereby relieving sequestration of the heterodimeric complex of c-Rel-p50 and v-rel reticuloendotheliosis viral oncogene homolog A (RelA). This will allow the p50-RelA heterodimer to translocate to the nucleus and control binding to specific promoter regions to facilitate transcription of target genes. This interaction enables classical or canonical NFκB signal transduction, a cascade culminating with pro-inflammatory and survival factors being transcribed. Therefore, cIAP1/2 are positive regulators of the classical NFκB pathway. (Figure 2)

Amongst prominent transcriptional targets of this pathway are major histocompatibility complex 1 and 2 (MHC1/2) and programmed death receptor ligand 1 (PD-L1). MHC1 and MHC2 are protein complexes required for the extracellular expression of endogenous material in the form of peptide fragments to cytotoxic T cells. MHC1 is expressed by all nucleated cells and interacts with the T cell receptors (TCRs) on CD8 T cells, whereas MHC2 is expressed selectively on phagocytes and interacts with CD4-expressing T cells. PD-L1 is the predominant ligand for programmed cell death protein 1 (PD-1), a receptor expressed

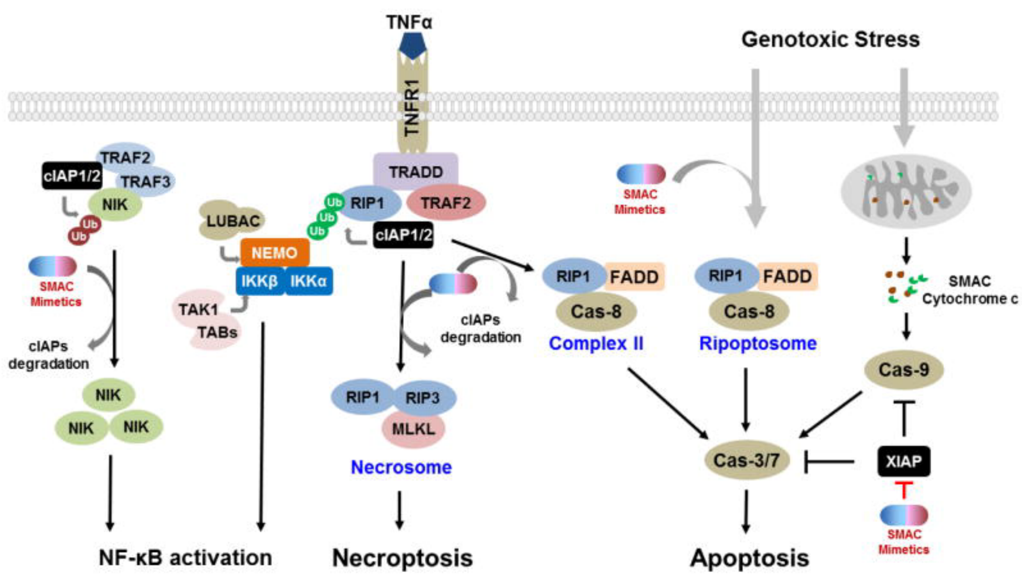
TNFα
TNFR1
Genotoxic Stress
TRADD
RIP1
TRAF2
cIAP1/2
LUBAC
NEMO
IKKβ
IKKα
TAK1
TABs
Ub
TRAF2
TRAF3
cIAP1/2
NIK
SMAC Mimetics
cIAPs degradation
NIK
NIK
NIK
RIP1
FADD
Cas-8
Complex II
RIP1
FADD
Cas-8
Ripoptosome
SMAC
Cytochrome c
Cas-9
Cas-3/7
XIAP
RIP1
RIP3
MLKL
Necrosome
NF-κB activation
Necroptosis
Apoptosis

Figure 2. IAPs promote classical NFκB activity

Schematic outlining the diversified involvement of the IAPs and impact of targeted antagonism using SMs on apoptosis, necroptosis, and NFκB signaling. In a basal state, cIAP1/2 will polyubiquitinate NIK, enabling its proteasomal degradation. Upon IAP antagonism using SMs, NIK will no longer be polyubiquitinated and will instead accumulate, thereby enabling alternative NFκB signaling. In the context of TNF/TNFR1 signal transduction, cIAP1/2 will polyubiquitinate RIPK1, precluding necrosome or complex II formation and thus enabling classical NFκB signaling in conjunction with LUBAC, NEMO, TAK1, and TAB1. XIAP inhibits caspase-3, -7, and -9 activation, preventing apoptosis. Adapted from [Bai et al., 2014] primarily on activated T cells. The interaction between these domains forms an axis that functions as a rheostat for immune activation. NFκB signalling also upregulates an extensive list of receptor ligands central to the immune response [Pahl et al., 1999]. Notably, TNF-alpha is also a target gene for NFκB, thereby enabling the feed-forward amplification of NFκB signalling in an autocrine or paracrine fashion. This mechanism rationalizes the toxicity of systemic TNF, as dissemination from a locale is strongly associated with the pathogenesis of endotoxic shock [Ceramil and Beutler, 1988]. This has limited the clinical oncology application of TNF thus far to isolated limb perfusion [Aderka et al., 1998].

The non-canonical, or alternative, NFκB pathway occurs when NFκB -inducible kinase (NIK) stabilizes. NIK, together with IKK-alpha, will phosphorylate p100, relieving its sequestration with v-rel avian reticuloendotheliosis viral oncogene homolog B (RelB). Activated p100 will then be processed into p52, forming a heterodimer with RelB. This complex will translocate to the nucleus and enable the transcription of target genes (Beug, 2012). Both cIAP1 and cIAP2 suppress alternative NFκB signal transduction by constitutively mediating the proteasomal degradation of NIK. TRAF2 will recruit cIAP1 and cIAP2, and TRAF3 will recruit NIK, forming a regulatory complex [Zarnegar et al., 2008]. cIAP1 and cIAP2 will then direct the K48 ubiquitination of NIK, enabling its proteasomal degradation. This establishes cIAP1 and cIAP2 as negative regulators of alternative NFκB signalling.

Within the context of TNF-alpha signal transduction, the absence of cIAP1/2 occlude the formation of cell-intrinsic complexes otherwise promoting inflammatory signalling, concomitantly enabling formation of spectral death complexes [Gyrd-Hansen & Meier, 2010]. In the absence of cIAP1/2, RIPK1 ubiquitination is attenuated, diminishing inhibitor of kB kinase-beta and thereby blunting classical NFκB signal transduction [Mahoney et al., 2008].

A secondary complex referred to as the ripoptosome will then form consisting of RIPK1, TRADD, Fas-associated death domain (FADD), initiator caspase-8, cellular FLICE (FADD-like IL-1-beta- converting enzyme)-inhibitory protein (c-FLIP) and RIPK3. Procaspase-8 will form a heterodimer with the long or short isoform of c-FLIP. Procaspase-8 dimerization with the long isoform of c-FLIP will cleave RIPK1, thereby disassembling the ripoptosome. This interaction however will not process procaspase-8 into activated form, thereby preventing executioner caspase activation and cell death. Procaspase-8 dimerization with the short isoform of c-FLIP will not cleave RIPK1, thereby allowing the RIPK1-RIPK3-Mixed Lineage Kinase domain-like pseudokinase (MLKL) necrosome to form [Tsuchiya et al., 2015]. Active RIPK1 will phosphorylate RIPK3, enabling RIPK3 to phosphorylate MLKL. MLKL will oligomerize and translocate to the cell membrane where it will form pores in the bilayer. This disruption will cause intracellular contents to be expelled into the extracellular space. The release of these damage-associated molecular patterns (DAMPs) stimulates an inflammatory response [Samson et al., 2020]. The degree to which an inflammatory response is initiated from these coordinated events is a gradient regarded as necroptosis. The configuration of the complexes determines the manner of cell death. Taken together, the presence or absence of cIAP1/2 are principal determinants of whether pro-survival signaling occurs or terminal death complexes form, respectively.

1.0.3 Smac Mimetics as anti-cancer compounds

Smac – second mitochondria-derived activator of caspases amphipathic protein, Diablo homolog – is the catalytic projectile of nuclear stress-factor DIABLO (direct IAP-binding protein with low isoelectric point) [Chai et al., 2000]. Upon apoptotic stimuli, mitochondrial-derived Smac tetrapeptide specifically binds the AVPI (Alanine-Valine-Proline-Isoleucine) cleft of BIR2/3 motif IAP members: cIAP1, cIAP2, XIAP, and Survivin (*Birc5*) [Huang et al., 2003] [Du et al., 2000]. The binding of Smac to IAPs antagonizes their function by triggering their auto-ubiquitination and proteasomal degradation, thereby allowing caspase activation and apoptosis [Darding et al., 2012].

Smac mimetics (SMs) define a class of experimental pharmacological drugs facilitating chemical ablation or allosteric inhibition of the IAP family members, exuding axial control of bifurcating mortality elements via translocation of intracellular proteins [Silke et al., 2013]. These synthetic small-molecule chemical compounds are designed to emulate endogenous Smac-AVPI interactions, thereby artificially antagonizing the IAPs [Table 1]. In essence, the pharmacological stability of SMs prolong the natural latency of IAP-regulated pathways, allosterically inhibiting complimentary signalling moieties [Fulda et al., 2015]. The effects are classically ascribed as perpetuation of cell death cascades, exploiting inherent vulnerabilities within neoplastic cell circuitry. Various SMs have been developed using the AVPI motif as a template, with further modifications to adjust binding to specific BIR domains. A monomeric SM developed by Novartis, LCL161, is the most clinically advanced SM (Figure 3). SM dimers have also been developed to enhance IAP inhibition or ablation. Monovalent SMs bind a single BIR domain on the IAPs, whereas bivalent SMs possess two binding motifs. The ability to inhibit both BIR2 and BIR3 domains enables bivalent SMs more effective at downregulating XIAP. Although well tolerated in patients, SMs have not had major clinical success within patients bearing advanced malignancies due to the lack of anti-cancer efficacy [Bai et al., 2014].

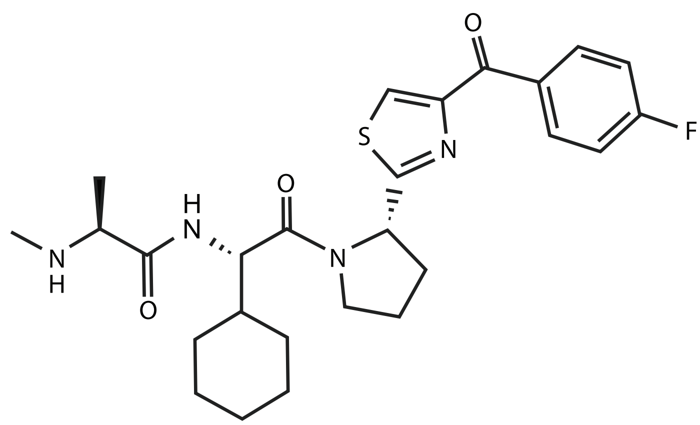

Figure 3. Smac Mimetic

Chemical structure of monovalent LCL161. Adapted from [Bai et al., 2014].

Cancer, the prevalence of abnormal cells with replicative immortality, arises from endogenous mutations in previously healthy cells driving unrestrained proliferation. The refractory nature of chemo- or radio-therapeutics to eliminate neoplastic cells is correlative with aberrations in apoptosis. Mutations in cIAP1/2 and XIAP have been verified to enable the progression of various cancers. Specifically, cIAP1 and cIAP2 have been identified as candidate oncogenes based on gene amplification within lung carcinoma and osteosarcoma [Dai et al., 2003] [Ma et al., 2001]. Similarly, XIAP over-expression is linked to cancer progression and resistance to therapy, thus associated with poorer prognosis [LaCasse et al., 2013]. Given the prevalence of these IAPs at critical nodes in both intrinsic and extrinsic cell death cascades, increased activity prevents the feed-forward amplification necessary to facilitate localized cell attrition. The renowned establishment of this principle has extensively endorsed the application of SMs as combinatorial anti-neoplastic therapeutics [Beug et al., 2015].

Several reports have explored the tendency of cancer cell lines to undergo attrition when treated with SM in vitro [Peterson et al., 2007; Raulf et al., 2014; Lueck et al., 2016]. The presence of TNF-alpha, either from endogenous production or exogenous addition of recombinant isoforms, potentiate sensitivity considerably [Fulda, 2015]. However, previous research from our lab has demonstrated that in vitro sensitivity to SM treatment does not correlate with in vivo anti-cancer efficacy with SM treatment. Accordingly, upon in vivo implantation of cell lines resistant to SM in vitro, in vivo SM treatment has demonstrated anti-cancer efficacy. This further suggests SMs may promote anti-cancer efficacy by engaging the host response to cancer cells.

Whether SM-mediated immune modulation or direct cytopathic effects are responsible for anti-cancer efficacy in immunocompetent settings remains unknown. Select biomedical literature evaluating prophylactic SM monotherapy report greater survival benefit among immunocompetent mice bearing subcutaneous rhabdomyosarcoma [Dobson et al., 2017] or systemic myeloma [Chesi et al., 2016].

1.0.4 IAPs and innate immunity

IAPs have been centrally implicated in the survival and activity of various innate immune compartments. Accordingly, the presence of cIAP1/2 may mediate resistance to apoptotic stimuli and regulate the functional plasticity of innate immune cells including macrophages and NK cells. In the context of microbial infection, bivalent SM Birinapant promoted an M2 phenotype within macrophages [Nadella et al., 2018], generally considered an anti-inflammatory and wound-healing phenotype. Conversely, monovalent SM LCL161 has demonstrated M1 inflammatory polarization within tumour-associated macrophages [Kim et al., 2017]. The variable expression of cIAP1 and cIAP2 within macrophage subsets may contribute toward these confounding results, as cIAP1 has been shown to be preferentially expressed in M2 macrophages, whereas cIAP2 being preferentially expressed in M1 macrophages [Moron-Calvente et al., 2018]. Human natural killer (NK) cells treated with SMs have demonstrated an increase in TNF-alpha and interferon-gamma (IFN-y) production, with an increase in target cancer cell cytotoxicity [Fishcer et al., 2017].

Previously, our lab has demonstrated SM in conjunction with an assortment of innate immune stimulants generate durable cures in an orthotopic syngeneic model of mammary carcinoma [Beug et al., 2014]. Specifically, LCL161 in combination with either oncolytic vesicular stomatitis virus delta-51 clone (VSVd51), polyinosinic:polycytidylic acid (poly (I:C)), or CpG-ODN 2216 eradicate EMT6 tumours in Balb/C mice. Oncolytic viruses, such as VSVd51, are engineered to specifically target and eliminate cancerous cells, while sparing normal host cells. Poly (I:C) is a synthetic mimic of double-stranded RNA, and thus a non-infectious substitute that will simulate viral infection by agonising Toll-like receptor 3 (TLR3). CpG-containing oligodeoxynucleotides (CpG-ODNs) are synthetic mimics of bacterial DNA, and thereby a TLR-9 agonist. The combinatorial anti-cancer efficacy was deemed dependent on TNF-alpha signalling. Given the systemic toxicity of TNF-alpha administration, stimulating the localized production of pro-inflammatory cytokines by the host immune system is considered an effective strategy to elevate cytokines in a safe and tolerable manner. Accordingly, selective replication of an oncolytic virus elicits a robust type-1 IFN response and produces cytokines enabling SM to enhance bystander killing of cancer cells [Cai et al., 2017]. This ‘cytokine storm’ consists of TNF-alpha, TRAIL, and both type-1 and type-II IFNs [Beug et al., 2014]

1.0.5 IAPs and adaptive immunity

A prevailing tactic to instigate cancer cell death, SMs are also potent stimulants, promoting the proliferation of pivotal immune cells required for sustaining antigen-specific immunity [Dougan, 2018]. Specifically, SM had a co-stimulating effect on both CD4+ and CD8+ T cells in the presence of T cell receptor (TCR) stimulation, wherein interleukin (IL-)-2, IL-4, IFNy production was elevated, alongside increased CD25 expression. Reported using murine and human T cells in vitro [Dougan et al., 2010], the pro-inflammatory activity of T cells following

SM treatment has not been visibly translated in a live disease model or clinical setting, suggesting a homeostatic control mechanism may restrain autoimmunity or the in vivo anti-cancer efficacy of SMs. Notably, SM effects on T cell proliferation and cytokine production are dependent on the prevalence of accessory signaling and the signature of costimulatory domains expressed [Murray et al., 2020].

Within B cells, cIAP1 and cIAP2 govern B cell activating factor (BAFF) and CD40 signalling pathways [Matsuzawa et al., 2008]. Constitutive loss of both IAPs generates a similar phenotype as CD40 deletion, as germinal centre formation is mitigated [Gardam et al., 2011]. Furthermore, B cells no longer require BAFF-receptor signalling for survival, enabling unrestrained proliferation and accumulation. Constitutive alternative NFκB signalling is a prevailing trait amongst B cell-lineage malignancies [Pham et al., 2011], which is further enhanced upon SM treatment. Accordingly, mutations or deletion of cIAP1 or cIAP2 occur in approximately 20% of multiple myelomas [Keats et al., 2007]. This would rationalize previous studies reporting lack of efficacy upon treating a mouse model of multiple myeloma with SM [Beug et al., 2017].

1.1 Adaptive Immune Cells and Cancer Immunity

1.1.1 Regulatory T cells

A distinct subset of CD4 T cells, Tregs are distinguished based on their immunosuppressive functionality. Tregs are essential to maintain immune homeostasis in the form of peripheral tolerance, moderating pathological inflammation and preventing autoimmunity (Vignali et al., 2008). Their actions prevent mature lymphocytes from responding to specific antigens, restraining self-reactivity. Forkhead box P3 is the primary transcription factor historically distinguishing effector T cells from Tregs, and is indispensable for their development, maintenance, and suppressive function (Hoi et al., 2003). FoxP3 deficiency in humans is associated with the development of immunodysregulation, polyendocrinopathy and enteropathy, X-linked syndrome (IPEX) in early infancy. Deletion of FoxP3 in mice is associated with hyper-responsive effector CD4 T cells, leading to the development of fatal autoimmunity (Fontenot et al., 2003). Tregs retain a diverse collection of inhibitory mechanisms including the secretion of inhibitory cytokines to paracrine effector T cells, direct cytolysis of effector T cells, metabolic disruption of effector T cells by depriving them of necessary growth factors such as IL-2 and inhibiting the maturation and function of antigen-presenting cells (Vignali et al., 2008). These mechanisms enable Tregs to suppress in both a contact-dependent or -independent manner.

IL-2, a cytokine required for T cell survival, binds to the IL-2 receptor. The receptor depicts variable affinity to IL-2 depending on the presence of specific chains constituting the overall receptor. The highest affinity conformation of the IL-2 receptor is a trimeric complex consisting of the alpha (CD25), beta (CD122), and gamma (CD132) chains. The gamma chain is regarded as the common gamma chain, given its tendency to complex with other transmembrane domains to form receptors for other cytokines, such as IL-4 [Kondo et al., 1993], IL-7 [Kondo et al., 1994], IL-9 [Kimura et al., 1995], IL-15 [Giri et al., 1994] and IL-21 [Asao et al., 2001]. The alpha chain on its own will bind IL-2 with low affinity, and the dimeric complex of the beta and gamma chain will bind IL-2 with intermediate affinity [Liao et al., 2011]. Experiments evaluating the stability of the complex have determined that IL-2 will initially bind the alpha chain, which then recruits the beta and gamma chain [Metz et al., 2012]

Tregs upregulate CD25 to a greater degree than effector CD4 T cells in a healthy state, thus depleting the available IL-2 required for clonal expansion (Thornton et al., 1998). Prior to the discovery of FoxP3 as a lineage-defining transcription factor, CD4 and CD25 co-expression was the predominant criteria to distinguish Tregs from other CD4 lineages. A defining characteristic, FoxP3 binds to the promoter and regulatory region of CD25 to enhance CD25 transcription, whereas upon binding to the IL-2 promoter it represses IL-2 transcription [Chen et al., 2006].

Given the ability of Tregs to restrain effector function of T cells and DCs, these cells are inherently involved in suppressing anti-tumour immunity. FoxP3-expressing Tregs are generally more prevalent in the peripheral blood of cancer patients compared to healthy donors [Woo et al., 2001]. Furthermore, the density of FoxP3+ cells is greater in cancerous tissue compared to healthy tissue [Miller et al., 2006]. Collectively, the abundance in the tumour microenvironment has been associated with poor prognosis in cancer patients [Xu et al., 2010] [Liotta et al., 2011], however exceptions have been reported. For example, greater density of FoxP3+ Tregs is associated with greater control in patients with head and neck cancer [Badoul et al., 2006], and improved survival in Hodgkin's lymphoma patients [Alvaro et al., 2005]. These counterintuitive results may be attributed to the shared activation signals needed for development compared to conventional T cells, along with the expansive control of gene expression by FoxP3 [Martin et al., 2010]. Treg differentiation requires activation of its TCR with peptides specific for self-antigen via MHC-2, along with CD28 co-stimulation. Indeed, transient expression of FoxP3 has been detected on non-regulatory conventional CD4+ T cells following TCR stimulation, without endowing the cell with immunosuppressive properties [Akbar et al., 2007]. FoxP3 is capable of binding approximately 700 genes, acting as either a transcriptional repressor or activator [Zheng et al., 2007]. This implicates FoxP3 as having a pleiotropic role in cancer biology, as its expression may be capable of repressing oncogenes driving cancer progression [Martin et al., 2010].

The targeted ablation of Tregs in the tumour microenvironment is a promising strategy to promote anti-tumour immunity. The removal of these pan-suppressive cells conceptually relieves the repression of effector cells, thereby enabling them to proceed with the clearance of malignant cells. Given the intrinsic diversity of FoxP3+ Tregs, methods to efficiently remove Tregs in a precise manner remain to be demonstrated in the clinic. Traditionally, antibodies targeting CD25 (e.g., PC61 clone in pre-clinical studies) have been utilized to ablate Tregs [Setiady et al., 2010]. The ablation is dependent on the presence of NK cells or macrophages that mediate antibody-dependent cytotoxicity (ADCC) or antibody-dependent cell-mediated phagocytosis (ADCP). Bi-functional molecules, IgG subclass of antibodies possess a variable F(ab) region along with a constant Fc domain that enables interaction with the complement component 1q (C1q) or surface-bound Fc-receptors [Zhang et al., 2016]. Complement proteins elicit an amplifying cascade of inflammation and mediate cell killing through labelling the cell for opsonization or puncturing the cell membrane by forming a membrane attack complex [Golay et al., 2020]. Fc-receptors are membrane-bound domains that specifically recognize the Fc region of immunoglobulins (Ig) [Ben Mkaddem et al., 2019]. The interaction between an antibody's F(ab) region and its surface-bound target domain, in tandem with the Fc-region binding to the appropriate Fc-receptor, enables cross-linking that allows two cells to remain in proximity with one another, developing a synapse. Studies evaluating PC61 administration in tumour-bearing mice demonstrate enhanced immunity to non-self antigens, with increased IFNy secretion by T cells isolated from lymph nodes peripheral to the tumour [Tanaka et al., 2002]. The effective generation of antigen-specific immunity following Treg ablation has enabled the simultaneous administration of tumour-antigen vaccination as a viable strategy to promote anti-cancer cytotoxic T cell immunity.

Clinically, a recombinant IL-2 diphtheria toxin conjugate known as denuleukin diftitox, or ONTAK, was developed to selectively eliminate Tregs from the tumour microenvironment or peripheral blood without inducing toxicity onto subsets that express intermediate and lower levels of the trimeric IL-2 receptor [Dannull et al., 2005]. Daclizumab, a humanized monoclonal antibody targeting CD25, has also been explored in combination with tumour-antigen vaccination to enhance anti-cancer immunity [Rech et al., 2009].

1.1.2 Dendritic Cells & T cell priming

Antigen-presentation to naïve T cells is necessary to form an adaptive response to a specific immunogen. As tumours evolve, the genetic alterations accumulated manifest as neo-antigens [Schumacher et al., 2015]. Developing an immune response against evolving tumours requires active sampling and presentation for the development of a de novo T cell response to tumours. Dendritic cells (DCs) are the professional antigen presenting cells (APCs) of the immune response, necessary for bridging innate and adaptive immune systems [Gardner et al., 2020]. These cells are generated and undergo differentiation in the bone marrow from common myeloid progenitor cells [Dominguez et al., 2010]. Distinct from other phagocytes, namely B cells and macrophages, DCs downregulate phagocytosis upon maturation and instead upregulate presentation-associated machinery: MHC molecules and co-stimulatory domains. DCs are generally subclassified into two generic subtypes: conventional (cDC) or plasmacytoid (pDC). cDCs are generally associated with antigen presentation and distinguished by the expression of zinc finger and BTB domain containing 46 (Zbtb46) [Satpathy et al., 2012], whereas pDCs are associated with response to viral DNA or RNA to facilitate type-1 interferon production and are distinguished by the expression of plasmacytoid dendritic cell antigen 1 (PDCA-1). Despite these distinctions, pDCs retain a considerable degree of plasticity which enables them to process and display antigen.

cDCs can be further subdivided into two functional classes known as type-1 or type-2 cDCs. Type-1 conventional dendritic cells (cDC1) are distinguished based on their enhanced ability to cross-present exogenous antigen to CD8 T cells [Segura et al., 2014]. Enhanced migration to lymphoid structures is necessary for enabling interaction with naïve T cells to facilitate their priming and subsequent clonal expansion. In comparison, macrophages are generally unable to migrate and present antigen to prime T cells, despite being the primary phagocytic population. Migratory cDCs are thus imperative for trafficking tumour-associated antigens to draining lymph nodes, where they will cross-present exogenous antigens to enable clonal expansion of tumour-associated antigen-specific T cells [Gutierrez-Martinez et al., 2015]. cDC1s are distinguished based on their expression of the basic leucine zipper activating transcription factors(ATF)-like 3 (BATF3) and interferon regulatory factor 8 (IRF8) transcription factors. Accordingly, deletion of Batf3 in mice ablated the generation of cross-presenting dendritic cells and were unable to generate antigen-specific CD8 T cells in response to West Nile virus infection [Hildner et al., 2008]. Type-2 conventional dendritic cells (cDC2) are distinguished by the expression of interferon regulatory factor 4 (IRF4). These cells are involved in the presentation of endogenous antigen to and shaping the polarization of CD4+ helper T cells [Sittig et al., 2016]. Notably, CD40-ligand (CD40L) on CD4+ helper T cells bind to CD40 expressed on DCs. A co-stimulatory protein required for DC activation, CD40 mediates signaling via the alternative NFκB pathway. Upon CD40 agonism, cIAP1/2 ubiquitinate TRAF3 for proteasomal degradation, allowing NIK to stabilize and promote cell survival [Elgueta et al., 2009]. Notably, NIK-deficient mice are commonly referred to as alymphoplasia mice, given their lack of developed secondary lymphoid structures, or lymph nodes [Shinkura et al., 1999].

DCs generally control the activation of T cells by interaction between DC-expressed B7 molecules, CD80 (B7-1) and CD86 (B7-2), and T-cell expressed co-stimulatory molecule CD28 [Lenschow et al., 1996]. A host of alternative co-stimulatory molecules and ligands have been a topic of intense research, each with slightly nuanced functionality compared to others [De Sousa Linhares et al., 2018], contributing toward the goal of improving anti-tumour T cell responses. Although cross-presentation has yet to be shown as an imperative process to elicit anti-tumour immunity in humans, the implied necessity of CD8 T cells for optimal anti-tumour immunity suggests this procedure is necessary to generate a targeted response to neoantigens [Figure 4]. In accordance, Batf3-deficient mice fail to eradicate immunogenic malignancy following immunotherapy regimens that otherwise engage and promote a successful anti-tumour cytotoxic T cell response [Sanchez-Paulete et al., 2016]

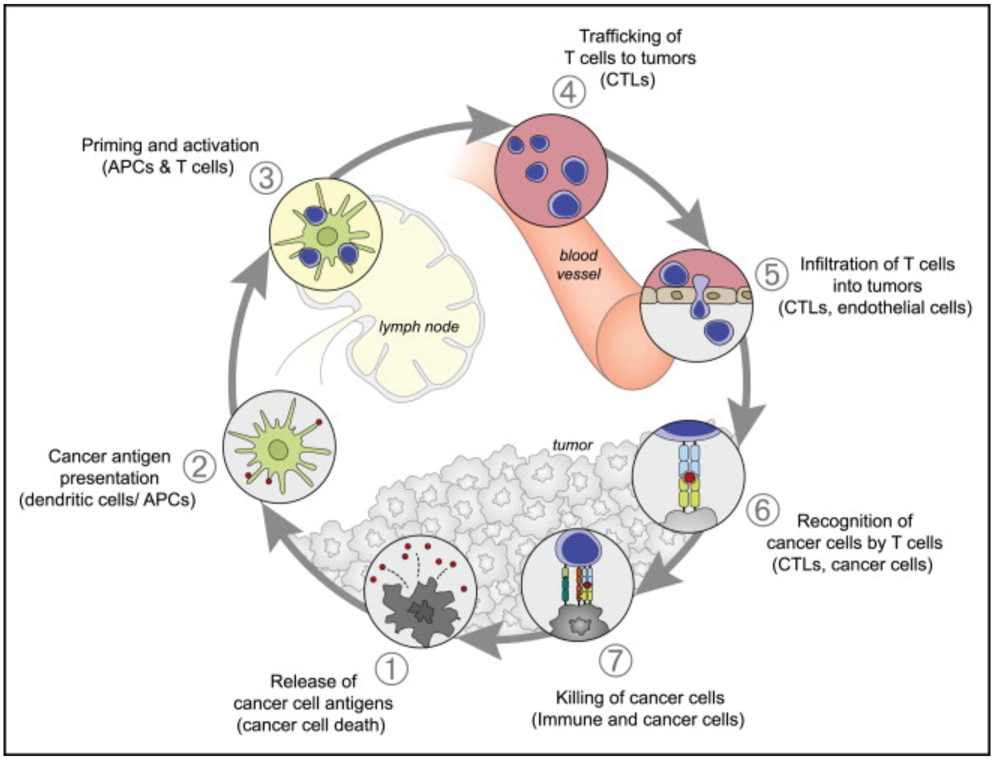
Trafficking of
T cells to tumors
(CTLs)
4
Priming and activation
(APCs & T cells)
3
blood
vessel
5
Infiltration of T cells
into tumors
(CTLs, endothelial cells)
lymph node
tumor
Cancer antigen
presentation
(dendritic cells/ APCs)
2
6
Recognition of
cancer cells by T cells
(CTLs, cancer cells)
1
Release of
cancer cell antigens
(cancer cell death)
7
Killing of cancer cells
(Immune and cancer cells)

Figure 4. Cancer Immunity cycle

Cancer-specific immunity is a cyclical and self-perpetuating process that amplifies T cell responses to eradicate tumours. Each of the seven outlined steps require the coordinated activity of stimulatory and inhibitory factors that either enhance or restrain immunity. Adapted from [Chen & Mellman, 2013].

1.2 Cancer Immunotherapy

1.2.1 Bladder Cancer & BCG

Bladder cancer is currently the tenth most common cancer diagnosed worldwide, with approximately 570,000 diagnosed cases and greater than 200,000 deaths [Sung et al., 2021]. Established risk factors include smoking and exposure to chemical carcinogens [Erdurak et al., 2014]. It is diagnosed nearly four times as frequently in men than in women, however the exact reason for this is unclear [Freedman et al., 2011]. Visible hematuria is the most common symptom presented upon diagnosis. Computed tomography urography and cystoscopy are used to assess both the upper and lower urinary tract in patients with suspected disease [Kamat et al., 2016]. Most cases are transitional carcinomas, otherwise known as urothelial carcinomas. The remaining proportion of cases are classified as non-transitional carcinomas, commonly identified as squamous cell carcinoma, adenocarcinoma, small cell carcinoma, or sarcomas. Approximately 75% of patients with urothelial carcinoma present with non-muscle invasive disease, with the remaining presenting with muscle invasive or metastatic malignancy. Urothelial carcinoma is further sub-classified based on grade and stage, which aids clinicians to accurately diagnose and treat patients. The World Health Organization (WHO)'s grading system is based on cellular anaplasia, or cellular dedifferentiation, whereas stage is determined based on the depth of tumour invasion [Kamat et al., 2016].

Bacillus Calmette-Guerin (BCG) is a vaccine developed to prevent pathophysiology from tuberculosis (TB), an infectious disease caused by infection with mycobacterium tuberculosis bacteria. Named after its creators Albert Calmette and Camille Guerin, the vaccine has been administered to adolescents since the 1920s and has been mandatory in most nations at some point in the 20th century. BCG is developed using mycobacterium bovis, the bovine strain of tuberculosis that does not inflict disease in humans. [Aspatwar et al., 2021]

Intravesical BCG instillation has been used clinically to treat non-muscle invasive bladder cancer (NMIBC) for nearly 50 years [Redelman-Sidi et al., 2014]. First practiced in 1976 [Morales et al., 1976], the concept of utilizing bacteria for cancer treatment was initially pioneered in the late 1800s by William B. Coley, creator of microbial products known as Coley's toxins. The specific use of mycobacteria stems from clinical observations that cancer did not manifest as frequently in patients that harboured active tuberculosis-associated lesions [Pearl et al., 1928]. This resistance was demonstrated in immunocompetent mice, wherein BCG inoculated animals developed resistance to tumour transplantation [Old et al., 1959]. Coincidentally, this study enabled the discovery of TNF itself, as it was isolated from the serum of BCG-infected mice [Carswell et al., 1975].

BCG internalization by bladder cancer cells is one possible mechanism that may contribute toward therapeutic efficacy. Although the internalization of BCG (which under general circumstances is internalized by professional phagocytes like macrophages) by urothelial cells is considered unusual, the presence of intrinsic mutations is hypothesized to enable uptake by malignant cells [Redelman-Sidi et al., 2013]. This direct cytotoxicity may foster a more robust immune response, as it may cause the release of cytokines like IL-6 or chemokines that will recruit pro-inflammatory immune cells to the tumour microenvironment [Esuvaranathan et al., 1995]. Despite this rationale, the internalization of BCG by bladder cancer cells has yet to be demonstrated as necessary for anti-tumour efficacy.

BCG anti-cancer efficacy requires a competent host immune response [Ratliff et al., 1987], and is thus considered the first immunotherapy to be successfully implemented in a clinical setting. The use of live bacteria instead of heat-killed, coupled with close physical contact between bacteria and cancer cells [Kavoussi et al., 1990], are necessary criteria to maximize therapeutic efficacy. This interaction enhances the recruitment of immune cells to the tumour microenvironment [Taniguchi et al., 1999]. These immune infiltrates are the central constituents mediating anti-tumour activity, however the precise mechanism explaining BCG's effectiveness has yet to be definitively elucidated. The recruitment of CD4 and CD8 T cells, along with NK cells, macrophages, DCs, and other polymorphonuclear cells suggest BCG elicits non-specific debulking of the tumour mass. The containment of both the tumour and instilled BCG by the bladder wall enables a potent immune response to be restricted to the localized tumour microenvironment. A TLR-2, -4, and -9 agonist, BCG enables the production of various cytokines that promote inflammation [Zhang et al., 1999].

Intravesical instillation of BCG mycobacteria is the standard regimen to resolve stage one bladder cancer [Morales et al., 1980]. Despite its effectiveness containing papillary neoplasms, BCG instillation fails to restrain advanced disease, with objective response to subsequent combinatorial MVAC (methotrexate – vinblastine sulfate – adriamycin – cisplatin) cocktail or rudimentary platinum-based chemotherapy declining sharply following focal invasion of the mesoderm [Sarkis et al., 1995]. The default surgical remedy, removal of bladder tissue significantly diminishes ensuing quality of life, as radical cystectomy requires artificial compensation through alternative urinary storage and excretion [Sanli et al., 2017]. A critical void in the oncology armamentarium remains, as non-resectable urothelial malignancy frequently precedes terminal metastatic disease within 5 years [Richters et al., 2020].

The grade of urothelial carcinoma inversely correlates with clinical pathological Smac/DIABLO expression, wherein one study reported 98% of NMIBC tissue expressed Smac, compared to approximately 40% in muscle-invasive tissues [Mizutani et al., 2010]. Furthermore, higher expression of Smac within muscle-invasive cases retained a longer post-operative recurrence-free period following transurethral resection [Mizutani et al., 2010]. Given these findings, the prognostic significance of Smac suggests SMs may confer greater reactivity upon treatment.

1.2.2 Immune Checkpoint Blockade

Immune checkpoint blockade has proven highly effective at restraining and eradicating a wide range of non-resectable advanced malignancies [Pardoll et al., 2012]. A new pillar of cancer treatment, the success of immune checkpoint blockade has promoted the application of immunomodulatory agents in the clinic. There are currently hundreds of ongoing clinical trials worldwide evaluating the efficacy of immune checkpoint inhibitor (ICI) treatment as stand-alone mono-therapies, or in combination with other agents [Darvin et al., 2018]. The potential increase in anti-tumour efficacy and objective response upon combining ICIs with other experimental drugs provides an opportunity for new treatments to enter the clinic. In accordance, our lab has previously demonstrated intraperitoneal injection of a murine monoclonal antibody targeting programmed cell death protein 1 (anti-PD-1, J43 clone) synergizes with simultaneous oral gavage SM (LCL161) treatment to potentiate anti-tumour immunity in an orthotopic model of murine glioblastoma [Beug et al., 2017].

Currently, pembrolizumab and nivolumab are two monoclonal antibodies targeting PD-1 approved for the treatment of metastatic melanoma, with new approvals emerging for various other malignancies [Twomey et al., 2021]. Notably, pembrolizumab has been granted approval for the treatment of advanced urothelial carcinoma [Bellmunt et al., 2017]. Cemiplimab is another antibody targeting PD-1 and is approved for cutaneous squamous cell carcinoma [Ahmed et al., 2019]. Atezolizumab, durvalumab, and avelumab are monoclonal antibodies specific for PD-L1. Atezolizumab is approved for the treatment of metastatic urothelial carcinoma following platinum-based chemotherapy [Ning et al., 2017], along with triple-negative breast cancer [Schmid et al., 2018], metastatic non-squamous non-small cell lung cancer [Socinski et al., 2018]. Durvalumab and avelumab are also approved for the treatment of advanced urothelial carcinoma [Wills et al., 2019] [Powles et al., 2020]. Avelumab is distinct from durvalumab and atezolizumab given it belongs to the IgG1 subclass of IgG antibodies. This enables avelumab to bind to Fc receptors with high affinity, thereby enabling ADCC of tumour cells to occur [Boyerinas et al., 2015].

ICIs operate by interrupting intercellular co-inhibitory signaling amongst immune cells interacting with other immune cells or tumour cells (Figure 5) [Darvin et al., 2018]. As a result, tumours with greater immunological infiltrates confer a higher degree of response to immunomodulatory therapies. PD-1 is primarily expressed on immune cells and upon binding its cognate ligand, programmed cell death ligand 1 (PD-L1), operates as a rheostat for immune cell activation [Okazaki et al., 2013]. A recent report demonstrates the PD-1/PD-L1 axis confers its inhibitory function by blunting traditional CD28 co-stimulatory signaling required for T cell activation [Hui et al., 2017]. Accordingly, the invigoration of T cells relative to tumour burden in melanoma patients correlates with response to pembrolizumab, a monoclonal antibody targeting PD-1 [Huang et al., 2017]. Notably, despite the association of PD-1 with T cell biology, the PD-1 molecule has also been detected on DCs [Lim et al., 2016],

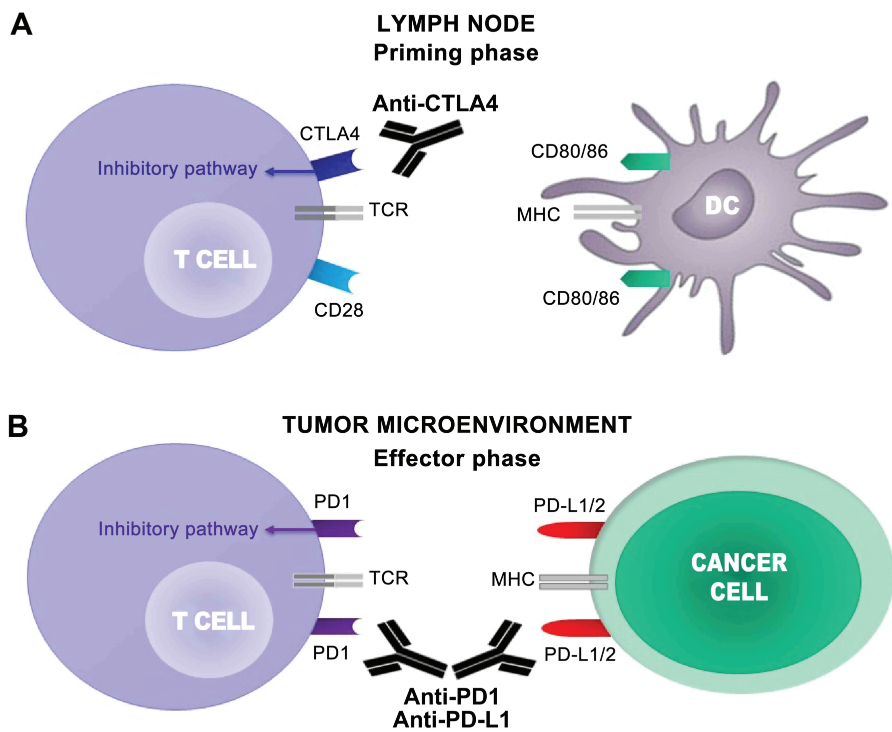
A
LYMPH NODE
Priming phase
Anti-CTLA4
CTLA4
Inhibitory pathway
TCR
T CELL
CD28
CD80/86
MHC
DC
CD80/86
B
TUMOR MICROENVIRONMENT
Effector phase
PD1
Inhibitory pathway
TCR
T CELL
PD1
PD-L1/2
MHC
CANCER CELL
PD-L1/2
Anti-PD1
Anti-PD-L1

Figure 5. PD-1/PD-L1 and CTLA-4 immune checkpoint blockade

PD-1 and CTLA-4 regulate disparate phases of the T cell response. A) In the peripheral lymph nodes, T cells are activated following sequential TCR agonism with a cognate peptide-MHC complex followed by associated co-stimulation through B7 molecules CD80/86 binding to CD28. CTLA-4 is a negative regulator of co-stimulation, binding to CD80/86 with greater affinity than CD28, thereby precluding co-stimulatory signaling. B) With greater antigen exposure, like in the tumour microenvironment, PD-1 is upregulated on T cells. Upon binding to PD-L1/L2, ligands expressed by tumour cells, T cell activation is inhibited. Adapted from [Stucci et al., 2017]

NK cells [Hsu et al., 2018], B cells [Thibult et al., 2013], and myeloid-derived suppressor cells (MDSCs) [Nam et al., 2019]. The precise molecular mechanism of PD-1 on these cell types is unclear. Although many factors have been associated with response to PD-1 blockade, including PD-L1 expression, density of immune infiltrates in the tumour microenvironment, mutational burden, or mismatch-repair deficiency, there are no definitive biomarkers that accurately predict efficacy [Yi et al., 2018].

Unabated PD-1 signalling, in conjunction with constitutive TCR agonism, suppresses activated T cells into an exhausted state. As antigen load elevates, T cells will progressively lose effector functionality and other properties necessary for optimal effector function [Wherry et al., 2011]. This hypo-responsive state is accompanied with an increase in the overall quantity and diversity of immunoregulatory receptors and cytokines. In tumours, given the prolonged exposure of infiltrating T cells to tumour-associated antigens, T cells may be eliminated, leading to the loss of tumour antigen-specific T cells [Jiang et al., 2015]. In the case where antigen persists, this hierarchical process culminates with the apoptosis of T cells. PD-1 is considered the major inhibitory receptor that regulates this process.

Cytotoxic T lymphocyte-associated antigen-4 (CTLA-4) is another inhibitory immune checkpoint receptor that has been successfully targeted by monoclonal antibodies for the treatment of advanced malignancies. The first ICI clinically approved was ipilimumab in 2011 for the treatment of metastatic melanoma [Hodi et al., 2010]. Ipilimumab is undergoing clinical trials for the treatment of various advanced malignancies in combination with ICIs targeting PD-1, including urothelial carcinoma [McGregor et al., 2019]. CTLA-4 is upregulated on T cells shortly following activation and binds to the same B7 receptors (CD80 and CD86) expressed on DCs as co-stimulatory CD28, however with greater avidity than

CD28 [Yokosuka et al., 2010]. This sequestration of co-stimulatory ligands restrains T cell priming. The cell-intrinsic mechanism of CTLA-4 has yet to be defined.

CTLA-4 is highly expressed on Tregs and is a transcriptional target of FoxP3 [Chen et al., 2006]. Antibodies targeting CTLA-4 that confer Fc receptor cross-linking may therefore enable Treg ablation by ADCC or ADCP [Simpson et al., 2013]. This implicates CTLA-4 as a pivotal factor in both the peripheral lymphoid structures and the tumour microenvironment. Accordingly, optimal anti-tumour activity from CTLA-4 blockade requires interaction with both regulatory and effector T cells [Peggs et al., 2009] [Simpson et al., 2013]. There are currently no definitive biomarkers that would indicate response to CTLA-4 blockade.

1.3.3 **Combination Immunotherapy**

The advent of combination immunotherapy has promoted the inclusion of various therapeutic modalities that hope to promote anti-tumour efficacy leading to enhanced survival benefit. The combination treatment regimen of Nivolumab and Ipilimumab has demonstrated greater tumour regression in advanced metastatic melanoma, compared to either treatment alone [Wolchok et al., 2013]. The concurrent treatments are tolerable, with a manageable safety profile. For bladder cancer, the objective response to nivolumab or nivolumab in combination with ipilimumab remains approximately 30% [Hakenberg et al., 2017] [McGregor et al., 2019]. Despite the promising results from clinical trials, ICIs are not sufficiently active for a large cohort of patients.

There is an ongoing clinical trial evaluating the efficacy of monovalent LCL161 in combination with a PD-1 targeting monoclonal antibody within non-small cell lung cancer (NSCLC), triple-negative breast cancer, colorectal cancer, or renal cell carcinoma patients

(NCT02890069) [Cetraro et al., 2022]. The emergence of combinatorial treatment platforms present significant promise to eradicate advanced disease. Drug cocktails perpetuate diversifying mechanisms of action, potentially synergizing to elicit greater efficacy than any given modality in isolation. The prevalence of ongoing clinical trials and established treatment standards against myriad cancers involving antibodies targeting immune checkpoints CTLA-4, PD-1 and PD-L1 are creating a sizeable financial burden on healthcare systems worldwide. Here I evaluate the use of a small-molecule chemical mimetic emulating a natural molecular procedure capable of sensitizing solid tumours to checkpoint blockade. The addition of this cost-effective adjuvant clinically may yield greater objective response rates or diminish the treatment duration required to achieve maximum benefit from checkpoint blockade. The therapeutic strategy is thereby posited to improve patient survival and economic cost by enhancing the efficacy of approved pharmaceutical drugs.

1.3 Hypothesis and Objectives

I hypothesized SM treatment in combination with monoclonal antibodies targeting prominent immune checkpoints, namely αCTLA-4, would synergize to facilitate immunological eradication of established murine urothelial carcinoma. My primary objective is to demonstrate durable cures in a murine model of cancer, with my secondary objective being to determine the general mechanism responsible for anti-tumour efficacy. By understanding the mechanism of action, we can incorporate this knowledge as insight toward developing an optimized strategy to adopt SMs as anti-cancer agents. To this end, I explore the effects of SM on specific immune cell compartments relevant for anti-tumour efficacy, in a tumour-free setting.

2.0 MATERIALS AND METHODS

2.1 Cell Culture & Time-lapse Microscopy

Cell line stocks were stored at -80°C (dry freezer; <3 years) or -130°C (liquid nitrogen; long term) in 90% heat-inactivated fetal calf serum (HI-FCS, Gibco) and 10% Dimethyl Sulfoxide (C_2H_6OS, DMSO, Sigma-Aldrich). Cell vials were thawed until partial melting of frozen homogenate in a 37°C water chamber. Immortalized cells (1mL) were diluted in Dulbecco's modified Eagle's medium (D-MEM) media (9 mL, HyClone™, Cytiva) supplemented with 10% heat-inactivated fetal calf serum (HI-FCS, Gibco), 1% non-essential amino acids (NEAA, Invitrogen), L-glutamine, and 1% sodium pyruvate ($C_3H_3NaO_3$, Gibco) in a sterile biosafety cabinet. In vitro cell density optimization was performed using a time-lapse microscopy instrument integrated into a humidified 37ºC incubator (Incucyte® Live-Cell Analysis System, Essen BioScience). Cells were seeded in serial dilutions and plates were immediately placed into designated slots in the imaging chamber. Cells were cultured for sufficient time to evaluate the impact of spatial segregation on bulk growth dynamics. Images were acquired using a 10x objective lens (1.24 μM/pixel, 1408x1040 pixels, 1.75x1.29 mm field of view). Phase imaging was generated using brightfield microscopy (Basler Ace 1920-155μM, CMOS sensor) and fluorescence channels (Red: 585_{EX} [565,605_{bp}] 635_{EM} [625,705_{bp}]; Green: 460_{EX} [440,480_{bp}] 524_{EM} [504,544_{bp}]) for overlay images. Data was analyzed used the Cell-by-Cell software module (Incucyte® Zoom™, Essen BioScience), and exported to Excel (Office 10, Microsoft) and Prism (9.1, GraphPad). Eccentricity measurements were generated from phase-mask overlay images and computational segmentation by pixel discrimination. Derived second order moments of regional ellipses define eccentric distance ratio of ellipse foci and semi-major axis length

2.1 Cell Health Assays

Log-growth phase cells were seeded at optimized densities in 100 μL of supplemented media in 96-well TC-plates and incubated for ~24 hours at 37ºC prior to treatment. For multiple treatments, cells were treated in 25-50μL increments for a maximum volume of 150-200uL. For biological treatments, PBS with bovine serum albumin (0.05% BSA, Sigma-Aldrich) was used as a negative control. For chemical treatments, recombinant cytokines, or all other chemicals reconstituted in DMSO and stored below -80, 0.05% DMSO (Sigma-Aldrich) was used as a negative control. Following incubation, 7x resazurin salt solution (Alamar™ Blue, ThermoFisher) or tetrazolium dye MTT [3-(4, 5 dimethylthiazol-2-yl)-2, 5-diphenyltetrazolium bromide] (MilliporeSigma) was diluted in cell-free media in a biohood with the lights turned off. Plates were removed from the incubator and aspirated of media. Cells were reconstituted with solution-diluted media and incubated for 2-6 hours. Following visual confirmation of colorimetric shift, plates were immediately analyzed for spectral absorbance using a spectrophotometer (Synergy™ microplate reader, Biotek®). Wavelength correction was applied to baseline readings and absorbance output was quantified to infer net metabolic activity (Gen5™ software). For normalized viability quantification the following equation was incorporated: % viability = [(experimental signal – background) / (control signal – background)] * 100%.

Cell cytotoxicity was assayed using a lactate dehydrogenase (LDH) release kit (Promega) to quantify LDH release from lysed or dead cells using the manufacturer's protocol. Target cells were plated in a 96-well flat-bottom plate the day prior to the assay. Various conditions were maintained as follows: spontaneous target cell LDH release, spontaneous effector cell LDH release at defined experimental ratios, maximum LDH release from target cells, effector cell baseline LDH release at defined experimental ratios relative to target cells, baseline LDH in media. Upon preparing target and effector cells for co-culture, cells were reconstituted in media with 2.5% FCS instead of 10% to minimize signal saturation from background. Triton X-100 was added to lyse cells and generate maximal LDH release readout. Immediately following target and effector cell co-culture, plate was centrifuged at 300 RCF for 5 minutes to ensure contact between targets and effectors. Co-cultures were incubated for 4-6 hours. Following incubation cells were centrifuged at 300 RCF for 5 minutes to pellet cells and debris. 50uL of supernatant was transferred to a new 96-well plate and 75uL of reaction cocktail was added to each well. Plate was incubated in the dark for 45 minutes at room temperature, then wavelength absorbance was quantified using a spectrophotometer. Calculation for cytotoxicity was performed as follows: Well signal = (490nm reaction signal reading – 620nm correction) – blank media signal. Following adjustment of each reading, the following formula was used to determine percent cytotoxicity: [experimental signal – (target spontaneous release signal + effector spontaneous release signal)] / (target maximum signal – target spontaneous signal).

2.3 Bacteria

The Connaught strain of Mycobacterium bovis Bacillus Calmette-Guerin (BCG) was a gift from Dr. Subash Sad (University of Ottawa), and technical guidance was provided by Renu Dudani (National Research Council, Ottawa). BCG was cultured in a polycarbonate Erlenmeyer flask (Thomas Scientific) with bacterial medium comprised of: Middlebrook 7H9 broth (Sigma-Aldrich), 10% albumin-dextrose-catalase (ADC) supplement (Sigma-Aldrich), 0.2% glycerol, 0.05% polyoxyethylene-[20]-sorbitan-monooleate (Sigma-Aldrich). BCG was selectively propagated by supplementing media with 15 μg/ml Kanamycin. To culture mycobacteria, media was warmed to 37ºC prior to culture, and otherwise stored at 4ºC in the dark. A frozen (-80ºC) vial containing 1e8 colony-forming units (cfu) per mL of bacteria was thawed and dispensed into warm media, and flask was capped with a 0.22μm hydrophobic membrane. Mycobacteria was cultured in a 37ºC humidified, rotating incubator (300 rpm) lacking CO_2. Optical density (OD_N) of bacterial cultures was determined by absorbance measurements using a spectrophotometer (Synergy™ HTX plate reader, Gen5 software, Biotek®). OD_N was utilized to infer bacterial density and growth phase, with all experiments incorporating mid-log phase bacterial culture. Colony forming units (CFU) per mL of bacteria was determined by plating serial dilutions on Middlebrook 7H10 solid medium (Sigma-Aldrich) agar plates supplemented with 10% oleic acid-albumin-dextrose-catalase (OADC, Sigma-Aldrich), 0.5% glycerol, with or without antibiotics. For long-term storage, mid-log cultures (OD_{600}= 0.7–1.0) were frozen in 20% glycerol at -80°C. For in vivo experiments, mid-log culture aliquots were centrifuged and reconstituted in D-PBS. Pre-log phase bacteria ($OD_{600} \cong 0.3$) was kept on ice for < 1 hour prior to animal inoculation. Clinical-grade lyophilized BCG (4ºC storage, <2 years) was reconstituted in D-PBS and utilized immediately for experiments (OncoTICE®, Merck GmBh).

2.4 Viruses

Vesicular stomatitis -(Indiana) virus (VSIV) and a derivative VSIV$^{\Delta M51}$ (deletion of 51st amino acid, methionine, in the central M domain), and **Vaccinia** virus (VV) were provided by Dr. David F. Stojdl (presently: Turnstone Biologics; formerly: Children's Hospital of Eastern

Ontario Research Institute) and Dr. John C. Bell (Ottawa Hospital Research Institute). $VSIV^{\Delta M51}$-$SIINFEKL^{luc}$ ($2e10^{10}$ pfu/mL stock at -80°C) was provided by Dr. Yonghong Wan (McMaster University). We kindly thank Dr. Fanny Tzelepis (presently: Health Canada, formerly: Ottawa Hospital Research Institute) for technical guidance and flow cytometric validation of ovalbumin epitope (SIINFEKL)-specific $CD8^+$ T cell expansion via tetramer expression. $VSIV_{-m}IFN\beta$, $VSIV_{-m}IFN\beta^{-NIS}$, $VSIV_{-h}IFN\beta$, $VSIV_{-h}IFN\beta^{-NIS}$, and $VSIV^{\Delta M51\text{-}NIS}$ were all purchased from Imanis Life Sciences. All VSIV variants were propagated in Vero cells. **Sendai** virus was purchased from Charles River. **Adeno**virus constructs were generated in-house.

2.5 Chemical Compounds

Lyophilized, clinical grade Smac mimetic (LCL161, Novartis) was reconstituted in acid buffer (30% 0.1M HCl, 70% 0.1M NaOAc, pH=4.63) until homogenous to a density of 50 mg/kg or 75mg/kg, < 1 hour prior to in vivo oral gavage. For in vitro treatments LCL161 was reconstituted in DMSO at a stock concentration of 10-100 mM. Pan-caspase inhibitor z-$VAD^{\cdot fmk}$ ((carbobenzoxy-valyl-alanyl-aspartyl-[O-methyl]-fluoromethylketone), R&D Systems) was reconstituted in DMSO as per manufacturer's protocol. NIK inhibitor (SMI1, Selleck Chemicals) was reconstituted in DMSO as per manufacturer's protocol.

2.6 Transitional Cell Carcinoma

The methodology for orthotopic instillation was developed based previous literature [Gunther et al., 1999]. $MB49^{luc}$ cells were thawed and sub-cultured in $100mm^2$ (~55 cm^2

growth area; 10 mL volume) circular tissue culture (TC)-treated plates (Corning) at 37°C and 5% CO_2 in a humidified direct-heat incubator (Forma, ThermoFisher). To verify allograft tolerance, subcutaneous inoculations of MB49^{luc} cells were visualized by bioluminescence (data not shown). Pre-instillation cell density optimization was conducted following pilot inoculations incorporating fold-change cell concentrations (data not shown). Cells were cultured for a maximum of 2-3 divisions, 4-5 days prior to the morning of surgery. Approximately 1.5 hours prior to invasive surgery, ~85-90% confluency was confirmed by light microscopy. Following qualitative (morphology) and quantitative (hemocytometer) verification of consistent vitality, cells were aspirated of residual medium, rinsed with D-PBS (sterile, 4°C) and incubated with trypsin (0.25%) at 37°C to abate adherence. Cells were reconstituted in 37°C supplemented media and triturated to maximize cell yield prior to centrifugation (300 RCF, 4°C, 5 minutes). Supernatant was aspirated and cells were reconstituted in 2x(mL) of 95% HI-FCS until pellet homogenized, followed by 5% DMSO by titration/10 cm^2 plate. Cells were stored in 1 mL aliquots in cryopreservation vials (Cryovial™, Fisher Scientific) within an isopropanol chamber at -80°C prior to storage. Cells were manually counted/discriminated by loading a hemocytometer with cell aliquots diluted 1:1 with 0.4% resazurin salt (Trypan Blue™, Sigma-Aldrich). Preoperative buprenorphine HCl (0.05 mg/kg) was administered subcutaneously to each mouse 1 hour prior to surgery to alleviate pain. 8–10-week-old female C57BL/6$^{N\text{-}Cr1}$ mice were utilized throughout the study to prevent inadvertent self-recognition of a Y-chromosome -linked antigen, as MB49 cells are derived from a male C57BL/6 mouse. Animals were weighed (BJ-C series, Intelligent Weighing Technology) anesthetized with 3-5% isoflurane inhalant (Baxter International) in a gas chamber and transferred to a dual 2-3% isoflurane & 4% O_2 ventilation manifold (15-cone, pressure-gauged ventilation apparatus; constructed in-house). Animals were kept on a water-based heating pad (37°C) to prevent surgery-induced hypothermia. Ophthalmic ointment (PuraLube™, Dechra) was applied to the eyes to prevent reticular dehydration/corneal damage. Hair at the surgical site was removed by topical administration of depilatory cream (Veet™, Reckitt) on the lower abdomen (not genitalia) for 3 minutes. Transurethral catheterization was performed using lubricated (K-Y Jelly, Reckitt), 1-inch, 20-gauge pediatric venous catheters (Terumo) by aiming the polyethylene tubing at a 45° angle and inserted completely by inferring the natural curvature of the urethra. Prior anesthesia and abdominal palpations expelled urine and minimized urine retention, and residual urine was removed using a pipette (PIPETMAN® P200L, Gilson) pointed precisely at the base of the catheter hub. 80μL of 1:1 ratio of equilibrated (37°C water bathe, ~5 minutes) 0.25% trypsin (Sigma-Aldrich) and non-supplemented (lacking HI-FCS & antibiotics) D-MEM was instilled into the bladder for 15 minutes to aggravate the transitional epithelium. Solution was retained by using an air-filled syringe as a pneumatic actuator (seal). Following incubation, solution was expelled by palpating the lower abdominal cavity. 25,000 $MB49^{luc}$ cells (100 μL) resuspended in Dulbecco's phosphate-buffered saline (D-PBS, Sigma-Aldrich) were injected by 0.5 mL syringe. Catheters were sealed and anesthetized animals were further incubated for 50 minutes. Anesthesia was halted and mice were placed in ventilated 37°C recovery chambers for 20 minutes. Post-operative recovery was aided with dietary supplements (Cheerios™, General Mills) and a cotton fiber pad to minimize overall stress, thereby mitigating the propensity of additional non-experimental variables (discomfort/pain-associated behavioral shifts disparate from tumour instillation). Buprenorphine (0.05 mg/kg) was administered within 2-4 hours post-instillation, and once more the next day. For all survival experiments, stable expression of firefly luciferase within animals was evaluated by in vivo imaging of animals on day 6 post-instillation to infer the presence of a non-metastatic allograft using a bioluminescence reporter. Photosensitive D-luciferin sodium salt (Sigma-Aldrich) was thawed immediately prior to subcutaneous administration in a dark biosafety cabinet and dim imaging suite. Animals were weighed (BJ-C series, Intelligent Weighing Technology) anesthetized with 2% isoflurane and transferred amongst apparatuses sharing a common source for anesthetic, remaining unconscious for the remainder of the imaging procedure. Animals were transferred from gas chamber to ventilation cones within an in vivo imaging system (IVIS® Spectrum, Perkin Elmer). An 8-minute incubation period preceded bioluminescent image acquisition (exposure time ≤ 60 seconds). This duration optimized workflow for studies with larger cohorts of animals (2-3 personnel, designated tasks), updating recursive software settings, and luciferin metabolism. Pilot experimentation to evaluate neoplastic invasiveness was designed based on survival probability data from articles incorporating similar inoculation methods [Gunther et al., 1999]. Ex vivo imaging of internal organs comparing bioluminescence from the primary tumour and isolated organs confirmed saturation of the urinary organ prior to metastases. We found untreated tumours metastasize to the lymph nodes, kidneys, liver, and lungs ≥ 8 days after intravesical instillation. We tailored the start of treatments to reflect the critical non-muscle to muscle invasiveness transition. This strategy represents medical intervention at the time wherein current clinical regimens begin to progressively diminish overall quality of life and anti-neoplastic efficacy relative to treatment toxicity. Furthermore, it ensured discrete and consistent evaluation of treatment efficacy against primary malignancy. Following visual verification of bioluminescence representative of urinary tumours (day 6), animals were randomized, and treatment groups were assigned to cages (day 7). All oral gavage treatments were conducted immediately prior to intraperitoneal injections for each animal. For intraperitoneal treatments, mice were tilted to enable the abdominal viscera to shift and thereby preclude accidental puncture of abdominal organs. A 25-gauge needle was utilized to inject solution into the lower right quadrant of the abdomen. For simultaneous co-treatments, the lower left quadrant was used as the injection site. Mice were treated in the afternoon, unless otherwise stated. For ex vivo tumour analysis, cystectomy was performed and if necessary remaining healthy urothelium was discarded. Specifically, for tumours extracted < 12 days post-inoculation, palpation-induced urine discharge was inferred as partial saturation of the organ with solid neoplasm. Urinary organs were instilled, akin to inoculation technique, by injecting ~50μL of cold D-PBS via the urethra. Urinary vertex perfusion verified partial organ saturation with neoplasm, requiring precise excision of non-neoplastic urothelium. For tissues extracted ≥ 12 days post-inoculation, urinary organs were visually verified for general enlargement, vertex sedimentation, and disfigurement (non-uniform ventral or basal eccentricity) as confirmation of neoplastic saturation. Ligation was performed with a ventral knot around the bladder neck and trigone, exposing the dorsal body. If necessary, healthy urothelium was peeled and discarded, and tumour samples were submerged in sterile PBS. Tumours were weighed, minced, and then resuspended in 2% FCS-PBS containing 25 μg/mL collagenase I & II (Liberase™ research-grade thermolysin medium, Sigma-Aldrich). Tumour fragments were mechanically (program: m_TDK_1; 45-minute runtime) and enzymatically (37°C heated manifold) dissociated (GentleMACS® OctoDissociator with heaters, Miltenyi Biotec®). Tumours were processed through a 70μM cell strainer (Corning) to generate single cell suspensions. For survival studies, additional clinical observation records were required due to dramatic changes in animal wellness of nontreatment/refractory treatment cohorts ~15 days following intravesical instillation. Animals were weighed and monitored 3 times a day starting on day 7 until the end of each study. Animals were euthanized when overall health diminished, a value comprised of the following characteristics: body weight changes (maximum of 20% decrease in total weight from original weight prior to intravesical instillation), activity (responsiveness/lethargy), body condition score (thin/normal/overweight), hair coat (rough hair coat/piloerect/porphyrin staining), posture (upright/hunched), respiratory distress, facial grimace (protruded ears and squinting eyes), colour (normal/pallor/jaundice), hydration (epithelial dexterity), fecal/urinary output (hematuria), and general nesting behavior (disassembly of housing & post-operative recovery pad). Bioluminescent imaging of animals with fold-change differences in survival benefit relative to control treatment cohorts were imaged using consistent acquisition and analysis settings. Absence of precise bioluminescence following IVIS® imaging and survival benefit exceeding 150 days post-intravesical instillation were inoculated subcutaneously with 500,000 $MB49^{WT}$ or histocompatibility-matched 500,000 $B16F10^{WT}$ cells reconstituted in D-PBS in the right flank. In a separate study, reinoculation strategy was partially modified to evaluate distinct allografts in the left (MB49) and right (B16F10) flank simultaneously. Wildtype strains of cells were utilized for inoculating healthy animals cured of $MB49^{luc}$ to preclude antigenicity and immunological memory responses specific towards luciferase and transfection-associated molecular structures. 20-fold greater cells were utilized for secondary inoculation to ensure allograft rejection required robust immunological memory and remained specific for the primary allograft. Subcutaneous tumour outgrowth was measured at least 3 times/week using electronic calipers (VWR). Animals were sacrificed if/when measurement foci traversed ellipse orthoptic in relation to injection site, implicit equation-derived tumour volume exceeded 250mm^2, or overall animal health and wellness diminished as per standard ethical guidelines. All experimentation and survival studies pertaining to orthotopic MB49^{luc} or MB49^{GFP} tumours contain $\geq$ 3 animals. Re-inoculation experiments contain $\geq$ 3 animals previously cured of MB49^{luc}. Tumour instillation was conducted in increments of 15 animals at a time (as per manifold capacity), with all animals within each survival study grafted within a 3-hour timeframe. Topical antibiotic (2% Taro-Mupirocin, GlaxoSmithKline) and local anesthetic (2.5% Lidocaine, EMLA) was applied to animals to treat minor injuries sustained extrinsic of experimental parameters, or $\geq$ 4 months after experimental endpoint, as required. MBT-2^{luc} cells were instilled in female C3H mice akin to MB49^{luc} instillation. C3H mice failed to establish orthotopic tumours or subcutaneous tumours following inoculation with MBT-2^{luc}, or wild-type MBT-2. Allograft rejection corroborates literary findings reporting type-C retroviral infection facilitating MBT-2 immunogenicity (De Boer et al., 2000). We thank Dr. Dorine Gilbert and Dr. Holly Orlando for guidance in developing the protocols (CHEO-1694), and the ACVS technical staff for their assistance throughout the duration of this study.

2.7 Surgical Dissection & Primary Cell Extraction

6-8-week-old naïve C57BL/6^J female mice were sacrificed by CO_2 exposure followed by cervical dislocation in a designated animal procedure suite. Mice were placed supine on a gauze pad in a level 2 biosafety cabinet (BSL-2) and sanitized with 70% ethanol for dissection. Ventral bilateral incisions piercing the subcutaneous skin and the peritoneal wall were created from the abdominal cavity to the hypogastric region. For **bone marrow** extraction, parietal tissue was removed from the left and right iliac regions, exposing the femoral heads (micro-forceps & assorted surgical scissors, Fisher Scientific). Femoral head ostectomy was conducted by fracturing the acetabulum and severing proximal tissue by shearing. Amputated femora were sheared to discard adjacent connective tissue. Perpendicular compound fractures proximal to the patella and femoral head enabled aspiration of single cell suspensions using a 22-gauge needle attached to a 2 mL syringe pre-loaded with supplemented RPMI. Liquid marrow was sieved using a 70µM nylon mesh filter (Corning). Single-cell suspensions were centrifuged (25°C, 300 RCF, 5 minutes) and reconstituted in RPMI supplemented with ammonium chloride (NH_4Cl) solution for a brief incubation (~25°C, 2 minutes) to lyse non-nucleated erythrocytes (Invitrogen). **Spleens** were harvested, weighed, and then stored in cold MACS® Tissue Storage Solution (Miltenyi Biotec) on ice. Efferent lymphatics were excised then discarded, and spleens were processed into homogenous suspension via mechanical dissociation (program: m_spleen_01; ~56 second runtime) using a GentleMACS® OctoDissociator (Miltenyi Biotec®). Sterile cells were pipetted (ART® 1000 REACH™, Molecular BioProducts) via septum-seal opening (C-tubes, Miltenyi Biotec®) and processed through 70µM nylon mesh filters (Corning). Single-cell suspensions were centrifuged (25°C, 300 RCF, 5 minutes) and reconstituted in ammonium chloride (NH_4Cl) solution and incubated (~25°C, ≤ 5 minutes, dependent on suspension viscosity) to lyse non-nucleated erythrocytes (RBC Lysis Buffer, Invitrogen). Suspension was diluted with PBS (1:5), centrifuged (25°C, 300 RCF, 5 minutes), and reconstituted in supplemented RPMI. Inguinal, cervical, and axillary **lymph nodes** were harvested (MF-1 curved micro-forceps, Thomas Scientific), stored, and processed in a physically similar manner to spleens excluding ammonium chloride incubation. Animal studies wherein surgery or inoculations are experimental variables required precise excision of proximal (draining) lymph nodes only. Gut-associated lymphoid follicles (**Peyer's Patches**) were isolated from the mucosal layers of the small intestine (ileum and jejunum).

Note, the structural integrity of the basal lamina is integral to avoid the retrieval of gastrointestinal microorganisms when excising tissue. **Peripheral blood** was collected by non-surgical tail-vein perfusion or following animal endpoint by cardiovascular perfusion. …

2.8 AST/ALT Assays.

Serum was isolated from animals 24 hours following final treatment and processed for liver enzyme activity. Colorimetric assays for Aspartate Trans-aminase (AST) and Alanine Trans-aminase (ALT) were used, according to manufacturer's protocols (Sigma-Aldrich).

2.9 BMDC Maturation

Immature dendritic cells were differentiated on day 6 following initial marrow extraction and cell propagation from a 6–8-week-old C57BL/6^{J} mouse. Approximately $2*10^{8}$ cells were collected from two tibiae and femurs. Cells were collected and reconstituted ($2*10^{5}$ cells/mL) in fresh media supplemented with $_{rm}$IL-4 (10ng/mL) and $_{rm}$GM-CSF (40ng/mL). GM-CSF (40ng/mL) was added, and media was refreshed on day 4. GM-CSF (40ng/mL) was added on day 6 without refreshing media. To differentiate cells, recombinant murine TNFα (100ng/mL, R&D Systems), LPS (1μg/mL, Invitrogen), αCD40 (1μg/mL, Bio X Cell®), monomeric SM (5μM, LCL161, Novartis), or dimeric SM (5μM, Birinapant) was administered and cells were incubated (3-4 days, 37ºC, 5% CO_2). For transfer of differentiated dendritic cells, a broad tip pipette was utilized to prevent aggregation of cells. To evaluate DC functionality, cells were pulsed with a photostable, pH-insensitive soluble antigen (chicken ovalbumin whole protein) conjugated to a fluorescent tag (AF^{647}-OVA, ThermoFisher), sealed to minimize photobleaching (Black Film Seal, VWR®), and incubated for 2 hours prior to collection for flow cytometric analysis.

2.10 Lymphokine-activated Killer Cells

Spleens were resected from a 10 week-old C57BL/6J female mouse, homogenized using a GentleMACs Dissociator, then passed through a 100μM filter mesh (Elko Filtering). Erythrocyte lysis was performed on the cell suspension and incubated for one minute with 1mL of ammonium-chloride-potassium buffer (0.15M NH4Cl, 10mM KHCO3, 0.1mM Na2-EDTA, pH = 7.2-7.3). Enrichment of lymphokine activated killer (LAK) cells was performed by magnetic selection using the EasySep mouse NK cell isolation kit (STEMCELL). Enriched cells were reconstituted in RPMI-1640 media supplemented with 10% heat-inactivated fetal calf serum (FCS) (Gibco), 10μM beta-mercaptoethanol, 1% penicillin-streptomycin, 1% non-essential amino acids (Invitrogen), 20mM 4-(2-hydroxyethyl)-1-piperazeineethanesulfonic acid (HEPES), and 1000 U/mL recombinant human interleukin-2 (Peprotech) and maintained at 37°C with 5% CO2. Cells were plated at an initial density of $1x10^6$ cells/mL and passaged on days 4 and 6. Flow cytometry was performed to verify purity of cells after 7 days (>90% viability).

2.11 T cell culture, proliferation assay, and polarization

Spleens were harvested from 6-8-week-old naïve C57BL/6J mice. Splenocytes were isolated following mechanical dissociation using GentleMACs Dissociator (Miltenyi) and processed through a 70μM cell strainer (ThermoFisher). EasySep™ mouse CD8α magnetic isolation kits were used to isolate purified CD8α cells or CD4 positive selection magnetic isolation kits for CD4 purification, as per manufacturer's protocol (STEMCELL). Protocol resulted in approximately 90% purity following flow cytometric verification. Cells were reconstituted in RPMI-1640 media supplemented with 20% heat-inactivated FCS (Gibco), 1% penicillin-streptomycin, 1% non-essential amino acids (Invitrogen), 20mM HEPES, and 200 U/mL of recombinant murine interleukin-2 (Peprotech) and maintained at 37°C with 5% CO2. Flow cytometry was performed to verify purity of cells after 7 days (>90% viability). Cells were treated with 10ng/mL of anti-CD3

To quantify lymphocyte division cells were labeled with carboxyfluorescein succinimidyl ester (CFSE, CellTrace, Thermofisher). Cell suspension was resuspended in 1mL of culture medium in a 15mL conical tube. Tube was laid horizontally and 110μL of PBS was pipetted onto the dry portion of the tube close to the cap, creating a liquid bubble separate from the cell suspension. 1.1μL of 5mM CFSE was resuspended into the 110μL PBS bubble. Tube was capped, inverted, then immediately vortexed to ensure uniform mixing of CFSE and cell suspension. Cells were incubated for 10 minutes at room temperature in the dark to prevent photobleaching. Cells were washed twice with PBS containing 20% FCS, then pelleted by centrifugation (300 RCF for 5 minutes).

For CD4 T cell polarization, cells were diluted to a concentration of $1*10^6$ cells/mL. Th0 CD4 cells were further treated with recombinant cytokines and neutralizing antibodies. For Th1 polarization, recombinant IL-12 (10ng/mL) and neutralizing anti-IL-4 (5000ng/mL) antibody was added. For Th2 polarization, recombinant IL-4 (10ng/mL) and neutralizing anti-IFN-gamma (1000ng/mL) antibody was added. For inducible Treg polarization, recombinant

TGF-beta (10ng/mL), neutralizing anti-IFN-gamma (1000ng/mL) antibody, neutralizing anti-IL-4 (1000ng/mL) antibody, and additional IL-2 (30U/mL) were added.

2.12 Flow Cytometry.

Tumours were harvested, weighed, and underwent mechanical and enzymatic dissociation. Tumours were minced and resuspended in 2% FCS-PBS containing 25μg/mL Liberase (Roche) and dissociated for 45 minutes at 37°C using a GentleMACs Dissociator (Miltenyi). Tumours were processed through a 70μM cell strainer (ThermoFisher) to generate single cell suspensions. Adherent cell lines and ex vivo cultured cells were harvested using enzyme-free cell dissociation PBS buffer (ThermoFisher). In some cases, ex vivo cultured cells were stimulated using 5ng/mL PMA and 500ng/mL ionomycin (Sigma Aldrich) for 4 hours at 37°C. Single cell suspensions were reconstituted in PBS containing fixable viability dye: Zombie Violet™ BV421 (1:400) or Zombie Green™ (1:400) in 100 μL for 7 minutes at 4°C in the dark (Biolegend). Cells were centrifuged at 300 RCF for 5 minutes at 4°C and reconstituted in PBS containing 1% BSA with 1μg/100μL Fc block (Biolegend) and incubated for 10 minutes at room temperature. Antibodies marking surface receptors were added onto samples: All antibodies were purchased from Biolegend except for CD8α (FITC, KT15) which was purchased from ThermoFisher and used for tetramer staining. Cells were incubated for 20 minutes at room temperature in the dark. Cells were centrifuged at 300 RCF for 5 minutes at 4°C and reconstituted in FACS buffer (Biolegend) and acquired on a cytometer. Samples requiring transcription factor staining or intracellular cytokine staining were fixed and permeabilized using Fixation/Permeabilization kit (BD) for a minimum of 60 minutes to a maximum of 18 hours at 4°C in the dark. Cells were washed and reconstituted in permeabilization buffer (BD), followed by the addition of antibodies: FoxP3 (PE, FJK-16s, 1:50, ThermoFisher), GFP (AF488, FM264G, 1:100) and incubated for 30 minutes at room temperature in the dark. Cells were centrifuged at 800 RCF for 5 minutes at 4°C and resuspended in FACS buffer (Biolegend) and acquired on a BD Fortessa cytometer (BD). Photomultiplier tube (PMT) voltages were set using single stained samples and compensation beads (UltraComp eBeads, Affymetrix). For negative gates, fluorescence minus one (FMO) samples were used for all panels, with the exception of isotype control antibodies used for intracellular staining. Data was analyzed using FlowJo (Tree Star).

2.13 Statistical Analysis.

Comparison of Kaplan-Meier survival plots was conducted using log-rank analysis and comparisons performed using Mantel-Cox method (Prism 9, GraphPad). Comparison across multiple groups was conducted using one-way analysis of variance (ANOVA) with post-hoc analysis using Tukey's multiple comparison test (Prism 9, GraphPad). Comparison of two treatment groups was conducted using an unpaired t test with Welch's correction (Prism, GraphPad).

RESULTS

3.1 SM eradicates immunotherapy-resistant murine bladder cancer

3.1.1 Smac Mimetic and TNF-alpha co-treatment diminish MB49 viability in vitro

To evaluate the potential of SM to eliminate bladder cancer cells directly, I performed in vitro assays quantifying metabolic activity as a measure of cell health. I co-treated a panel of mouse (MB49 & MBT2) and human (T24 & TCCSUP) urothelial carcinoma cell lines with SM alongside additional relevant recombinant cytokines or BCG in search of sensitivity (Figure 6). Cells were co-treated with TNF-alpha, universal type-1 interferon, or BCG at different doses. SM consistently decreased average absorption of metabolites within each cell line. Within MB49 samples, the addition of TNF-alpha or IFN-beta alone did not alter metabolic activity. Infection with high dose BCG (1e7 cfu/mL) significantly decreased viability, however upon comparison with lower doses of BCG (1e6 and 1e5) viability increased significantly. This disparity demonstrates the dose of BCG being a significant factor determining whether cells would increase or decrease viability. Within the SM treated samples, the addition of TNF-alpha and high-dose BCG both diminished viabilities. Within MBT2 cells TNF-alpha diminished viability, while intermediate- and low-dose BCG increased viability. These results remain consistent with the addition of SM. For the human cell line TCCSUP, apart from intermediate-dose BCG slightly elevating viability, no treatment with or without SM was capable of significantly diminishing overall viability. The human T24 cell line was sensitive to the addition of TNF-alpha and BCG. The addition of TNF alpha diminished viability, however the addition of BCG uniformly increased overall viability. SM in combination with stimulants failed to significantly alter viability, apart from intermediate-dose BCG elevating viability. Collectively, these results suggest the addition of TNF-alpha

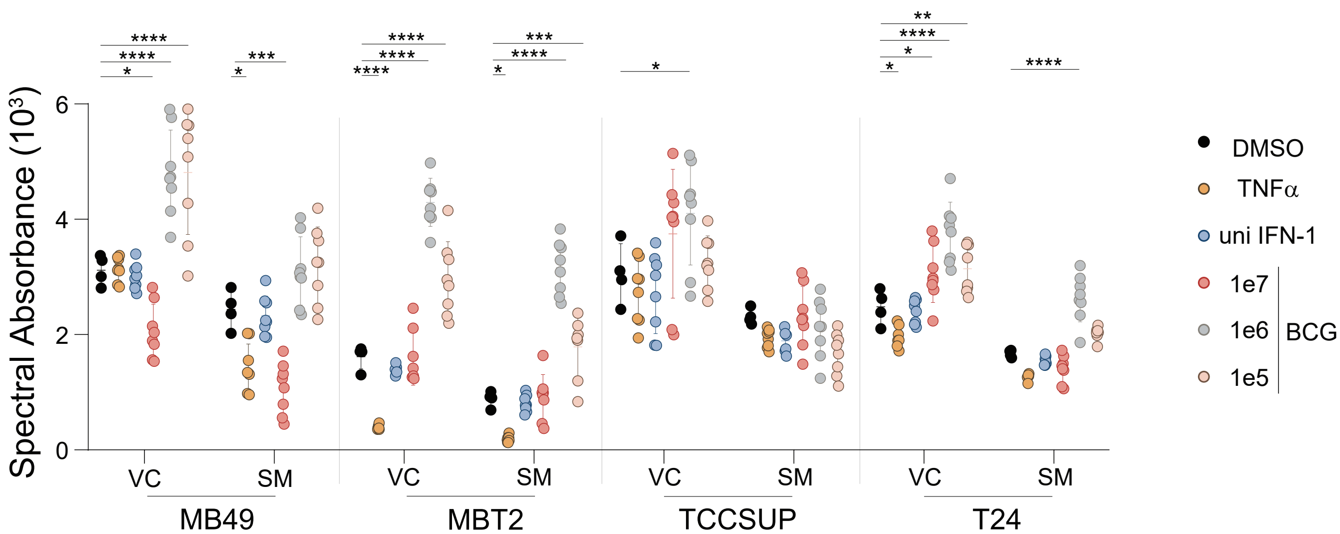

Spectral Absorbance (10^3)
6
4
2
0
VC
SM
MB49
MBT2
TCCSUP
T24
DMSO
TNFα
uni IFN-1
1e7
1e6
1e5
BCG

Figure 6. Viability of urothelial carcinoma cell lines co-treated with cytokines/BCG and SM.

10,000 murine (MB49 & MBT2) or human (TCCSUP & T24) cells were seeded in a 96-well flat-bottom TC-treated plate. After 24 hours cells were co-treated with VC (DMSO) or SM (5μM, LCL161) and recombinant murine or human TNF-alpha (10ng/mL), universal type-1 interferon (10ng/mL), or BCG (1e7, 1e6, or 1e5 cfu/mL). Colorimetric MTT assay was performed following an additional 48 hours. Statistical analysis was performed using ordinary one-way ANOVA with Tukey's multiple comparisons test with reference to the DMSO control treated group. **** $p < 0.0001$, *** $p < 0.001$, ** $p < 0.01$, * $p < 0.05$.

in combination with SM may enable metabolic quiescence in murine urothelial cell carcinoma cell lines. The addition of BCG, however, yields dose-dependent effects in both murine and human cell lines, with discrete doses generating polarizing effects on metabolic activity.

I performed an equivalent assay 24 hours after MB49 cells were co-treated with SM and recombinant TNF, TNF-related apoptosis inducing ligand (TRAIL), interferon (IFN)-beta, or discrete toll-like receptor (TLR) agonists poly-IC and Imiquimod (Figure 7A). Within vehicle control samples, TNF-alpha alone slightly increased average viability, a finding not seen with the previous assay. TNF-alpha stimulating growth suggests the endogenous pathway remains intact. Another finding distinct from the previous assay was the decrease in viability with IFN-beta treatment, albeit not to a significant degree. The addition of TRAIL or discrete TLR-7 and TLR-3 agonists did not affect viability. Upon combining with SM, the combination with TNF significantly diminished metabolic activity. Exclusive treatment with either inhibitor or TNF of MB49 cells in vitro augmented viability, suggesting intrinsic components of the ensuing molecular pathway regulating growth remain intact. I confirmed by flow cytometry SM did not change the expression of TNFR1, as overall expression remained uniform across the collective population (Figure 7B). I reaffirmed divergent sensitivity of TNF, as TNF treatment elevated metabolic activity, whereas co-treatment with SM diminished metabolic activity in a dose-dependent manner (Figure 7C). To further substantiate the cell-intrinsic toxicity of SM treatment, I pre-treated cells with a pan-caspase inhibitor (zVAD-fmk) or RIPK-inhibitor (Necrostatin-1) and co-treated cells with SM and TNF-alpha. Caspase inhibition and RIPK inhibition rescued viability (Figure 7D), implicating both apoptosis and necroptosis as active pathways enabling cell death upon SM and TNF-alpha co-treatment. Flow cytometry of SM and TNF co-treatment reported diminished acquisition of events

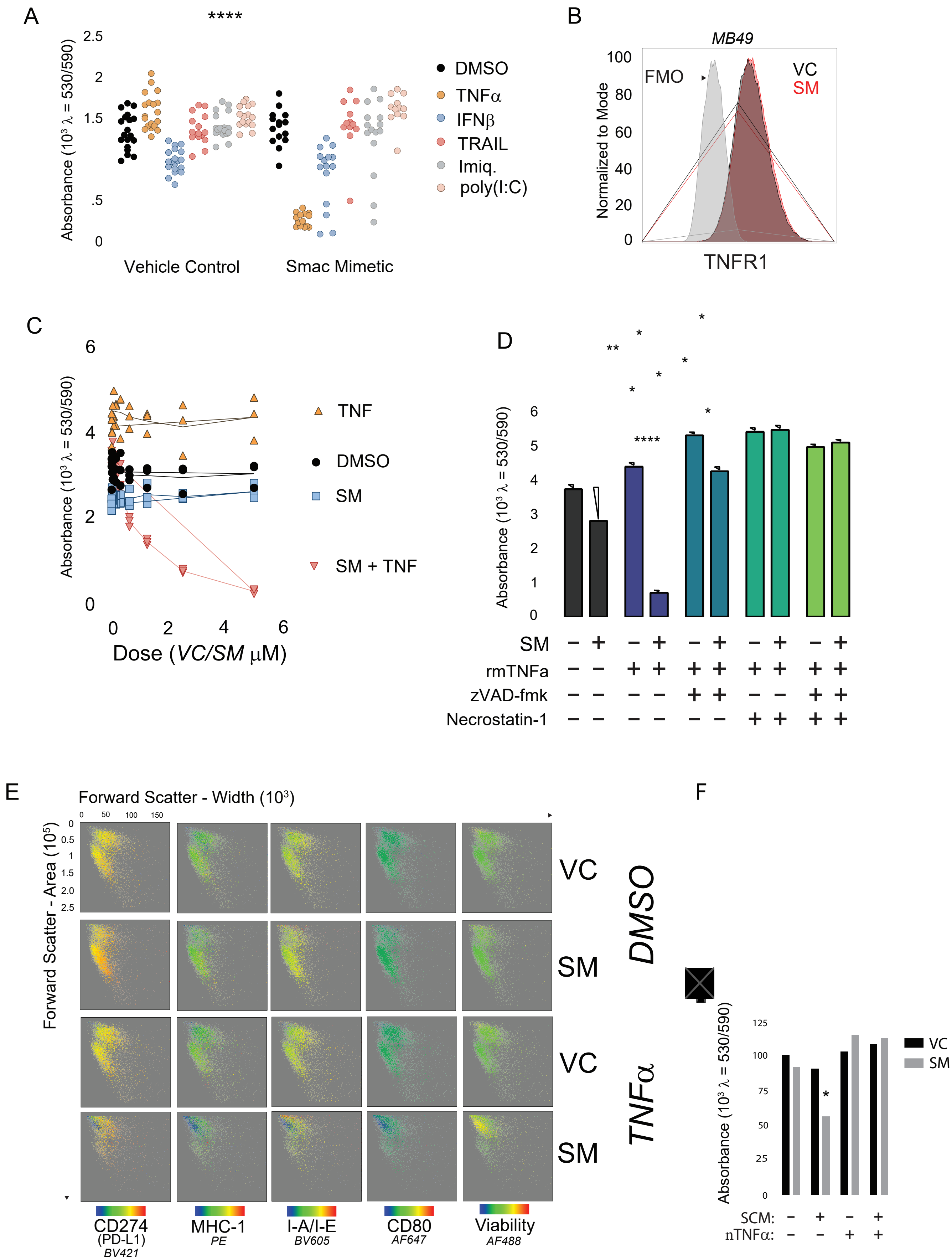

A
****
Absorbance (10³ λ = 530/590)
DMSO
TNFα
IFNβ
TRAIL
Imiq.
poly(I:C)
Vehicle Control
Smac Mimetic
B
MB49
FMO
VC
SM
Normalized to Mode
TNFR1
C
Absorbance (10³ λ = 530/590)
TNF
DMSO
SM
SM + TNF
Dose (VC/SM μM)
D
****
Absorbance (10³ λ = 530/590)
SM
rmTNFa
zVAD-fmk
Necrostatin-1
E
Forward Scatter - Width (10³)
Forward Scatter - Area (10⁵)
VC
SM
VC
SM
DMSO
TNFα
CD274
(PD-L1)
BV421
MHC-1
PE
I-A/I-E
BV605
CD80
AF647
Viability
AF488
F
Absorbance (10³ λ = 530/590)
VC
SM
SCM:
nTNFα:

Figure 7. MB49 is sensitive to SM and TNF-alpha combination in vitro

10,000 MB49 cells were seeded in a flat-bottom TC-treated plate overnight. A) Cells were co-treated with VC (DMSO) or SM (5μM, LCL161) and recombinant murine TNF-alpha (10ng/mL), recombinant murine IFN-beta (1000U/mL), recombinant murine TRAIL (100ng/mL), Imiquimod (10ng/mL), or poly I:C (10ng/mL). Resazurin salt absorption was quantified following 24 hours. Statistical analysis was performed using ordinary one-way ANOVA with Tukey's multiple comparisons test. **** $p < 0.0001$. B) Histogram overlay of in vitro VC (DMSO) or SM (5μM, LCL161) treated MB49 cells stained with PE-TNFR1 fluorescent antibody. Fluorescence minus one (FMO) refers to unstained mixture of both treatments. C) Cells were co-treated with VC (DMSO) or dose-escalating SM (LCL161) and recombinant murine TNF-alpha (10ng/mL) in triplicate. Resazurin salt absorption was quantified following 24 hours. D) Cells were pre-treated with zVAD-fmk (25μM) and/or Necrostatin-1 (25μM) for 2 hours then co-treated with recombinant murine TNF-alpha (10ng/mL) and/or SM (5μM, LCL161). Resazurin salt absorption was quantified following 24 hours. Two-way ANOVA (mixed-effects analysis) with Tukey's multiple comparisons test and Geisser-Greenhouse correction. Error bars, mean +/- s.e.m. * $p < 0.05$. **, $p < 0.01$. E) Flow cytometric analysis plotting forward scatter area (y-axis) vs forward scatter width (x-axis). Colorimetric gradients represent individual fluorophores as listed. F) Cells were treated with VC (DMSO) or SM (5μM LCL161) either in fresh RPMI-1640 medium or supernatant from splenocyte culture (SCM = splenocyte-cultured medium). Cells were further treated with control IgG or neutralizing TNF-alpha antibody (1ug/mL, XT3.11). Two-way ANOVA with Tukey's multiple comparisons test evaluating significance relative to VC control. * $p < 0.05$.

representative of larger ellipsoids, inferred using forward scatter light projections (Figure 7E). The co-treatment yielded fluctuating expression of PD-L1, MHC-1, MHC-2 (I-A/I-E) and CD80 compared to uniform expression from VC+DMSO, SM+DMSO, and VC+TNF-alpha treated samples. I noticed a marginal increase in PD-L1 expression amongst larger events, identified by greater forward scatter area, with SM treatment.

To evaluate whether TNF-alpha was the primary immunological constituent enabling sensitivity upon SM treatment, I cultured splenocytes from a naïve mouse and transferred supernatant onto MB49 cells. Samples were then treated with VC (DMSO) or SM, then supplemented with a neutralizing antibody specific for TNF-alpha. The splenocyte-conditioned medium alone did not affect viability, nor did TNF-alpha neutralization alone. The addition of SM diminished viability to approximately 50%, which was completely abated upon TNF-alpha neutralization. This verifies TNF-alpha as the predominant host-derived constituent sensitizing MB49 to SM treatment. (Figure 7F)

Despite the robust cytotoxicity of SM and TNF-alpha in combination, the transient activity of chemical compounds will likely allow cancer cells to eventually proliferate in vitro. Furthermore, the co-dependence of SM and TNF-alpha to enable metabolic quiescence suggests a marginal delay in either treatment would allow cancer cells to survive. Time-lapse imaging of cells treated with dose-escalating SM with constant TNF-alpha was performed. Protracted over 120 hours, most treatment groups presented a similar pattern of growth quantified as percent confluency (Figure 8A). Distinctly, SM+TNF-alpha treatments were less confluent as the dose of SM increased, with the highest dose preventing growth completely. Maximum-dose SM and TNF-alpha reduced average eccentricity of cells, indicating surviving cells were more circular and thus depict apoptotic morphology (Figure 8B). Notably, despite the near-complete elimination of cells, at 48-72 hours previously diminished cells begin to expand rapidly. The transience of growth inhibition is reflective of the short-term activity limiting the efficacy of chemical intervention.

In vitro dose-escalating infection of MB49 cells with BCG, with or without SM co-treatment, did not visibly alter cell size, membrane permeability, or expression of major histocompatibility complex (MHC)-I or -II, PD-L1, or CD80 (Fig. 9A). In addition, dose-escalating BCG, a non-specific agonist of multiple TLRs, did not significantly affect aggregate metabolic activity (Fig. 9B). This finding remained consistent despite the inclusion of additional stimuli, suggesting the cells are predominantly insensitive to BCG infection.

Viral vectors present a promising intervention strategy to circumvent oncogenic circuitry. Specifically, intrinsic defects in the cellular IFN response enables viral replication [Stojdl et al., 2000]. I proceeded to perform time-lapse analysis with parallel assays quantifying metabolic activity and cytotoxicity of cells infected with a panel of viruses. Cells were successfully infected with high titre adenovirus (Ad), or vesicular stomatitis Indiana virus (VSV) delta-51 constructs encoding GFP (Figure 10A). Infection was inferred by quantifying cumulative green fluorescence. Adenovirus replication occurred after a delay of ~72 hours, whereas VSV successfully replicated within the first 24 hours. Distinctly, wildtype VSV infection successfully diminished confluency, whereas adenovirus infection failed to restrain proliferation (Figure 10B). Despite not significantly altering confluency relative to PBS

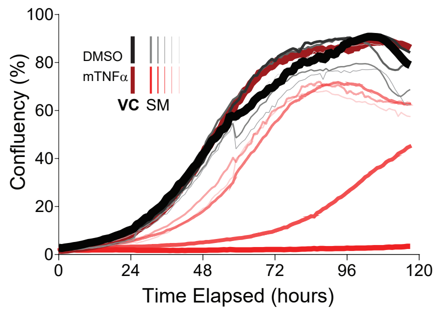

DMSO
mTNFα
VC SM
Confluency (%)
Time Elapsed (hours)

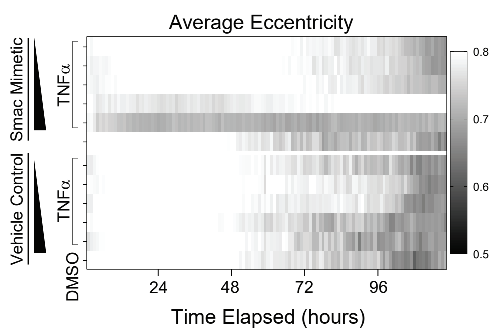

Average Eccentricity
Smac Mimetic
TNFα
Vehicle Control
TNFα
DMSO
Time Elapsed (hours)

Figure 8. Time-lapse analysis of MB49 treated with SM and TNF-alpha in vitro

10,000 MB49 cells were plated in a flat-bottom TC-treated plate. Cells were immediately treated with DMSO or constant recombinant murine TNF-alpha (10ng/mL), and 2-fold dose-diminishing vehicle control (VC, DMSO) or Smac mimetic (SM, LCL161) beginning at 10μM. Samples were incubated and imaged in quadruplicate at fixed intervals. A) Confluency over time. Black line denotes DMSO control. Gray lines of diminishing thickness denote dose-diminishing SM. Maroon line denotes murine TNF-alpha alone. Red lines of diminishing thickness denote dose-diminishing SM, co-treated with constant TNF-alpha. B) Average eccentricity of polygons over time.

A

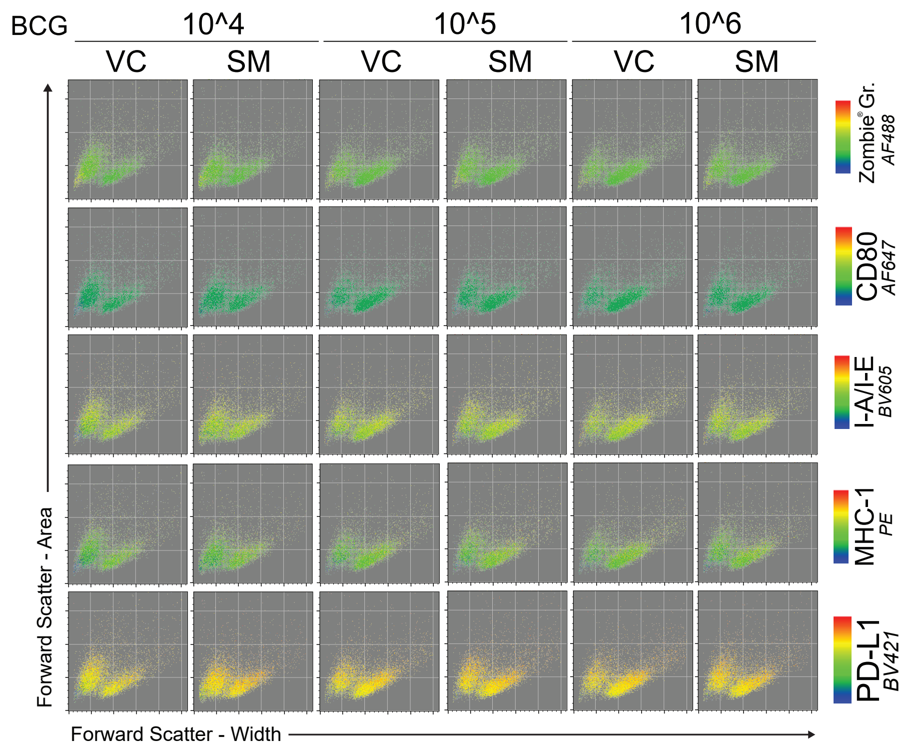
BCG
10^4
10^5
10^6
VC
SM
VC
SM
VC
SM
Zombie® Gr. AF488
CD80 AF647
I-A/I-E BV605
MHC-1 PE
PD-L1 BV421
Forward Scatter - Area
Forward Scatter - Width

B

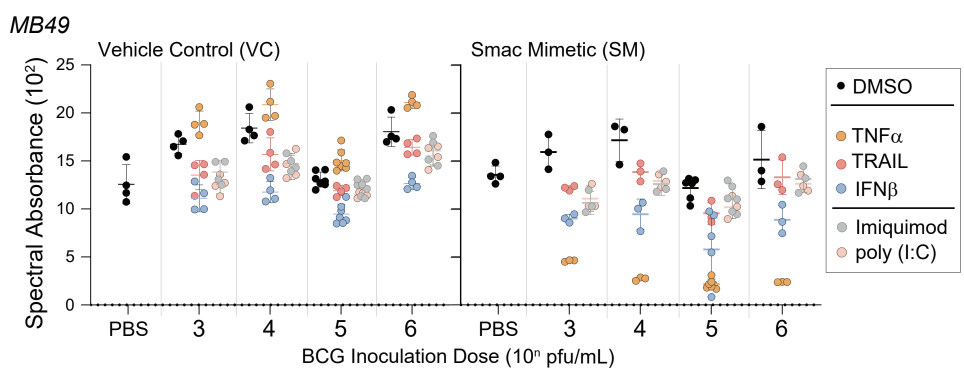
MB49
Vehicle Control (VC)
Smac Mimetic (SM)
Spectral Absorbance (10²)
BCG Inoculation Dose (10ⁿ pfu/mL)
PBS
3
4
5
6
DMSO
TNFα
TRAIL
IFNβ
Imiquimod
poly (I:C)

Figure 9. MB49 is resistant to BCG in vitro

A) MB49 cells were infected with 10^4, 10^5, or 10^6 cfu/mL of BCG then co-treated with VC (DMSO) or SM (5µM, LCL161). Cells were stained with Zombie Green (AF488) membrane permeability dye, and fluorescent antibodies specific for CD80 (AF647), I-A/I-E (BV605), MHC-1 (PE), and PD-L1 (BV421). Samples are plotted forward scatter area vs. forward scatter width, with colorimetric gradients outlining fluorescence. B) Cells were co-treated with VC (DMSO) or SM (5µM, LCL161) and recombinant murine TNF-alpha (10ng/mL), recombinant murine IFN-beta (1000U/mL), recombinant murine TRAIL (100ng/mL), Imiquimod (10ng/mL), or poly I:C (10ng/mL). Cells were further infected with 10^3, 10^4, 10^5, or 10^6 cfu/mL of BCG. Resazurin salt absorption was quantified following 24 hours. Statistical analysis was performed using ordinary one-way ANOVA with Tukey's multiple comparisons test.

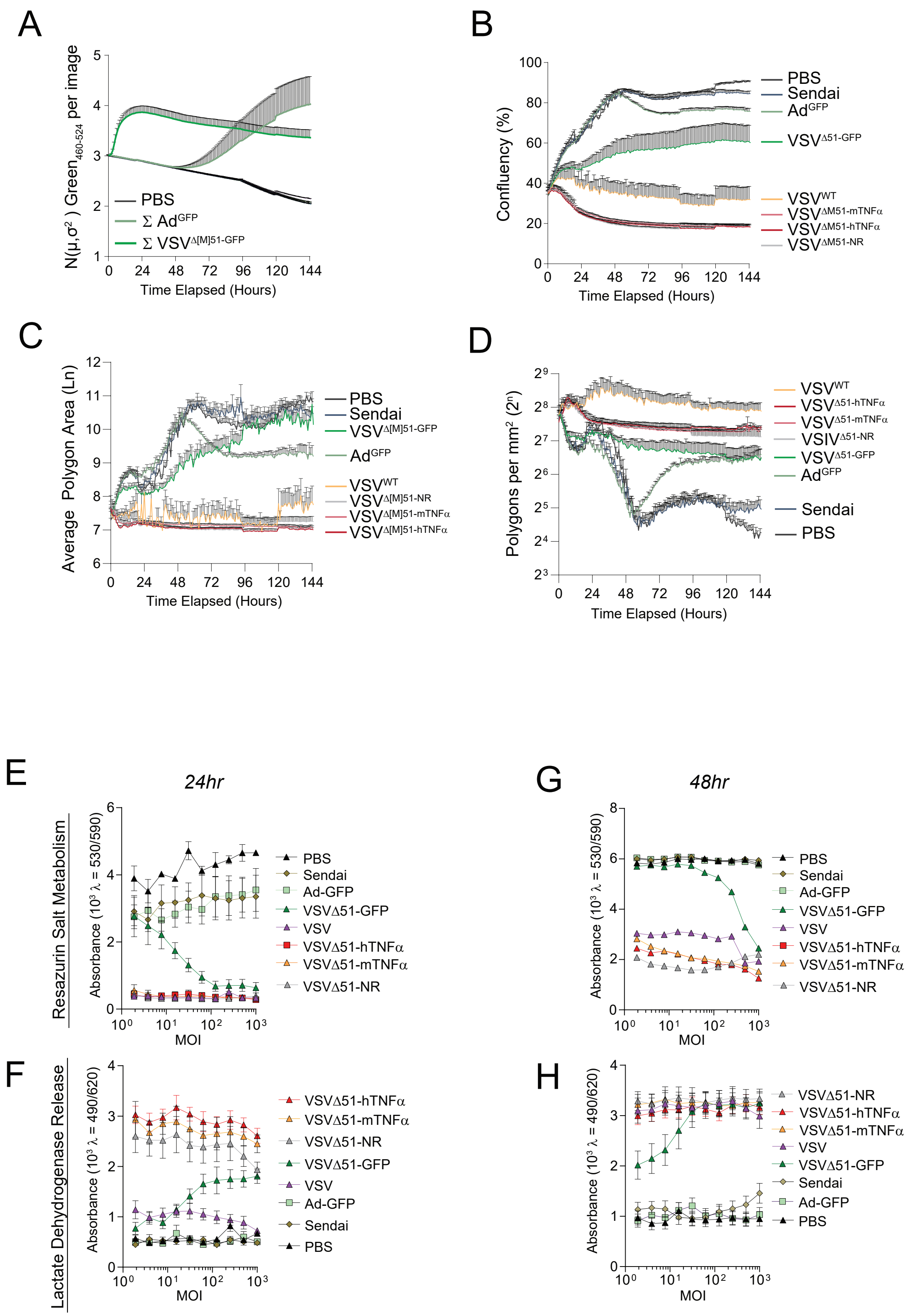

A
N(μ,σ²) Green460-524 per image
Time Elapsed (Hours)
PBS
Σ AdGFP
Σ VSVΔ[M]51-GFP
B
Confluency (%)
Time Elapsed (Hours)
PBS
Sendai
AdGFP
VSVΔ51-GFP
VSVWT
VSVΔM51-mTNFα
VSVΔM51-hTNFα
VSVΔM51-NR
C
Average Polygon Area (Ln)
Time Elapsed (Hours)
PBS
Sendai
VSVΔ[M]51-GFP
AdGFP
VSVWT
VSVΔ[M]51-NR
VSVΔ[M]51-mTNFα
VSVΔ[M]51-hTNFα
D
Polygons per mm² (2ⁿ)
Time Elapsed (Hours)
VSVWT
VSVΔ51-hTNFα
VSVΔ51-mTNFα
VSIVΔ51-NR
VSVΔ51-GFP
AdGFP
Sendai
PBS
E
24hr
Resazurin Salt Metabolism
Absorbance (10³ λ = 530/590)
MOI
PBS
Sendai
Ad-GFP
VSVΔ51-GFP
VSV
VSVΔ51-hTNFα
VSVΔ51-mTNFα
VSVΔ51-NR
G
48hr
Absorbance (10³ λ = 530/590)
MOI
PBS
Sendai
Ad-GFP
VSVΔ51-GFP
VSV
VSVΔ51-hTNFα
VSVΔ51-mTNFα
VSVΔ51-NR
F
Lactate Dehydrogenase Release
Absorbance (10³ λ = 490/620)
MOI
VSVΔ51-hTNFα
VSVΔ51-mTNFα
VSVΔ51-NR
VSVΔ51-GFP
VSV
Ad-GFP
Sendai
PBS
H
Absorbance (10³ λ = 490/620)
MOI
VSVΔ51-NR
VSVΔ51-hTNFα
VSVΔ51-mTNFα
VSV
VSVΔ51-GFP
Sendai
Ad-GFP
PBS

Figure 10. MB49 is sensitive to oncolytic VSV in vitro

10,000 MB49 cells were plated in a flat-bottom TC-treated plate overnight. Cells were treated with PBS or infected with increasing multiplicity of infection (MOI) of Adenovirus-GFP (Ad-GFP), wildtype Vesicular stomatitis Indiana Virus (VSV), VSV-delta51 mutated strains encoding either GFP ($VSV^{d[m51]\text{-}GFP}$), murine TNF-alpha ($VSV^{d[m51]\text{-}mTNFa}$), human TNF-alpha ($VSV^{d[m51]\text{-}hTNFa}$), or a non-replicating variant ($VSV^{d[m51]\text{-}NR}$), or Sendai virus. Data is represented as: A) Average of all green spots detected from PBS, B) confluency, C) polygon area. D) polygons per mm^2. Error bars indicate standard deviation. Resazurin salt absorption was quantified following E) 24- and G) 48-hours. Supernatant was assayed for lactate dehydrogenase release following F) 24- and H) 48-hours.

between 24 and 48 hours, the average area of Ad-GFP infected polygons increased (Figure 10C), with a corresponding decrease in the sum of polygons per unit area (Figure 10D). Together, this suggests cells began clustering. This trend reversed between 48 and 72 hours, as the average area of polygons decreased and the sum of polygons increased, corresponding with the gradual increase in green fluorescence. This demonstrates productive viral replication coincides with disaggregation of cell clusters. Upon infection with oncolytic rhabdovirus VSV variant – delta-51 – engineered to encode mouse or human TNF transgenes [Beug et al., 2018], I recorded a pronounced decline in bulk growth compared to the milder effects of wildtype VSV. I verified these findings by evaluating metabolic activity in tandem with cytotoxicity 24- and 48-hours post-infection (Figure 10E-H). PBS, Sendai virus (murine parainfluenza virus type-1, or murine respirovirus), and Ad-GFP did not significantly diminish metabolic activity or promote cytotoxicity after 24 or 48 hours. High titre VSVd51-GFP infection diminished metabolic activity, correlating with an increase in cytotoxicity. Notably, although wildtype VSV uniformly diminished metabolic activity, this did not correspond to an increase in cytotoxicity, at either 24- or 48-hour timepoints. This corroborates the oncolytic potency of the engineered delta-51 strain of VSV relative to the wildtype virus. Furthermore, the wildtype or VSVd51-GFP-encoding strains did not diminish overall confluency to levels achieved by VSVd51 encoding murine or human TNF. The addition of the TNF transgene profoundly diminished confluency immediately following infection, with sustained effects throughout the duration of the analysis. After 24 and 48 hours, metabolic activity remained significantly lower, and cytotoxicity remained elevated.

3.1.2 MB49 is resistant to UCC-approved immunotherapies

To consistently graft multifocal yet non-invasive malignancy, I opted for chemical perfusion of the urothelium in lieu of precision radiation. Despite robust focal amplification of cancer cells in vitro, the distention of the urinary parenchyma warrants verifying localized graft establishment prior to administering experimental treatments. I adopted a bioluminescent reporter system, wherein MB49 cells stably transfected with a lentivirus encoding bioluminescent firefly luciferase ($MB49^{luc}$ sub-lineage) ensured transient graft(luciferin-catabolic)-host discrimination. In vivo engraftment was piloted (Figure 11) and a seven-day incubation interval prior to treatment intervention was selected to ensure robust establishment antecedent to kidney metastasis. This interval ensured consistency across mice and treatment of a localized, non-invasive, or non-metastatic cancer. Although tumour development enlarged the bladder beyond natural distention, benign tumours retained an opaque white hue, suggesting they did not comprise necrotic death – principally characterized by the darkening of neoplastic tissue (data not shown).

I verified the suitability of the orthotopic MB49 model for evaluating novel treatment strategies against bladder cancer by demonstrating resistance toward the present conventional therapeutic practice. To evaluate treatment efficacy, I compared focal bioluminescence (before/after) the treatment interval and recorded survival longevity. Live-culture extract or reconstituted lyophilized clinical-grade BCG vaccines were instilled for 45 minutes within tumour-bearing bladders of sedated mice, representative of the standard clinical regimen [Kamat et al., 2015]. Given mice would tend to urinate any residual BCG following the procedure, the use of both forms of BCG was merited. Live-culture BCG isolated at log-phase of growth enacts active infection, whereas lyophilized BCG requires a set amount of time to

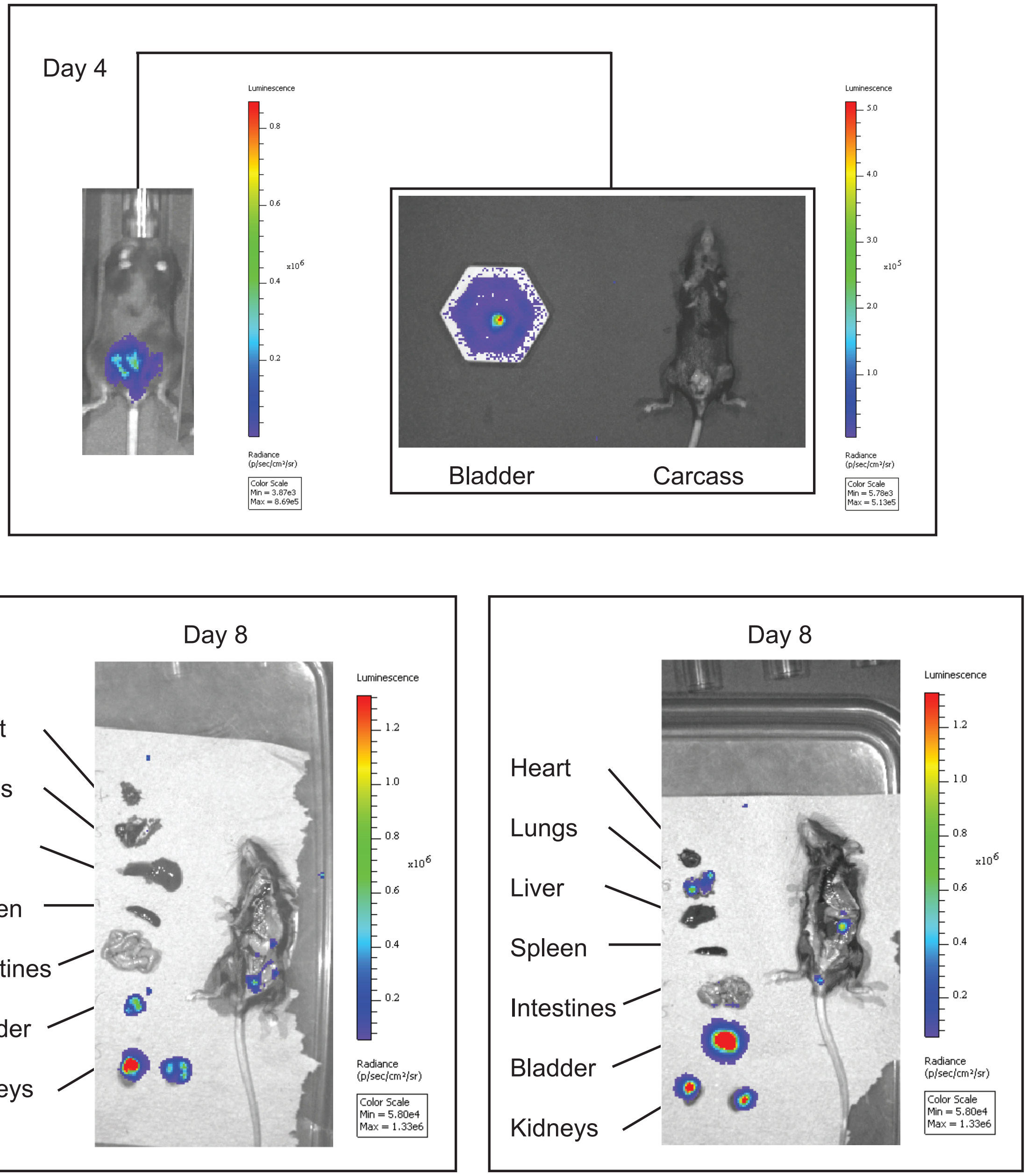
Day 4
Luminescence
0.8
0.6
x10^6
0.4
0.2
Radiance
(p/sec/cm²/sr)
Color Scale
Min = 3.87e3
Max = 8.69e5
Bladder
Carcass
Luminescence
5.0
4.0
3.0
x10^5
2.0
1.0
Radiance
(p/sec/cm²/sr)
Color Scale
Min = 5.78e3
Max = 5.13e5
Day 8
Heart
Lungs
Liver
Spleen
Intestines
Bladder
Kidneys
Luminescence
1.2
1.0
0.8
x10^6
0.6
0.4
0.2
Radiance
(p/sec/cm²/sr)
Color Scale
Min = 5.80e4
Max = 1.33e6
Day 8
Heart
Lungs
Liver
Spleen
Intestines
Bladder
Kidneys
Luminescence
1.2
1.0
0.8
x10^6
0.6
0.4
0.2
Radiance
(p/sec/cm²/sr)
Color Scale
Min = 5.80e4
Max = 1.33e6

Figure 11. Bioluminescent imaging of necropsied MB49-bearing mice.

25,000 MB49-luc cells were intravesically instilled into the mouse bladder of 8-week-old naïve female C57BL/6 mice. After the indicated number of days mice were injected with 200uL of working concentration luciferin intraperitoneally. Subject was then imaged or sacrificed after an 8-minute interval to allow luciferin to metabolize. Within 2 minutes necropsy was performed, wherein organs were excised and arranged as indicated. Carcass and organs were imaged for bioluminescence at the indicated scale for a total exposure time of 1 minute. Luminescence represents the presence of luciferase-tagged MB49 cells. Diagrams are of 2 representative mice. Radiance scale: p/sec/cm^2/sr.

productively regain infectability. This occurs because the viability of lyophilized BCG is reduced from prior exposure to freezing temperatures. I incorporated both forms of BCG as the lyophilized form (OncoTICE) is used clinically, and the live-culture form (Connaught) maximizes the likelihood of productive infection of cancer cells. Furthermore, different sub-strains of BCG have been shown to differentially promote immune cell activation, thereby affecting the overall capacity to elicit anti-tumour immunity [Esteso et al., 2021].

Notably, the intravesical instillation of BCG within tumour-bearing mice was deleterious toward the overall well-being of the animals. The prolonged anesthesia required to sedate the mice proved difficult to recover from, as a sizeable proportion of animals did not survive the procedure or succumbed during the 24-hour post-operative recovery period. The inhalant was preferred in place of the injectable anesthetic, as our initial protocol was altered as the injectable proved lethal in a cohort of 10 mice during pilot studies. To adjust for the adverse reaction to the anesthetic, BCG instillations were limited to a maximum of 2 with 4 days between each procedure, providing adequate time for animals to recover. Furthermore, the catheterization of animals bearing bladder tumours would often exacerbate hematuria, possibly compromising graft integrity. Consistent with prior literature, neither form of adjuvant therapy significantly enhanced survival benefit in the MB49 model [Mangsbo et al., 2010] (Figure 12A, B). These results, coupled with previous data confirming metastases at approximately 8 days following initial implantation, reaffirmed the aggressive nature of the model as the first control-treated animals reached endpoint at or before 20 days. Bioluminescent imaging was performed routinely to track tumour growth in this experiment, however, was strictly used to verify tumour presence prior to initial treatments in subsequent experiments. Minimizing luciferin injections ensured minimal immunogenicity resulting from

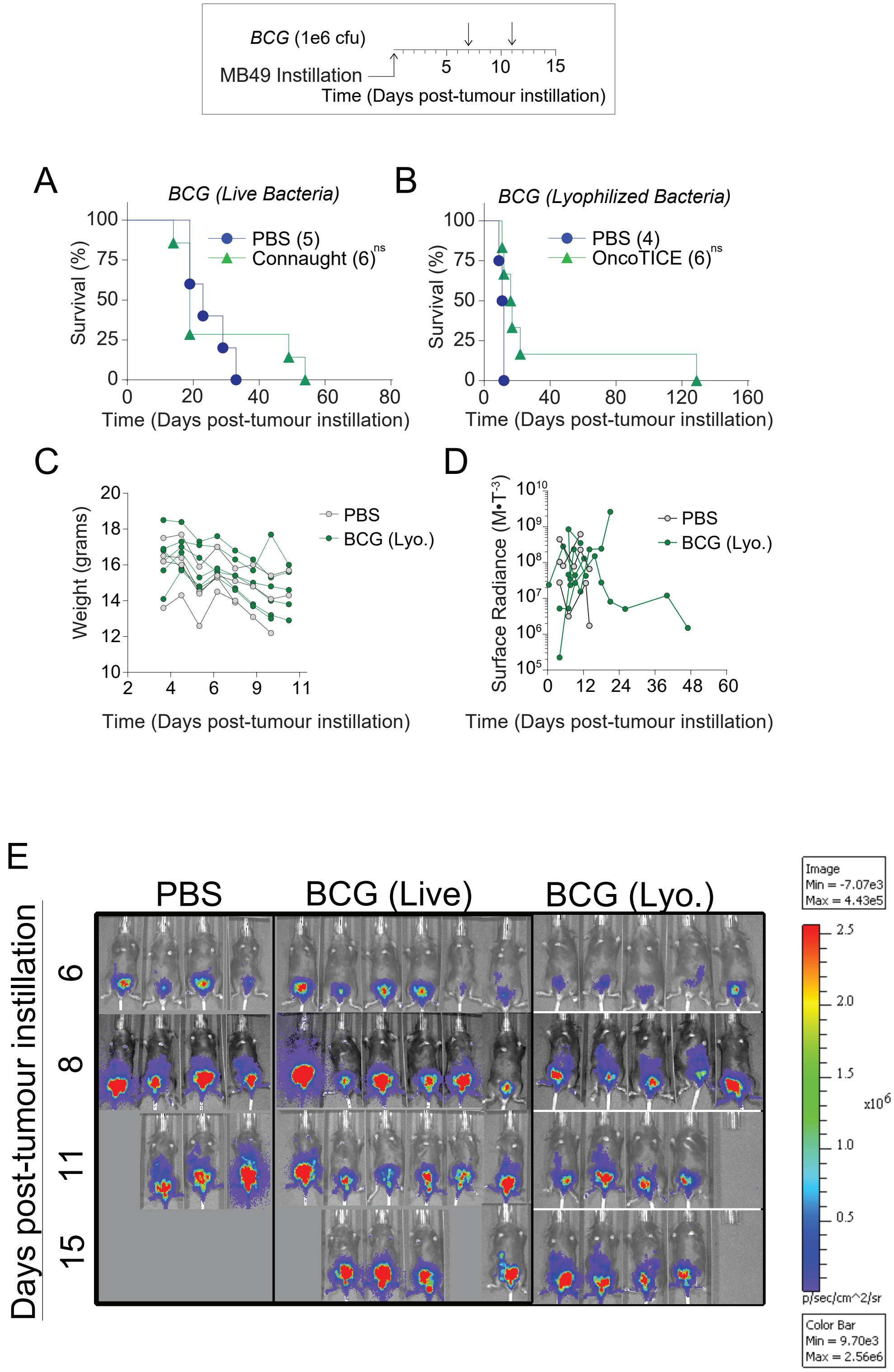
BCG (1e6 cfu)
MB49 Instillation
5 10 15
Time (Days post-tumour instillation)
A
BCG (Live Bacteria)
PBS (5)
Connaught (6)ns
Survival (%)
Time (Days post-tumour instillation)
B
BCG (Lyophilized Bacteria)
PBS (4)
OncoTICE (6)ns
Survival (%)
Time (Days post-tumour instillation)
C
Weight (grams)
PBS
BCG (Lyo.)
Time (Days post-tumour instillation)
D
Surface Radiance (M•T-3)
PBS
BCG (Lyo.)
Time (Days post-tumour instillation)
E
PBS
BCG (Live)
BCG (Lyo.)
Days post-tumour instillation
6
8
11
15
Image
Min = -7.07e3
Max = 4.43e5
x10^6
p/sec/cm^2/sr
Color Bar
Min = 9.70e3
Max = 2.56e6

Figure 12. BCG fails to prolong survival in MB49-bearing mice

25,000 MB49-luc cells were intravesically instilled into the mouse bladder of 8-week-old naïve female C57BL/6 mice. Mice were intravesically instilled with PBS or 1e6 colony-forming units of either log-phase live-cultured BCG (Connaught strain) or lyophilized BCG (OncoTICE) on day 7 and day 11 post-tumour instillation. A, B) Representative Kaplan-Meier survival plots with Mantel-Cox survival curve comparison test. Parentheses indicate number of mice in the treatment group. C) Progressive weight change of mice treated with PBS or live-cultured BCG. D) Select quantification of E) bioluminescent imaging performed on indicated days is shown. Absence of images in specific slots indicate subject reached endpoint prior to imaging. Radiance scale: p/sec/cm^2/sr.

procedures excluding designated treatments, as bioluminescence is generated from cancer cells metabolizing injected luciferin.

Humanized monoclonal antibodies specific for PD-L1 are approved for the treatment of advanced forms of urothelial cell carcinoma, however not for the treatment of non-muscle invasive bladder cancer. Given the aggressive nature of the MB49 model, I surmised treatments at timepoints past day 8 would constitute treatment of advanced muscle-invasive disease. I thus opted to evaluate whether prolonged blockade of the PD-1/PD-L1 axis would increase survival benefit. Intraperitoneal injections (6 doses total; 2-week regimen) of antibodies with clonal specificity toward inhibitory immune checkpoint moieties PD-1 (RMP1-14) or PD-L1 (10.9F) were performed and overall survival was used to evaluate efficacy. Notably, our lab has previously utilized the J43 antibody clone of PD-1 [Beug, 2017], however I opted to use the RMP1-14 clone. This decision was made based on unpublished data indicating the latter clone interacts with PD-1 on NK cells with greater avidity, thereby eliciting potentially superior anti-tumour activity (Ardolino, personal communication). Neither strategy could generate significant survival benefit as discrete mono-therapies (Figure 13A, B).

CTLA-4, the first monoclonal antibody mediating immune checkpoint blockade approved for clinical use, elicits maximal therapeutic effect via Fc receptor-dependent depletion of regulatory T cells [Simpson et al., 2013]. There are 3 commercially available murine clones of CTLA-4, each with different reactivity to CTLA-4. I found treatment with regulatory T cell-depleting clones of CTLA-4, 9H10 and 9D9 but not 4F10, eradicated MB49 tumours in part of the subject cohort (Figure 14). I opted to utilize the 9H10 clone for the remainder of

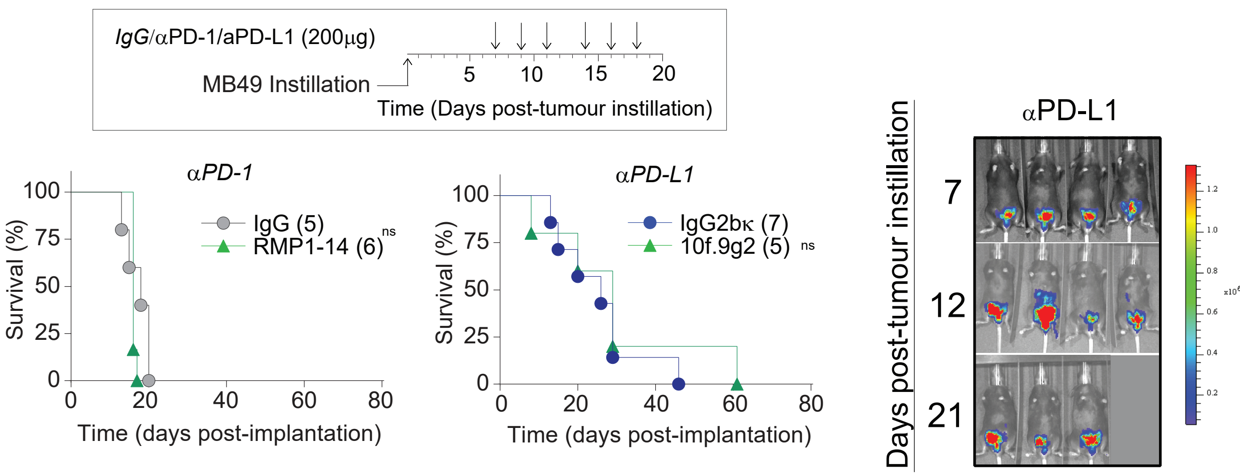
IgG/αPD-1/aPD-L1 (200µg)
MB49 Instillation
5
10
15
20
Time (Days post-tumour instillation)
αPD-1
Survival (%)
IgG (5)
RMP1-14 (6)
ns
Time (days post-implantation)
αPD-L1
IgG2bκ (7)
10f.9g2 (5)
ns
Days post-tumour instillation
7
12
21

Figure 13. PD-1/PD-L1 axis blockade fails to prolong survival benefit in MB49-bearing mice

25,000 MB49-luc cells were intravesically instilled into the mouse bladder of 8-week-old naïve female C57BL/6 mice. Mice were intraperitoneally injected with 200μg of control IgG/IgG2b-kappa or anti-PD-1 (RMP1-14 clone) or anti-PD-L1 (10f.9g2 clone) on days 7, 9, 11, 14, 16, and 18. A, B) Representative Kaplan-Meier survival plots with Mantel-Cox survival curve comparison test. Parentheses indicate number of mice in the treatment group. C) Bioluminescent imaging performed on indicated days is shown. Absence of images in specific slots indicate subject reached endpoint prior to imaging. Radiance scale: p/sec/cm^2/sr.

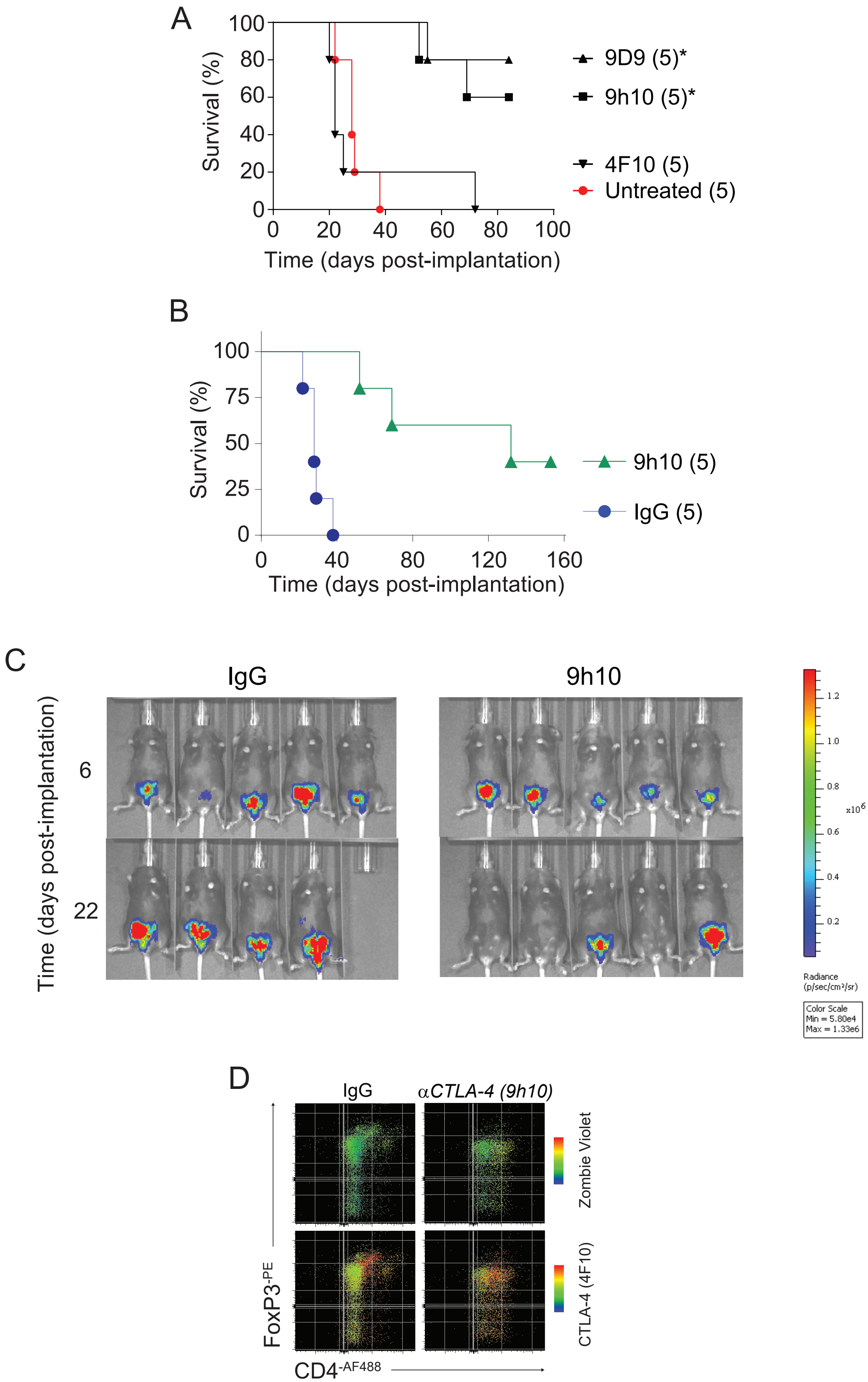

A
Survival (%)
100
80
60
40
20
0
0
20
40
60
80
100
Time (days post-implantation)
9D9 (5)*
9h10 (5)*
4F10 (5)
Untreated (5)
B
Survival (%)
100
75
50
25
0
0
40
80
120
160
Time (days post-implantation)
9h10 (5)
IgG (5)
C
IgG
9h10
Time (days post-implantation)
6
22
1.2
1.0
0.8
0.6
0.4
0.2
x10^6
Radiance (p/sec/cm²/sr)
Color Scale
Min = 5.80e4
Max = 1.33e6
D
IgG
αCTLA-4 (9h10)
Zombie Violet
CTLA-4 (4F10)
FoxP3-PE
CD4-AF488

Figure 14. Treg depleting clones of CTLA-4 enhances MB49 survival benefit

25,000 MB49-luc cells were intravesically instilled into the mouse bladder of 8-week-old naïve female C57BL/6 mice. A) Mice were left untreated or intraperitoneally injected with 200µg of anti-CTLA-4 clones 9H10, 9D9, or 4F10 on days 7, 9, 11, 14, 16, and 18. Representative Kaplan-Meier survival plots with Mantel-Cox survival curve comparison test. Parentheses indicate number of mice in the treatment group. * $p < 0.05$ B) Mice were intraperitoneally injected with control IgG or 200µg of anti-CTLA-4 clones 9H10 on days 7, 9, 11, 14, 16, and 18. Representative Kaplan-Meier survival plots with Mantel-Cox survival curve comparison test. Parentheses indicate number of mice in the treatment group. C) Bioluminescent imaging performed on indicated days is shown. Absence of images in specific slots indicate subject reached endpoint prior to imaging. Radiance scale: p/sec/cm^2/sr. D) Flow cytometric analysis of tumour-infiltrating lymphocytes from an IgG or 9H10-treated subject sacrificed on day 10 following tumour instillation. Plots are depicting FoxP3 (PE) expression among CD3+ (APC-Cy7) CD4+ (AF488) gated events. Colorimetric gradients represent viability (Zombie Violet, BV421) and CTLA-4 (APC) expression. Intersecting grey lines distinguish logarithmic change in probe expression.

my studies given its efficacy and prevalence in published reports, thereby ensuring equivalence with other reports. Furthermore, the 9D9 and 4F10 clones of CTLA-4 are also the predominant clone commercially available as a conjugate with a fluorophore, thereby making it the default clone for use in flow cytometry experiments. It is imperative to use a different clone for detection versus treatment given the treatment antibody may remain tethered to the target antigen, thereby allosterically inhibiting the detection antibody and masking the expression of the antigen. To verify the presence of regulatory T cells and their expression of CTLA-4 I conducted flow cytometry on tumour-infiltrating lymphocytes. Upon comparing CD3+ CD4+ populations from a control IgG-treated subject and a 9H10-treated subject I verified the tumours harboured regulatory T cells and confirmed that 9H10 treatment affected the phenotype of this population. Specifically, 9H10 treatment reduced the proportion of FoxP3- high events, which otherwise expressed a high degree of CTLA-4. 9H10 treatment did not however eliminate the expression of CTLA-4 overall, as the FoxP3-low populations expressed CTLA-4, in contrast with the FoxP3-low populations from the control IgG-treated subject which did not express CTLA-4 to the same degree (Figure 14D).

3.1.3 SM treatment enables immune-mediated cures of orthotopic MB49 tumours

Oral gavage SM treatment (4 doses LCL161 total; 2-week regimen) cured approximately half of the mice tested (Figure 15A). The absence of vestigial bioluminescence alongside a statistically significant increase in survival benefit collectively demonstrate SM monotherapy generated long-term, durable cures (Figure 15B). To assess the propensity for tumour relapse. we inoculated mice previously cured of $MB49^{luc}$ with 20-fold greater quantity of homologous, parental-lineage wildtype MB49 cells subcutaneously. Compared to age-matched naïve mice, the complete absence of ectopic growth in cured mice was attributed to immunological memory recall, as co-inoculation with numerically equivalent histo-compatible heterologous B16F10 melanoma in opposing flanks generated substantial tumours (data not shown). Long-term, relapse-free survival benefit in an immunocompetent model indicates development of host memory of eradicated, tumour-associated antigens. This finding prompted evaluating the necessity of discrete immune compartments to ascertain their overall involvement in regulating tumour growth alongside treatment efficacy.

Simultaneous antibody-mediated systemic ablation of immune cells during therapeutic intervention identified the necessity of major-histocompatibility complexes required to sustain survival benefit. Specifically, the absence of class II-recognition CD4 populations, expressed upon a wider range of immune cells of innate and adaptive lineage, correlated with a complete loss of treatment-induced survival benefit (Figure 16A). Similarly, the absence of class I-recognition CD8β (cluster of differentiation-8 beta, integral surface membrane glycoprotein) complexes, strictly expressed upon T cells, correlated with significant loss of treatment-induced survival benefit (Figure 16B). Negligible dependency toward CD161 (NK1.1 – killer cell lectin-like receptor subfamily B, member 1) populations, expressed nearly

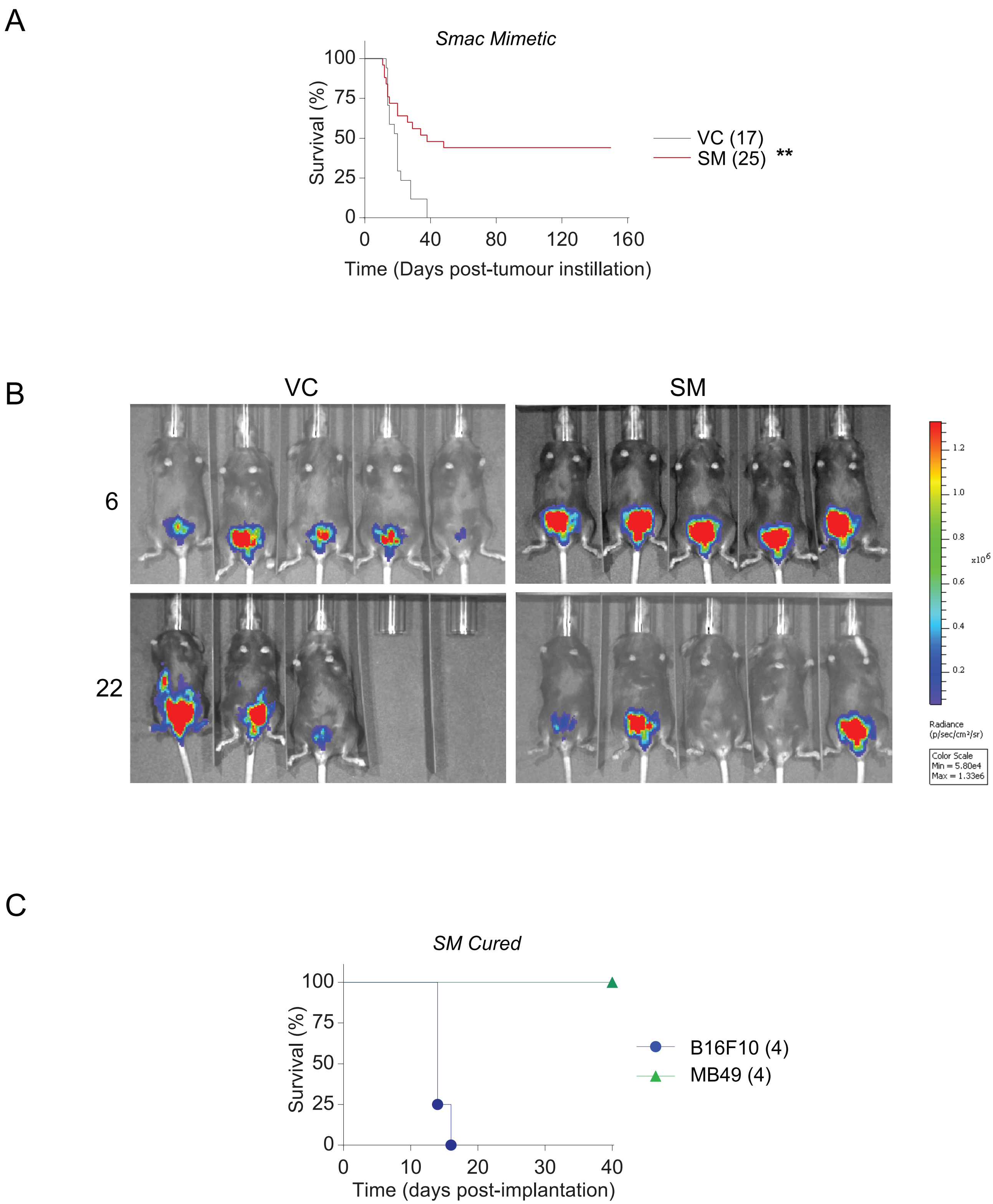
A
Smac Mimetic
Survival (%)
100
75
50
25
0
0
40
80
120
160
Time (Days post-tumour instillation)
VC (17)
SM (25) **
B
VC
SM
6
22
Radiance (p/sec/cm²/sr)
Color Scale
Min = 5.80e4
Max = 1.33e6
C
SM Cured
Survival (%)
Time (days post-implantation)
B16F10 (4)
MB49 (4)

Figure 15. SM increases MB49 survival benefit and generates anti-tumour immune memory

25,000 MB49-luc cells were intravesically instilled into the mouse bladder of 8-week-old naïve female C57BL/6 mice. Mice were treated with vehicle control (VC; acid buffer) or Smac mimetic (SM, LCL161, 75mg/kg) by oral gavage on days 8, 10, 15, and 17. A) Representative Kaplan-Meier survival plots with Mantel-Cox survival curve comparison test. Parentheses indicate number of mice in the treatment group. **, $p < 0.01$. Results are pooled from 3 representative experiments. B) Bioluminescent imaging performed on indicated days is shown. Absence of images in specific slots indicate subject reached endpoint prior to imaging. Radiance scale: p/sec/cm^2/sr. C) 150 days following initial MB49 instillation, cured mice were inoculated subcutaneously with 500,000 B16F10 or wildtype MB49 cells. Representative Kaplan-Meier survival plots with Mantel-Cox survival curve comparison test. Parentheses indicate number of mice in the treatment group.

exclusively on natural killer cells, excluded innate lymphocyte contribution to survival benefit (Figure 16C). The dispensable requirement of the natural killer cell compartment, decisively established in the production of TNF [Nandi et al., 1994], suggests SM treatment may promote anti-tumour immunity beyond established mechanisms perpetuating cancer cell-intrinsic death cascades.

I verified comprehensive depletion of the targeted cell compartments by flow cytometry using a panel comparing CD3-expressing CD4 and CD8 events alongside CD3-null NKp46 events (Figure 17). This experiment also verified the presence of T cells (CD3+NKp46-), NK cells (CD3-NKp46+) as well as NKT cells (CD3+NKp46+). The depletion of either CD4, CD8-beta, or NK1.1-expressing cells had a profound impact on the tumour microenvironment, as non-depleted cells would retain a greater proportion of the immunological niche. Accordingly, the depletion of either CD4- or CD8-beta-expressing cells did not alter the overall number of CD3+ NKp46- events in the spleen, lymph nodes, or tumours, however the depletion of NK1.1-expressing cells increased the overall number of CD3+ NKp46- events. This finding was interesting given the sparsity of CD3-NKp46+ events detected in nearly all samples. The majority of CD3+NKp46- events in the lymph nodes were either CD4+ or CD8-alpha+, without any detection of double-positive events.

Given the inherent requirement of adaptive immune constituents in promoting anti-tumour efficacy, I evaluated CD11c-expressing cells from the tumour microenvironment. I found SM treatment increased the number of CD11c+ events per gram of tumour tissue, with a corresponding increase in the expression of co-stimulatory CD40 and CD86. This was further

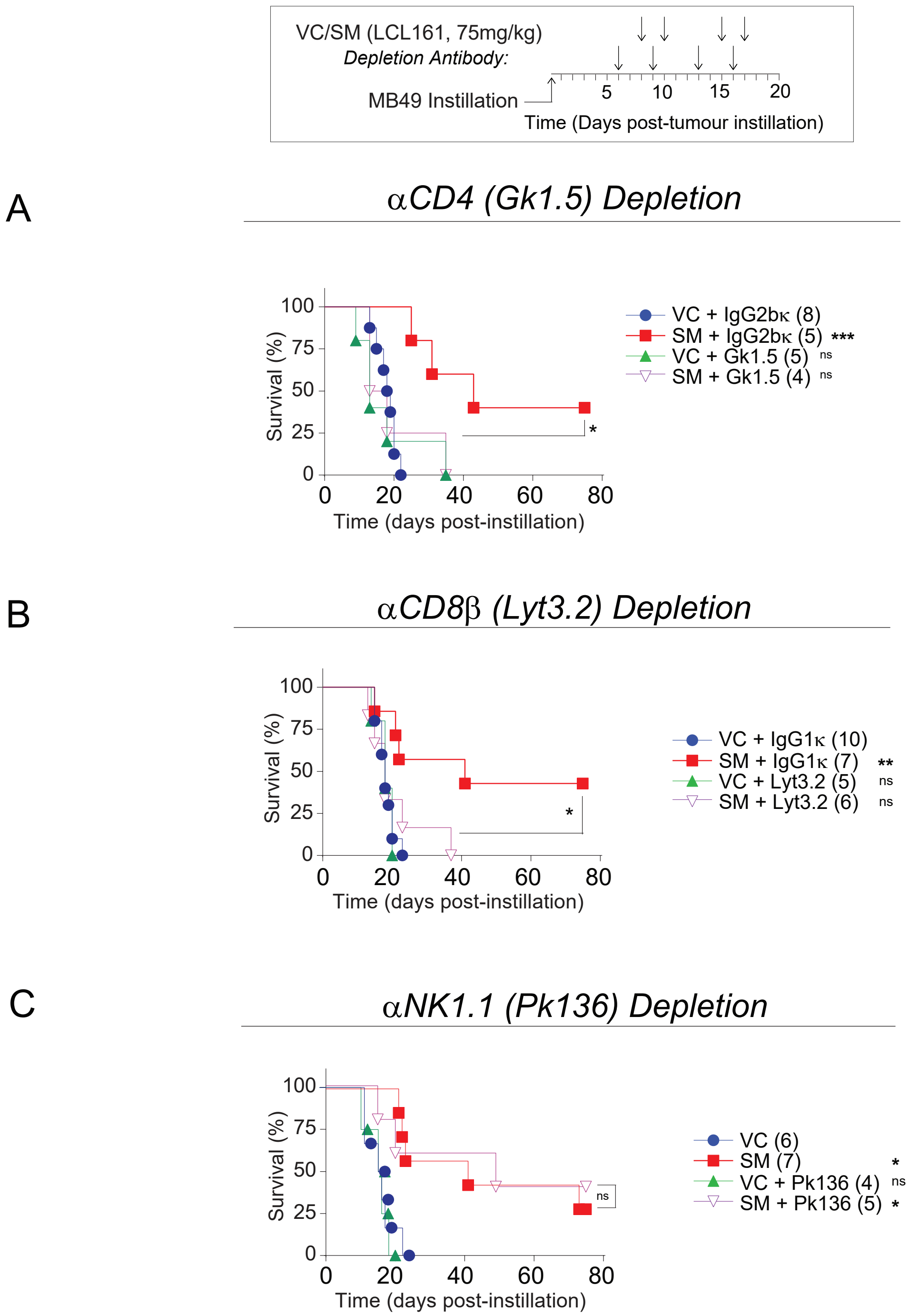

VC/SM (LCL161, 75mg/kg)
Depletion Antibody:
MB49 Instillation
5 10 15 20
Time (Days post-tumour instillation)
A
αCD4 (Gk1.5) Depletion
Survival (%)
100 75 50 25 0
0 20 40 60 80
Time (days post-instillation)
VC + IgG2bκ (8)
SM + IgG2bκ (5) ***
VC + Gk1.5 (5) ns
SM + Gk1.5 (4) ns
*
B
αCD8β (Lyt3.2) Depletion
Survival (%)
100 75 50 25 0
0 20 40 60 80
Time (days post-instillation)
VC + IgG1κ (10)
SM + IgG1κ (7) **
VC + Lyt3.2 (5) ns
SM + Lyt3.2 (6) ns
*
C
αNK1.1 (Pk136) Depletion
Survival (%)
100 75 50 25 0
0 20 40 60 80
Time (days post-instillation)
VC (6)
SM (7) *
VC + Pk136 (4) ns
SM + Pk136 (5) *
ns

Figure 16. SM-mediated survival benefit is dependent on CD4 and CD8 but not NK cells

25,000 MB49-luc cells were intravesically instilled into the mouse bladder of 8-week-old naïve female C57BL/6 mice. Mice were treated with vehicle control (VC; acid buffer) or Smac mimetic (SM, LCL161, 75mg/kg) by oral gavage on days 8, 10, 15, and 17, and intraperitoneally injected with 250μg of control IgG/IgG2b-kappa or A) anti-CD4 (GK1.5 clone), B) anti-CD8-beta (Lyt3.2 clone), or C) anti-NK1.1 (Pk136 clone) on days 6, 9, 13, and 16. Representative Kaplan-Meier survival plots with Mantel-Cox survival curve comparison test. Parentheses indicate number of mice in the treatment group. ***, $p < 0.001$. **, $p < 0.01$. *, $p < 0.05$.

A

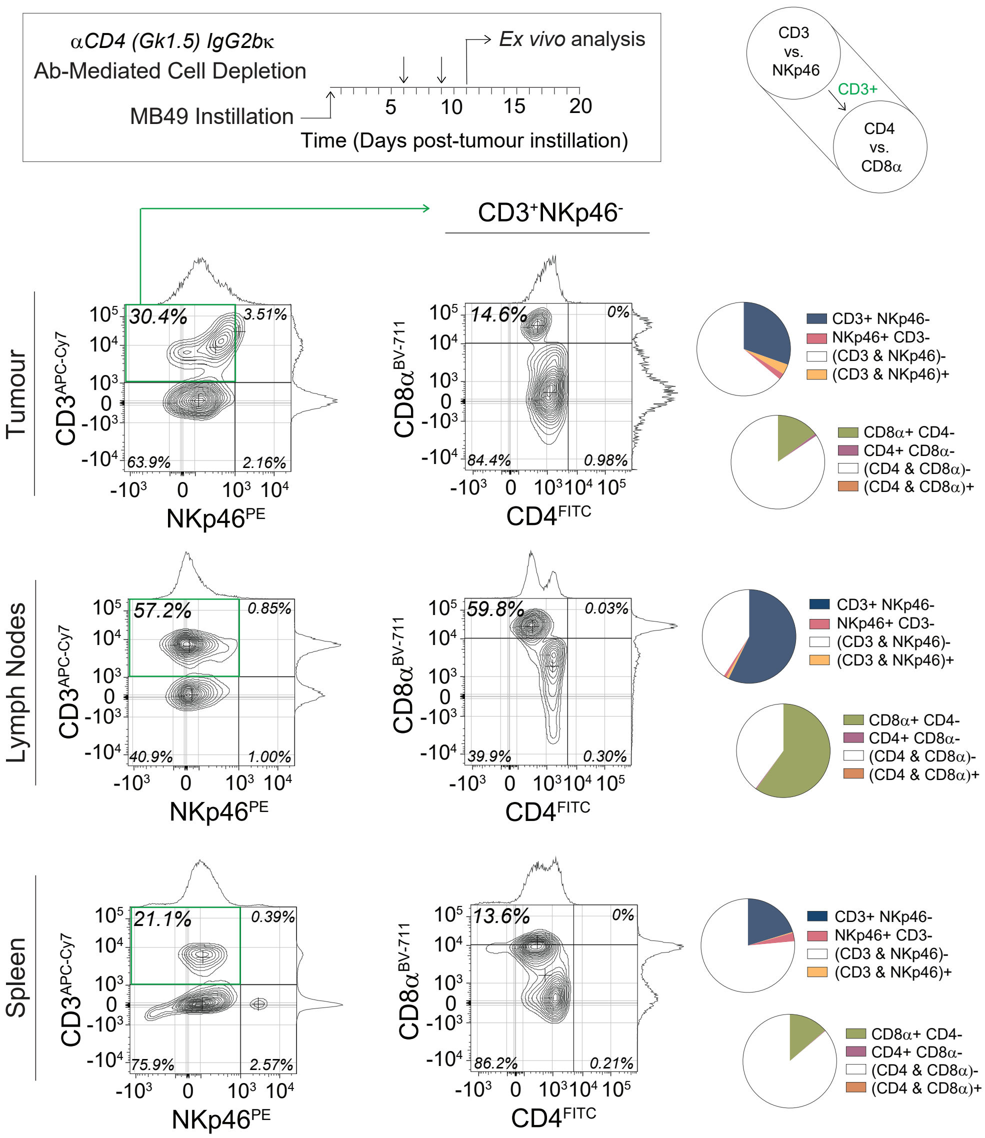

αCD4 (Gk1.5) IgG2bκ
Ab-Mediated Cell Depletion
Ex vivo analysis
MB49 Instillation
5 10 15 20
Time (Days post-tumour instillation)
CD3 vs. NKp46
CD3+
CD4 vs. CD8α
CD3+NKp46-
Tumour
Lymph Nodes
Spleen
CD3APC-Cy7
NKp46PE
CD8αBV-711
CD4FITC
30.4%
3.51%
63.9%
2.16%
14.6%
0%
84.4%
0.98%
57.2%
0.85%
40.9%
1.00%
59.8%
0.03%
39.9%
0.30%
21.1%
0.39%
75.9%
2.57%
13.6%
0%
86.2%
0.21%
CD3+ NKp46-
NKp46+ CD3-
(CD3 & NKp46)-
(CD3 & NKp46)+
CD8α+ CD4-
CD4+ CD8α-
(CD4 & CD8α)-
(CD4 & CD8α)+

B

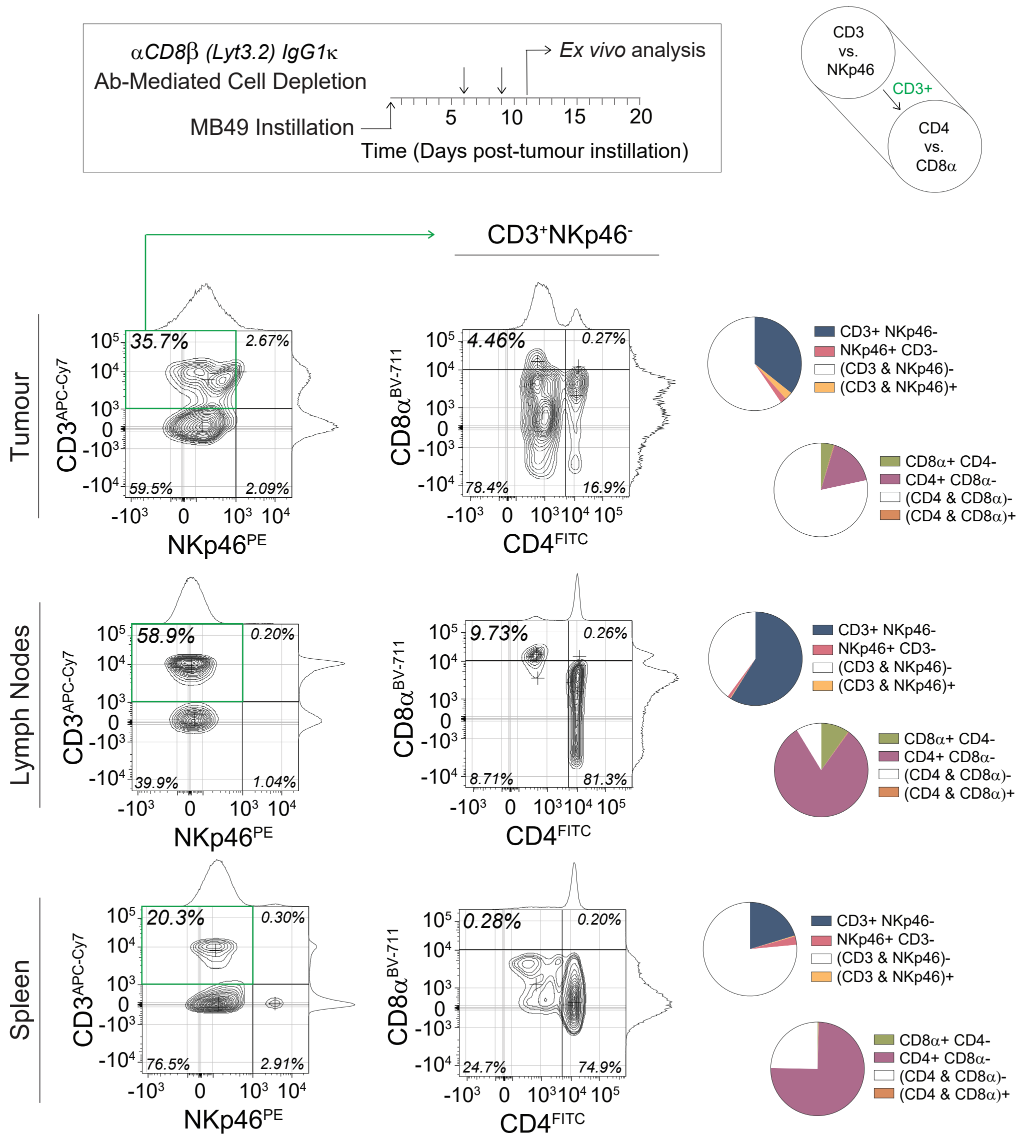
αCD8β (Lyt3.2) IgG1κ
Ab-Mediated Cell Depletion
Ex vivo analysis
MB49 Instillation
5
10
15
20
Time (Days post-tumour instillation)
CD3 vs. NKp46
CD3+
CD4 vs. CD8α
CD3+NKp46-
Tumour
Lymph Nodes
Spleen
CD3APC-Cy7
NKp46PE
CD8αBV-711
CD4FITC
35.7%
2.67%
59.5%
2.09%
4.46%
0.27%
78.4%
16.9%
58.9%
0.20%
39.9%
1.04%
9.73%
0.26%
8.71%
81.3%
20.3%
0.30%
76.5%
2.91%
0.28%
0.20%
24.7%
74.9%
CD3+ NKp46-
NKp46+ CD3-
(CD3 & NKp46)-
(CD3 & NKp46)+
CD8α+ CD4-
CD4+ CD8α-
(CD4 & CD8α)-
(CD4 & CD8α)+

C

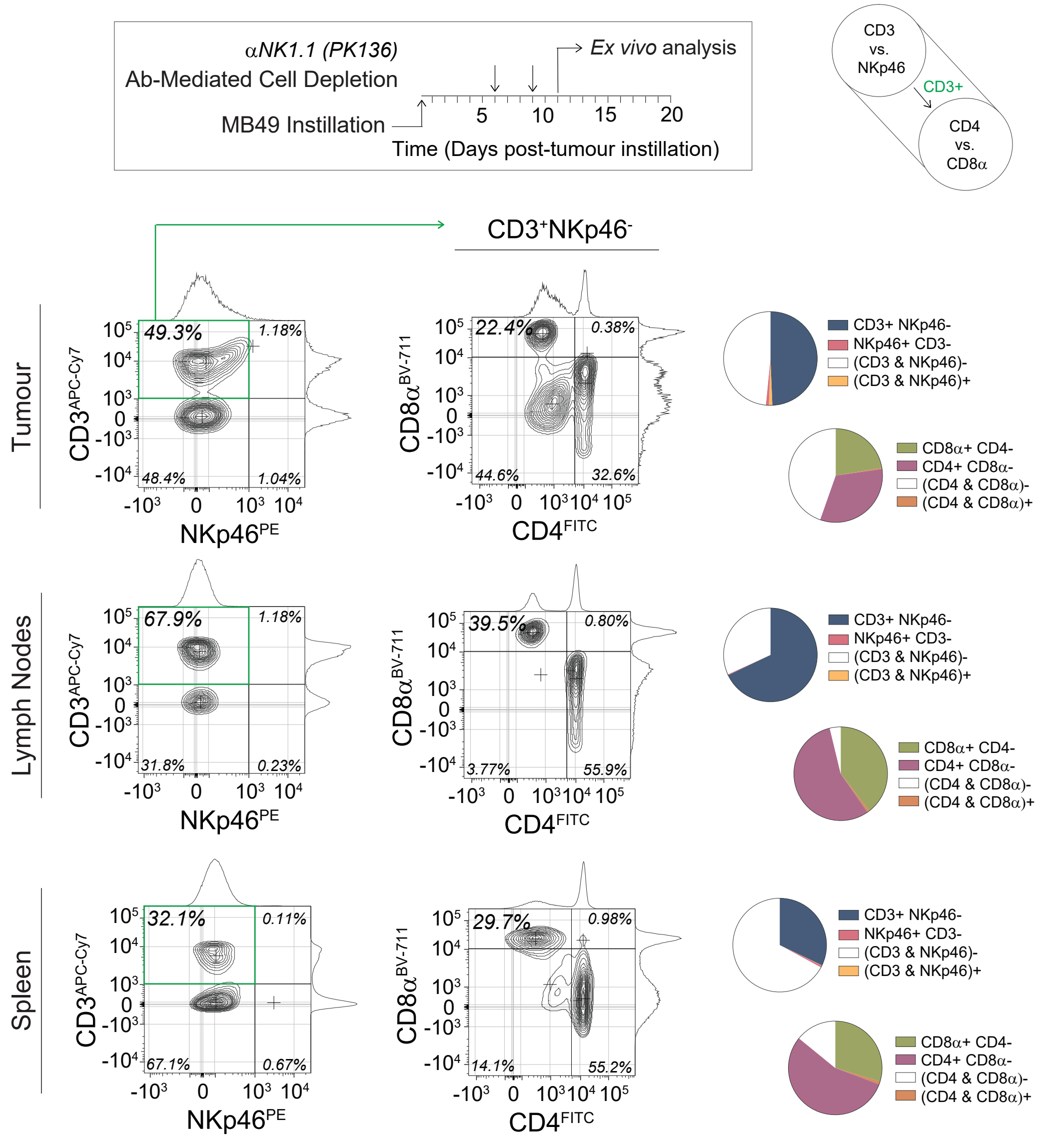
αNK1.1 (PK136)
Ab-Mediated Cell Depletion
Ex vivo analysis
MB49 Instillation
5
10
15
20
Time (Days post-tumour instillation)
CD3
vs.
NKp46
CD3+
CD4
vs.
CD8α
CD3+NKp46-
Tumour
Lymph Nodes
Spleen
CD3APC-Cy7
NKp46PE
CD8αBV-711
CD4FITC
49.3%
1.18%
48.4%
1.04%
22.4%
0.38%
44.6%
32.6%
67.9%
1.18%
31.8%
0.23%
39.5%
0.80%
3.77%
55.9%
32.1%
0.11%
67.1%
0.67%
29.7%
0.98%
14.1%
55.2%
CD3+ NKp46-
NKp46+ CD3-
(CD3 & NKp46)-
(CD3 & NKp46)+
CD8α+ CD4-
CD4+ CD8α-
(CD4 & CD8α)-
(CD4 & CD8α)+

Figure 17. Verification of intratumoural depletions

25,000 MB49-luc cells were intravesically instilled into the mouse bladder of 8-week-old naïve female C57BL/6 mice. Mice were intraperitoneally injected with 250µg of A) anti-CD4 (GK1.5 clone), B) anti-CD8-beta (Lyt3.2 clone), or C) anti-NK1.1 (Pk136 clone) on day 6 and 9. Mice were sacrificed on day 11 and tumours (upper plots), lymph nodes (middle plots), and spleens (lower plots) were resected for analysis by flow cytometry. Samples were stained with antibodies specific for CD3 (APC-Cy7), NKp46 (PE), CD4 (FITC, RM4-5 clone), and CD8-alpha (BV711). Left side plots identify CD3+ NKp46- events with a green box, from which events are further plotted on the right side (CD8-alpha vs. CD4). Crosses within individual quadrants identify median expression amongst events within the respective quadrant. Adjacent pie graphs illustrate event distribution from quadrants within both plots.

accompanied with an increase in DEC-205, the prevailing marker associated with the internalization of apoptotic material. (Figure 18A).

I further evaluated CD11b-expressing cells and found SM treatment increased the proportion of Ly6G+ and Ly6C+ co-expression, suggesting an increase in the absolute quantity of myeloid-derived suppressor cells in the tumour microenvironment (Figure 18B).

The inherent necessity of CD4 and CD8-beta T cells for SM treatment to generate survival benefit indicates an adaptive immune response specific to the tumour was generated, underscoring the immunogenicity of the MB49 model. The formation of an adaptive response to the tumour requires the capture, processing, and presentation of tumour-associated antigens to cognate T cells, which then undergo clonal expansion and traffic to the tumour microenvironment and elicit targeted cytotoxicity. To substantiate these findings, I propagated a fluorescent-reporter lineage of MB49 cells ($MB49^{GFP}$) (Figure 19A-C) to assess acquisition of tumour-associated material within integrin-alpha-X (ITGAX/CD11c)-expressing dendritic cells (DCs) using flow cytometry. I verified autofluorescence at discrete wavelengths, as fluorescence intensity was elevated in channels synonymous with green expression. I compared other reporter lines in parallel to verify that lentiviral transfection did not significantly alter the morphology of MB49 cells. Although MB49-GFP cells were on average smaller than wildtype MB49 cells, this was also the case with MB49-luc cells used for in vivo survival studies (Figure 19C). The consistency between cells used for in vivo studies ensures the results may be interpreted in a mutually-equivalent manner.

I implanted $MB49^{GFP}$ tumours to verify stable expression of GFP relative to increasing tumour burden. I resected tumours with a mass greater or fewer than 50mg, treated with either VC or SM, along with their draining lymph nodes (Figure 19D, E). I performed flow cytometry

A

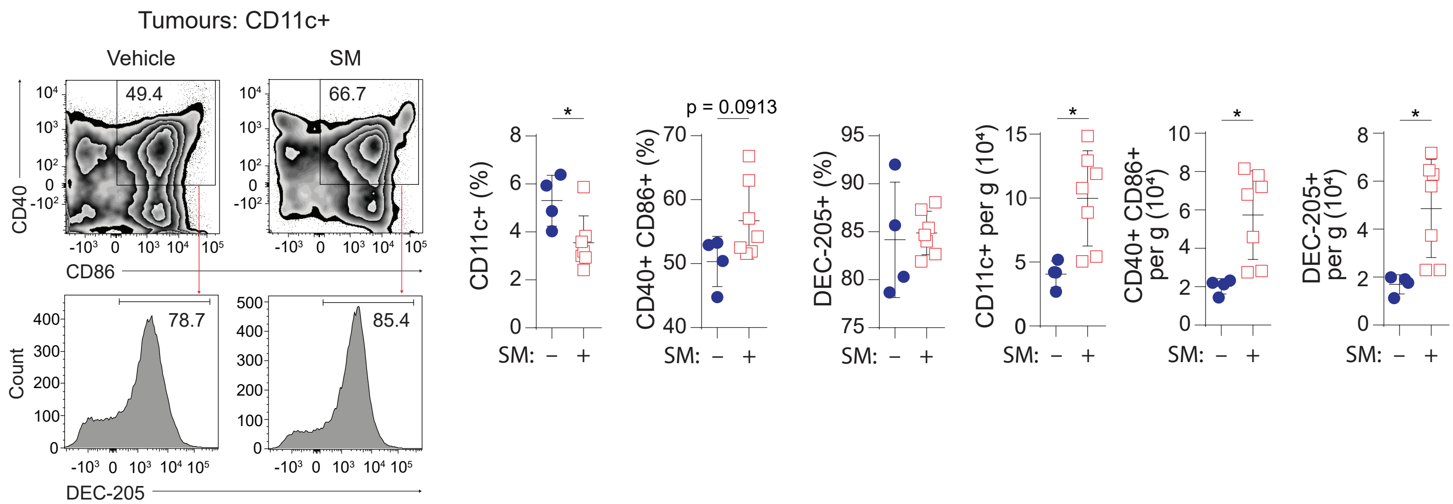
Tumours: CD11c+
Vehicle
SM
49.4
66.7
CD40
CD86
78.7
85.4
Count
DEC-205
p = 0.0913
CD11c+ (%)
CD40+ CD86+ (%)
DEC-205+ (%)
CD11c+ per g (10⁴)
CD40+ CD86+ per g (10⁴)
DEC-205+ per g (10⁴)
SM: – +

B

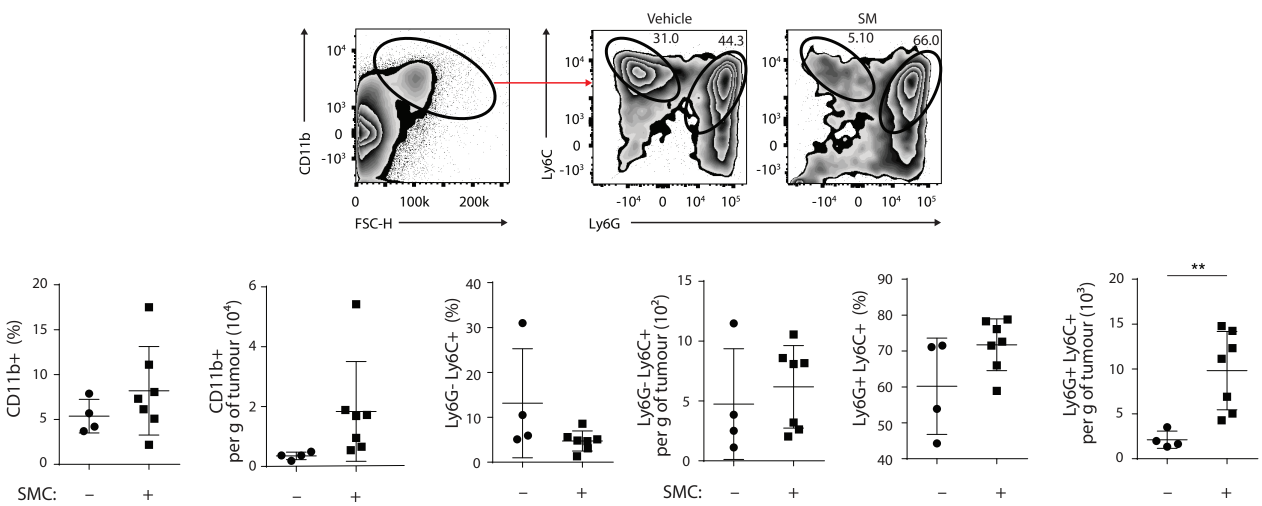
Vehicle
SM
31.0
44.3
5.10
66.0
CD11b
FSC-H
Ly6C
Ly6G
CD11b+ (%)
CD11b+ per g of tumour (10⁴)
Ly6G- Ly6C+ (%)
Ly6G- Ly6C+ per g of tumour (10²)
Ly6G+ Ly6C+ (%)
Ly6G+ Ly6C+ per g of tumour (10³)
SMC: – +

Figure 18. SM increases intratumoural DCs and myeloid-lineage cells

25,000 MB49-luc cells were intravesically instilled into the mouse bladder of 8-week-old naïve female C57BL/6 mice. Mice were treated with vehicle control (VC; acid buffer) or Smac mimetic (SM, LCL161, 75mg/kg) by oral gavage on days 7 and 9. Tumours were resected then processed for flow cytometry on day 11. A) Plots represent tumour-associated viable (Zombie Green, AF488) CD11c+ (PE-Cy5) events, with box inserts depicting CD40 (PE) + and CD86 (PE-Cy7) + events. Subsequent histograms depict DEC-205 (AF647). B) Plots represent CD11b (BV605) + events with further sub-gating on Ly6C (PerCP-Cy5.5) + and either high or low expression of Ly6G (BV711). Statistical analysis was performed using an unpaired T test with Welch's correction. **, $p < 0.01$.

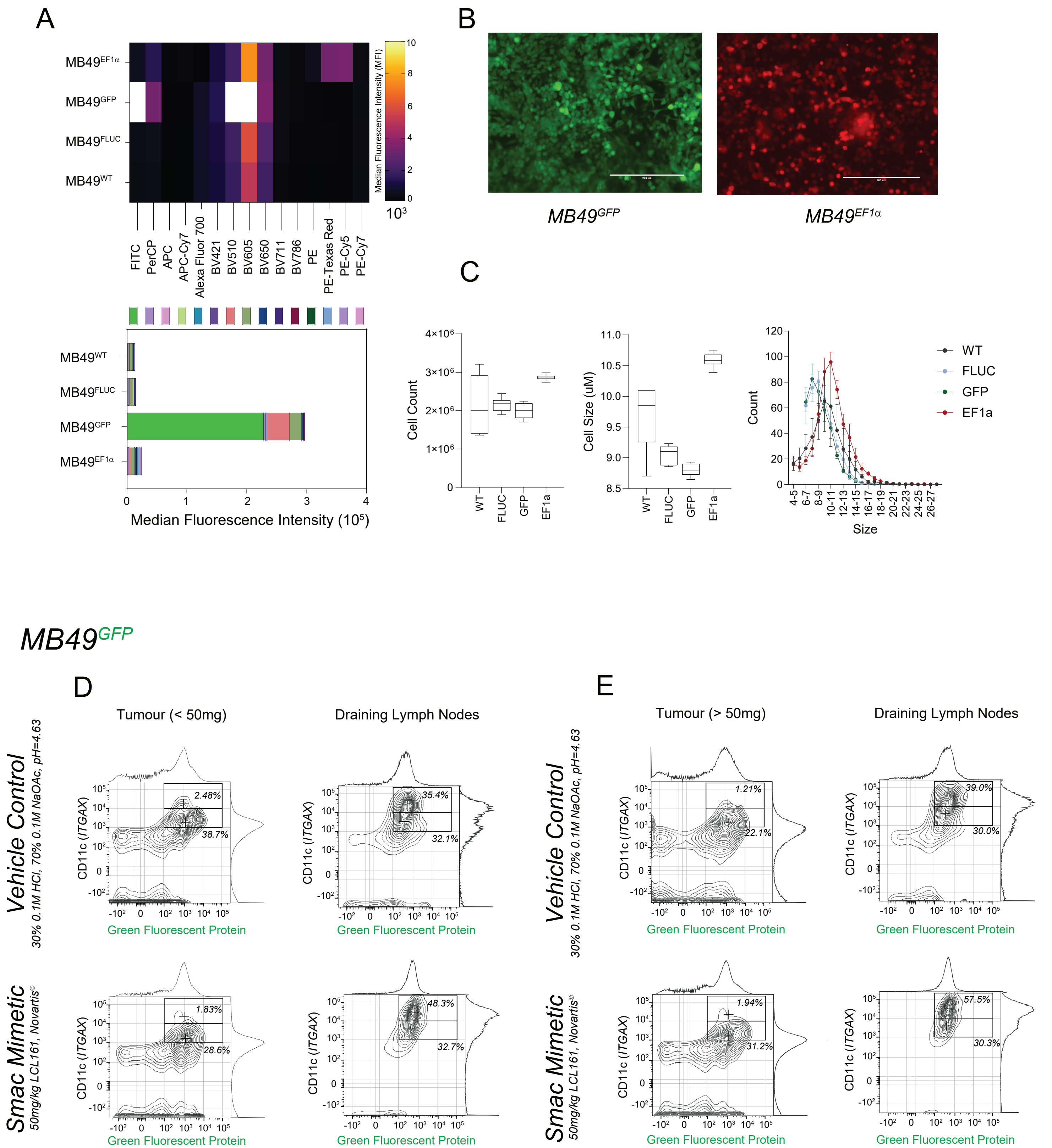
A
MB49EF1α
MB49GFP
MB49FLUC
MB49WT
Median Fluorescence Intensity (MFI)
10³
FITC
PerCP
APC
APC-Cy7
Alexa Fluor 700
BV421
BV510
BV605
BV650
BV711
BV786
PE
PE-Texas Red
PE-Cy5
PE-Cy7
Median Fluorescence Intensity (10⁵)
B
MB49GFP
MB49EF1α
C
Cell Count
Cell Size (uM)
Count
Size
WT
FLUC
GFP
EF1a
MB49GFP
D
Tumour (< 50mg)
Draining Lymph Nodes
E
Tumour (> 50mg)
Draining Lymph Nodes
Vehicle Control
30% 0.1M HCl, 70% 0.1M NaOAc, pH=4.63
Smac Mimetic
50mg/kg LCL161, Novartis©
CD11c (ITGAX)
Green Fluorescent Protein
2.48%
38.7%
35.4%
32.1%
1.21%
22.1%
39.0%
30.0%
1.83%
28.6%
48.3%
32.7%
1.94%
31.2%
57.5%
30.3%

Figure 19. SM increases prevalence of tumour-associated antigen in peripheral lymph nodes

A) MB49 reporter lines were processed for flow cytometry without any staining. Listed fluorophore parameters were enabled, and median fluorescence intensity (MFI) was quantified. B) Representative images were acquired using EVOS light microscope under the green (upper) and red (lower) filters. C) Cell count and cell size data was acquired using Corning cell counter. D, E) 25,000 MB49-GFP cells were intravesically instilled into the mouse bladder of 8-week-old naïve female C57BL/6 mice. Mice were treated with vehicle control (VC; acid buffer) or Smac mimetic (SM, LCL161, 75mg/kg) by oral gavage on days 7 and 9. Tumours and draining lymph nodes were resected then processed for flow cytometry on day 10.

and gated upon CD11c+ and GFP+ events, using this strategy to infer the uptake of tumour-associated antigens by dendritic cells. Within all tumours, as well as their draining lymph nodes, GFP expression was detected. These results suggest tumour-associated antigens were successfully trafficked via lymphatic drainage to proximal lymphoid structures, at different stages of tumour progression. Notably, the presence of CD11c(low) GFP+ events represent acquisition of tumour cells, a finding that was restricted to data from tumour samples only. The lack of CD11c(low) GFP+ events within draining lymph nodes relative to tumour samples suggest tumour cells were not present in the draining lymph nodes. Furthermore, the co-expression of CD11c within most GFP+ events indicate tumour-antigens were actively trafficked by dendritic cells to the draining lymph nodes. Within tumours <50mg [Figure 19D], the VC-treated subject retained a greater percentage of CD11c (mid + high) GFP+ events (38.7+2.48) than SM-treated subject (28.6+1.83). Equivalent gating on draining lymph nodes demonstrated DCs from the SM-treated subject (32.7+48.3) retained a greater percentage than the VC-treated subject (32.1+35.4). The discrepancy between tumour and draining lymph nodes from both treatments may be rationalized by SM increasing overall trafficking of tumour-associated antigens from the tumour to the draining lymph nodes. Within tumours >50mg [Figure 19E], the VC-treated subject retained fewer CD11c+ GFP+ events (22.1+1.21) than the SM-treated subject (31.2+1.94). Lymph node samples found the_SM-treated subject (30.3+57.5) retained a greater percentage than the VC-treated subject (30+39). Collectively, upon comparing VC- and SM-treated samples, I found CD11c+ events from the draining lymph nodes of SM-treated mice were consistently saturated with tumour-associated GFP to a greater extent than VC-treated mice. This suggests SM treatment may diversify the antigenicity of the T cell-driven, adaptive –or, derived – anti-tumour immune response.

Motivated by these novel findings, I partitioned focus toward distinguishing SMs as potent immunomodulatory agents through investigating derived immunological mechanism(s) of action.

3.2 Modulatory effects of SMs on T cell immunity

3.2.1 SM modulates dendritic cells in vitro

To begin, I isolated splenic CD11c+ cells then treated these cells with differing doses of the monovalent SM LCL161, or bivalent SM Birinapant. I recorded greater yield of CD11c cells from low doses in both treatment cohorts (Figure 20). High dose SM either had no effect on overall event count or diminished event count. Notably, a significant proportion of isolated cells did not express CD11c at high levels following treatment and culture period.

Surprised by the expansion of these immune cells derived from secondary lymphoid structures, I expanded my inquiry to incorporate cells from a primary lymphoid organ. Murine femoral bone marrow aspirate was treated ex vivo with recombinant granulocytic macrophage colony stimulating factor (GM-CSF) alongside IL-4 to propagate immature mesenchymal stem cell precursors toward professional APCs – bone marrow-derived dendritic cells (BMDCs) – then pulsed with established stimulants. Specifically, CD95 (or Fas ligand – TNF superfamily type 2 transmembrane apoptotic protein)-engagement increases the susceptibility of DCs to undergo apoptosis [McLellan, 2000], whereas TNF-alpha is critical for DC maturation [Trevejo et al., 2001]. Time-lapse microscopy quantified cell expansion or contraction in real-time. Detection of caspase-3 cleavage was measured by quantifying the intensity of a fluorescent green dye specific for the DEVD domain. To ensure consistent image acquisition, cells were not supplemented with additional growth factors upon initializing imaging. Within BSA, anti-CD95, and TNF-alpha-treated samples viable cells began to diminish in number after approximately 48 hours and continued to decrease gradually, as indicated in confluency measurements (Figure 21A). Interestingly, SM increased proliferation and augmented focal clustering, adjudged by the corresponding elevation in basal confluency

A

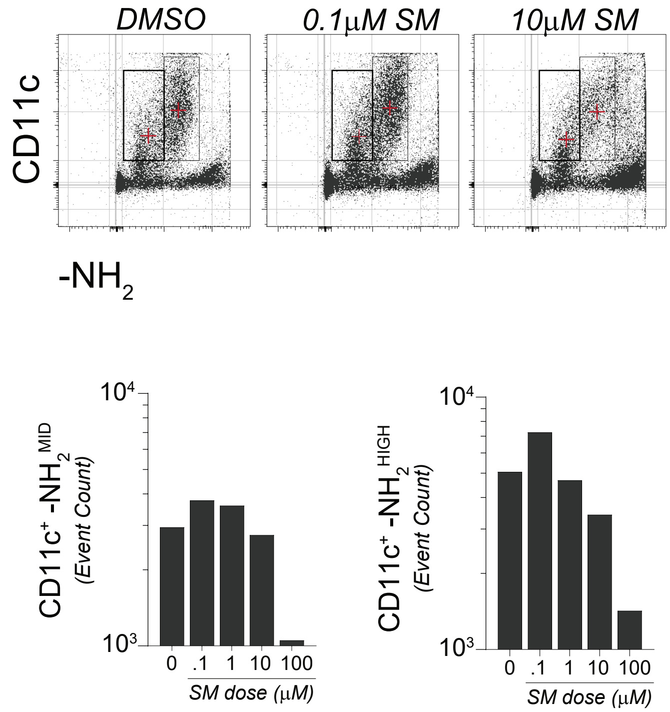
DMSO
0.1μM SM
10μM SM
CD11c
-NH2
CD11c+ -NH2MID
(Event Count)
CD11c+ -NH2HIGH
(Event Count)
10⁴
10³
0
.1
1
10
100
SM dose (μM)

B

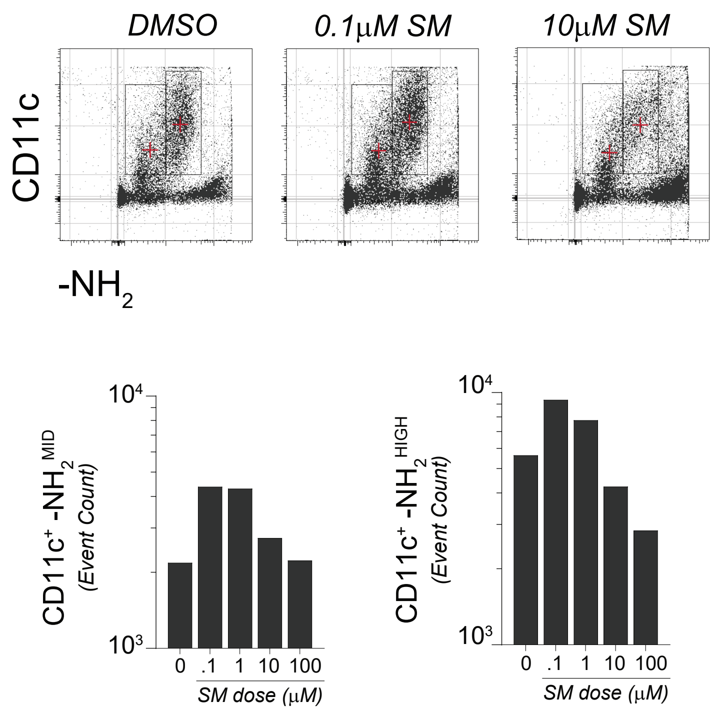
DMSO
0.1μM SM
10μM SM
CD11c
-NH2
CD11c+ -NH2MID
(Event Count)
CD11c+ -NH2HIGH
(Event Count)
10⁴
10³
0
.1
1
10
100
SM dose (μM)

Figure 20. Low dose SM increases CD11c yield in vitro

Splenic CD11c cells were magnetically isolated from a 8-week-old naïve female C57BL/6 mice. Samples were treated with dose-escalating A) monovalent (LCL161) or B) bivalent (Birinapant) SM. After 24 hours samples were collected and processed for flow cytometry. Events were plotted with a fluorescent probe specific for CD11c (FITC, y-axis) and an amine dye (-NH2, Zombie Violet, BV421). Gates identify CD11c mid vs. high expression and representative event counts are graphed.

with sharp increase in average congregate area of software-generated polygons (Figure 21A, B). Both attributes oscillated proportional to fold-increases in dosage within the first 24 hours following treatment administration. The decrease in the overall number of polygons, denoted by count per image (Figure 21C), while the average area of each polygon increased demonstrates individual cells began to aggregate (Figure 20G), an indicator of cell activation [Steinman, 1991]. This trend reverses for all samples, except for low-dose SM (0.5μM), after 24 hours, as the confluency and average area plateau or decrease while count per image increases.

Quantification of caspase-3 activation detected stable confluency and count within BSA control samples (Figure 21D, E). Detection in anti-CD95-treated samples was slightly elevated in comparison yet also remained stable, as expected. Notably, the average intensity of green fluorescence at individual spots in respective images quantifies the degree of caspase activation within individual cells (Figure 21F). Since cultures were not supplemented with additional growth factors, BSA-control and anti-CD95-treated samples reveal increasing caspase activity after 48 hours, as expected. SM-treated samples, however, depict sharp increases in caspase activity in a dose-escalating manner within the first 24 hours of imaging, as determined by confluency, count, and intensity. Following this increase, all caspase metrics diminish. Notably, caspase intensity is lowest for high dose SM after 72 hours, while its confluency remains highest, compared to all other treatment groups. This suggests SM treatment may differentiate multi-potent hematopoietic stem cell progenitors to a stable lineage following the proliferation and attrition of select cells in the milieu. By comparison TNF-alpha, a bona fide maturation agent for BMDCs, generates a similar trend albeit with reduced phase-contrast and caspase confluency. A significant distinction however is that TNF-

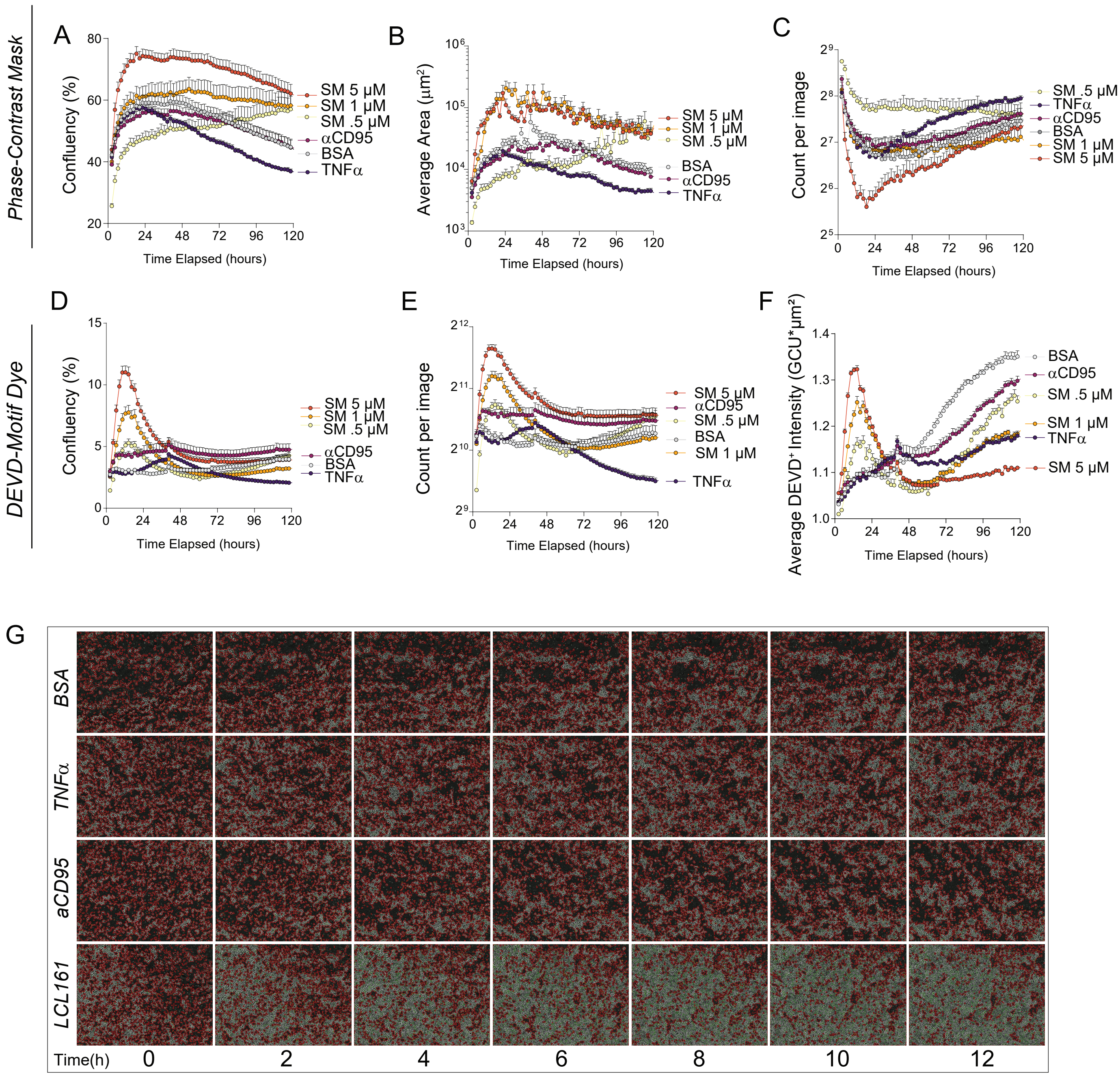

Phase-Contrast Mask
DEVD-Motif Dye
A
Confluency (%)
Time Elapsed (hours)
SM 5 µM
SM 1 µM
SM .5 µM
αCD95
BSA
TNFα
B
Average Area (µm²)
Time Elapsed (hours)
C
Count per image
Time Elapsed (hours)
D
Confluency (%)
Time Elapsed (hours)
E
Count per image
Time Elapsed (hours)
F
Average DEVD⁺ Intensity (GCU*µm²)
Time Elapsed (hours)
G
BSA
TNFα
aCD95
LCL161
Time(h) 0 2 4 6 8 10 12

Figure 21. SM enables BMDC expansion and clustering

BMDCs were pulsed with a fluorescent dye specific for the DEVD death-domain motif, then stimulated with PBS-BSA (0.1%), recombinant murine TNF-alpha (10ng/mL), anti-CD95 (FasL, 1ug/mL), or indicated concentrations of SM (0.5, 1, or 5μM, LCL161) then imaged every 2 hours in a time-lapse microscope. A) Phase-contrast confluency of polygons outlining cells, as a percent of total surface area. B) Average area of each polygon. C) Average number of polygons per image. D) Green DEVD-motif dye confluency. E) Average number of green spots per image. F) Average intensity of green spots per unit area, green calibrated unit per um^2. G) Phase contrast imaging of PBS-BSA, TNF-alpha, anti-CD95, and 5μM LCL161 every 2 hours for the first 12 hours, with overlay of software-generated polygons outlined in red. Green spots represents DEVD detection.

alpha has fewer instances of caspase activation overall (Figure 21E). This suggests SM treatment likely facilitates activity distinct from its regulation of TNF-alpha signaling.

I expanded on the prior experiment to evaluate whether SM treatment would promote the expression of shear-sensitive transcription factor zinc-finger BTB-domain containing 46 (Zbtb46) (Figure 22A), a preminent identification marker distinguishing type-1 conventional dendritic cells (cDC-1) [Satpathy et al., 2012]. This subset of DCs is established to preferentially enable cross-presentation of exogenous antigen, thereby enabling priming of CD8+ cells required for an adaptive immune response. Zbtb46 has been shown to be induced upon LPS treatment [Satpathy et al., 2012], a finding confirmed in the assay as nearly all events were Zbtb46+. Comparatively, treatment with anti-CD40 antibody or recombinant TNF-alpha yielded a heterogenous population, lacking significant distinction from the control PBS-treated sample. Upon treatment with SM, most events retained high expression of Zbtb46, which was partially rescued by adding neutralizing TNF-alpha antibody. This suggests SM treatment may promote the cross-presentation of soluble antigen.

I verified NIK expression specifically within CD11c cells from bulk BMDC culture (Figure 22B). Notably, SM treatment saturated all viable CD11c events with high levels of NIK, compared to a gradient of expression with the DMSO control-treated sample. To discretely quantify cross-presentation of soluble antigen while evaluating NIK dependency, I pulsed magnetically isolated CD11c+ cells with soluble peptide, preconditioned cell culture with or without a chemical inhibitor specific for NIK, further stimulated with treatments, then processed for

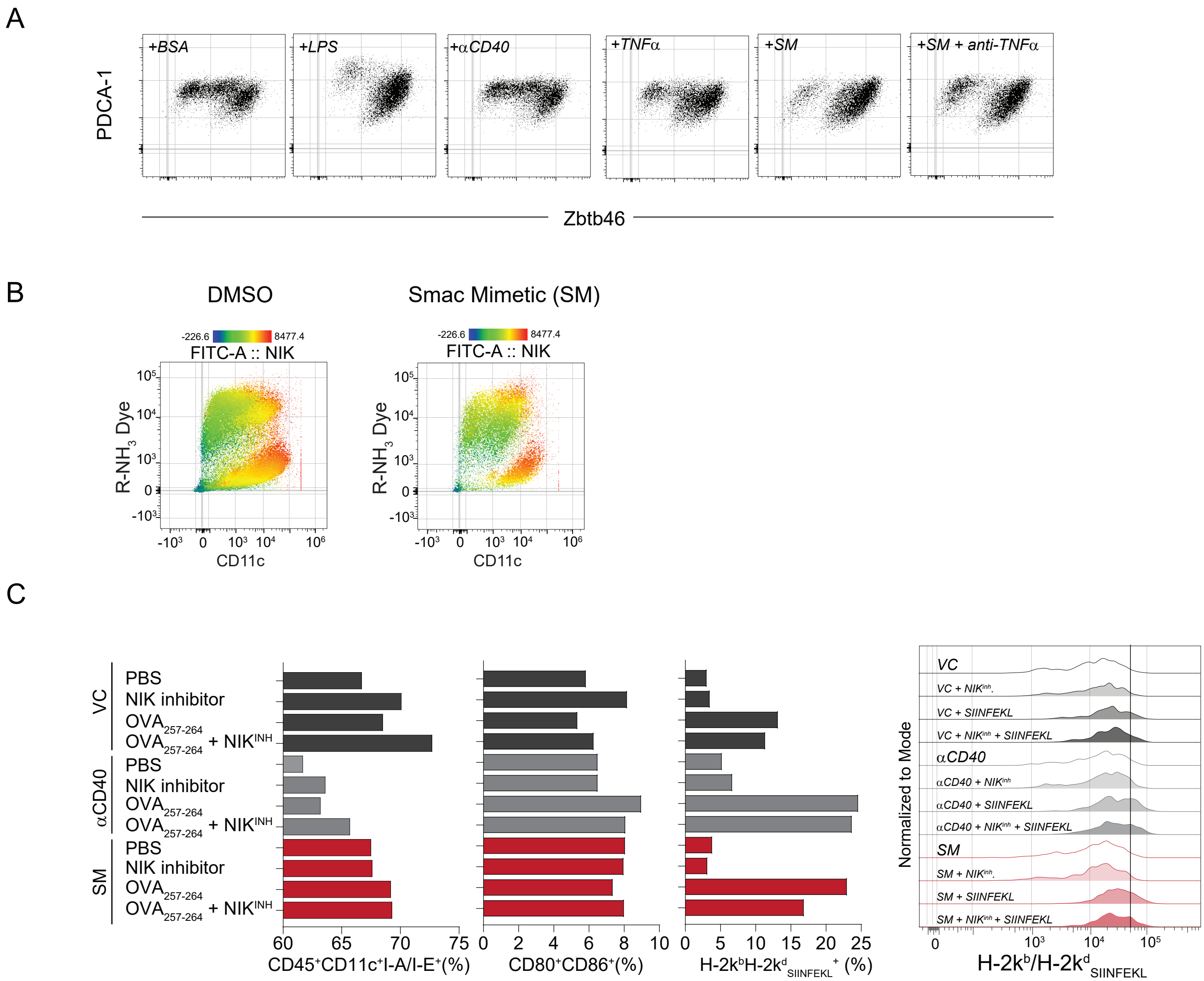

A
+BSA
+LPS
+αCD40
+TNFα
+SM
+SM + anti-TNFα
PDCA-1
Zbtb46
B
DMSO
Smac Mimetic (SM)
FITC-A :: NIK
R-NH3 Dye
CD11c
C
VC
αCD40
SM
PBS
NIK inhibitor
OVA257-264
OVA257-264 + NIK^INH
CD45+CD11c+I-A/I-E+(%)
CD80+CD86+(%)
H-2kbH-2kd SIINFEKL + (%)
Normalized to Mode
H-2kb/H-2kd SIINFEKL

Figure 22. SM enhances soluble antigen-presentation with partial dependency on NIK

Immature BMDCs were treated with 1% PBS-BSA, LPS (1 ug/mL), anti-CD40 antibody (1ug/mL), recombinant murine TNF-alpha (10ng/mL), or SM (LCL161, 5μM) with or without neutralizing TNF-alpha antibody (XT3.11, 1ug/mL) for 24 hours.) A) Events gated CD11b (PE-Cy5) + CD11c (FITC) + I-A/I-E (BV605) + and plotted PDCA-1 (y-axis, AF647) against Zbtb46 (x-axis, PE). B) Samples were further pulsed with soluble AF647-OVA fluorophore-peptide conjugate for 2 hours prior to evaluation by flow cytometry. Back-gating of CD11c (PE-Cy7, high expression) R-NH3 dye (Zombie Violet, BV421, low expression) is displayed, with colourized panel visualizing gradient of NIK (FITC). C) CD11c cells were magnetically isolated from a naive female C57BL/6 spleen then treated with 1% PBS-BSA, anti-CD40 antibody (1ug/mL), or SM (5μM, LCL161), alongside simultaneous treatment with or without a NIK inhibitor (1μM). Cells were then pulsed with SIINFEKL peptide (10ug/mL) for 2 hours, then collected for flow cytometry. Events were gated CD45 (PerCP-Cy5.5) +, CD11c (FITC) +, I-A/I-E (BV605) +, CD80 (AF647) +, CD86 (PE-Cy5) +, prior to gating H2kb/kd (PE). Solid line overlaid on histograms denotes division between positive and negative expression of an MHC-1-(H2kb/kd)-SIINFEKL-specific (PE) antibody.

flow cytometry using a fluorescently-tagged antibody targeting major histocompatibility complex-1(H2kb/H2kd) specific for the pulsed peptide (Figure 22C). Apart from a slight decrease in the overall quantity of αCD40 treated groups, I did not record significant fluctuation in the consensus population of DCs, gated as triple-positive for CD45, CD11c, and I-A/I-E. Quantification within elevated expression B7 domains, CD80 and CD86, did not reveal significant differences among the treatment groups. Lastly, upon evaluating H2kb/H2kd-SIINFEKL expression, I expectedly quantified ~3 to 5-fold increase within all groups pulsed with peptide. This pronounced expression was most elevated in the SM- or αCD40-treated cohorts. I recorded approximately one-third decrease in expression when comparing SM preconditioned with a NIK inhibitor. These results suggest SM treatment enabled epitope presentation, with partial dependency on the alternative NFκB pathway.

3.2.2 SM stimulates T cells in vitro

SM treatment has been reported to enable co-stimulation of T cells in vitro [Dougan et al., 2011]. Given antigen presentation facilitates the clonal expansion of T cells, I explored whether SM treatment would intrinsically polarize or preferentially expand specific sub-lineages of CD4 T cells. I found that SM treatment expanded co-stimulated CD4 T cells based on an increase in metabolic activity [Figure 23A] and diminishing expression of a dilutable dye (Figure 23B). Notably, unpolarized CD4 T cells further gated on transcription factors representative of Th1 (T-bet), Th2 (GATA3), or Treg (FoxP3) lineages suggested SM treatment preferentially enabled the proliferation of Th2 and Treg but not Th1 CD4 T cells. Interestingly, upon evaluating the polarization of Th0 cells following SM treatment, increasing dose of SM increased the expression of T-bet and FoxP3, with a negligible effect on GATA3 expression. This indicated that SM treatment enables pronounced polarization of neutral CD4 T cells into Th1 cells, and less substantially into Tregs (Figure 23C). Notably, Th1 and Th2 cells are countervailing lineages that collectively regulate immune homeostasis [Kidd et al., 2003]. To verify whether SM treatment could preferentially polarize CD4 T cells toward the Th1 phenotype, I generated Th2 cells and treated with SM. I found SM comprehensively diminished GATA3 expression, coupled with a slight increase in T-bet and FoxP3 expression. Collectively, this data suggests SM treatment enables the proliferation of possibly various lineages of CD4 T cells, however, preferentially up-regulates the expression of the Th1 lineage-defining transcription factor.

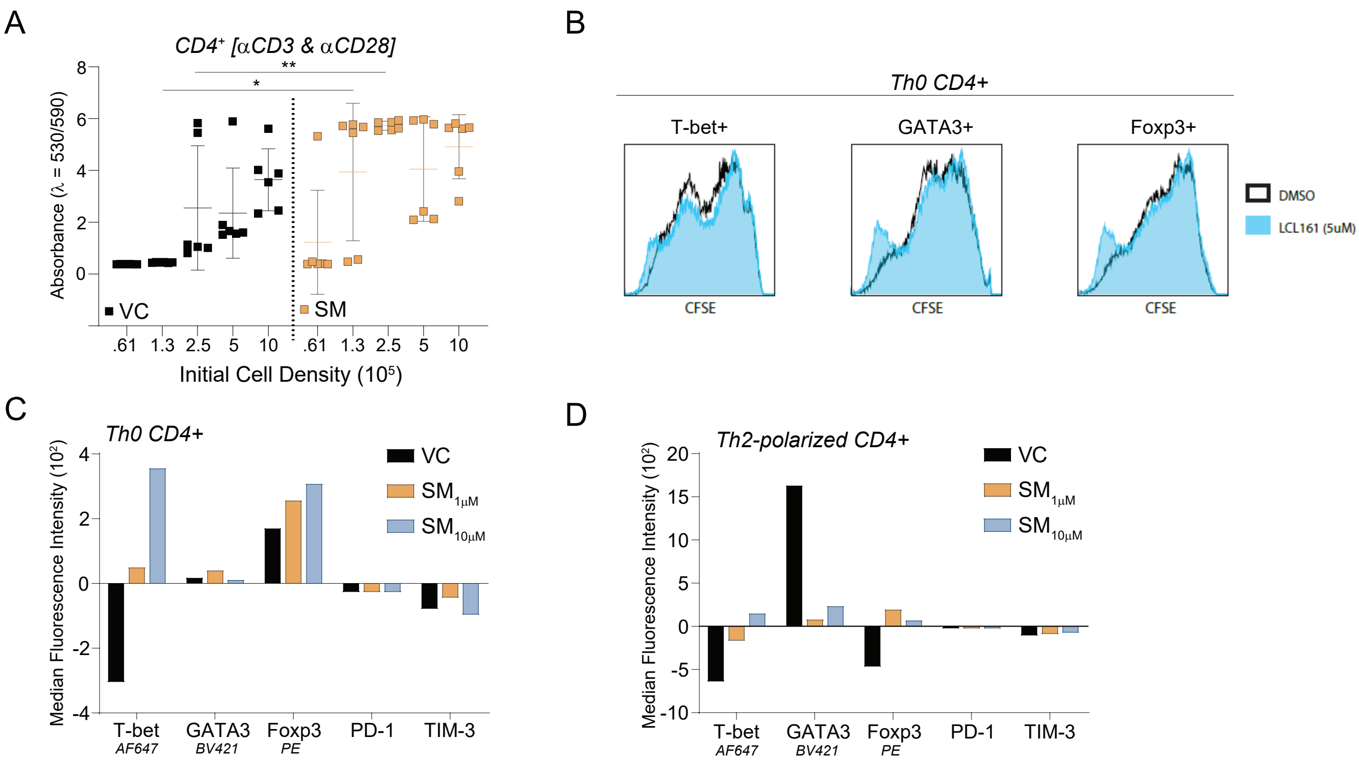
A
CD4+ [αCD3 & αCD28]
Absorbance (λ = 530/590)
VC
SM
Initial Cell Density (10^5)
.61 1.3 2.5 5 10 .61 1.3 2.5 5 10
B
Th0 CD4+
T-bet+
GATA3+
Foxp3+
CFSE
DMSO
LCL161 (5uM)
C
Th0 CD4+
Median Fluorescence Intensity (10^2)
VC
SM1μM
SM10μM
T-bet AF647
GATA3 BV421
Foxp3 PE
PD-1
TIM-3
D
Th2-polarized CD4+
Median Fluorescence Intensity (10^2)
VC
SM1μM
SM10μM
T-bet AF647
GATA3 BV421
Foxp3 PE
PD-1
TIM-3

Figure 23. SM enables expansion or polarization of CD4 T cells

A-D) CD4 T cells were magnetically isolated from a naïve female C57BL/6 spleen. Cells were supplemented with purified anti-CD3 (10 μg/mL), anti-CD28 (2 μg/mL), and recombinant murine IL-2 (200U/mL). A) Cells were seeded at 2-fold increasing densities as indicated and treated with vehicle control (VC, DMSO) or SM (LCL161, 5μM). After 48 hours supernatant was removed, and cells were assayed for resazurin salt metabolism. Absorbance is graphed and statistical analysis was performed using ordinary one-way ANOVA with Tukey's multiple comparisons test. *, $p < 0.05$. **, $p < 0.01$. B-D) Cells were either left B, C) undifferentiated to form Th0 cells, or D) differentiated into type-2 sub-lineage then treated with indicated dose of SM. B) CFSE dilution is plotted with DMSO SM treatment overlaid in blue. C, D) Median fluorescence intensity of indicated transcription factors or surface receptors following VC (DMSO) or SM (1 or 10 μM treatment).

3.2.3 SM treatment promotes soluble vaccine-specific T cell priming.

To evaluate clonal expansion of antigen-specific effectors, I adopted the classical approach wherein CD8-expressing T cells specific for ovalbumin-specific peptide sequence (SIINFEKL) were isolated from OT-1 T cell receptor-transgenic mice and then adoptively transferred into naïve syngeneic recipients. I verified the specificity of the donor OT-1 T cells using a dextramer specific for SIINFEKL-bound MHC-1 (Figure 24).

Mice were treated with soluble peptide, co-treated with established stimulants or SM, then incubated for the standard duration compulsory to propagate donor T cell-specific clones prior to ex vivo analysis of lymphocytes by flow cytometry [Williams et al., 2006] (Figure 25A). A mixture of agonistic CD40 antibody, the predominant surface transmembrane domain identified in stimulating DC activation, coupled with synthetic double-stranded viral RNA (poly I:C) was utilized as a reference threshold simulating acute viral infection. Without peptide vaccination, SM treatment failed to increase donor CD45.1+ CD8a+ cells or alter conventional phenotypic markers CD44 – up-regulated shortly following TCR agonism and is commonly used to distinguish T cell activation [Baaten et al., 2010] – or CD62L – associated with homing to specialized lymphoid structures [Galkina et al., 2007] – to a significant degree compared to baseline VC treatment with peptide vaccination. Upon co-treating SM with peptide vaccination, I noted a log-fold increase in the percentage of CD45.1+ CD8a+ donor T cells present, with fewer proportion expressing a naïve precursor phenotype. The expanded population depicted a marginal decrease in CD8a expression, commonly associated with the activation of T cells, however this was more pronounced in the anti-CD40 antibody- and poly (I:C)-treated samples.

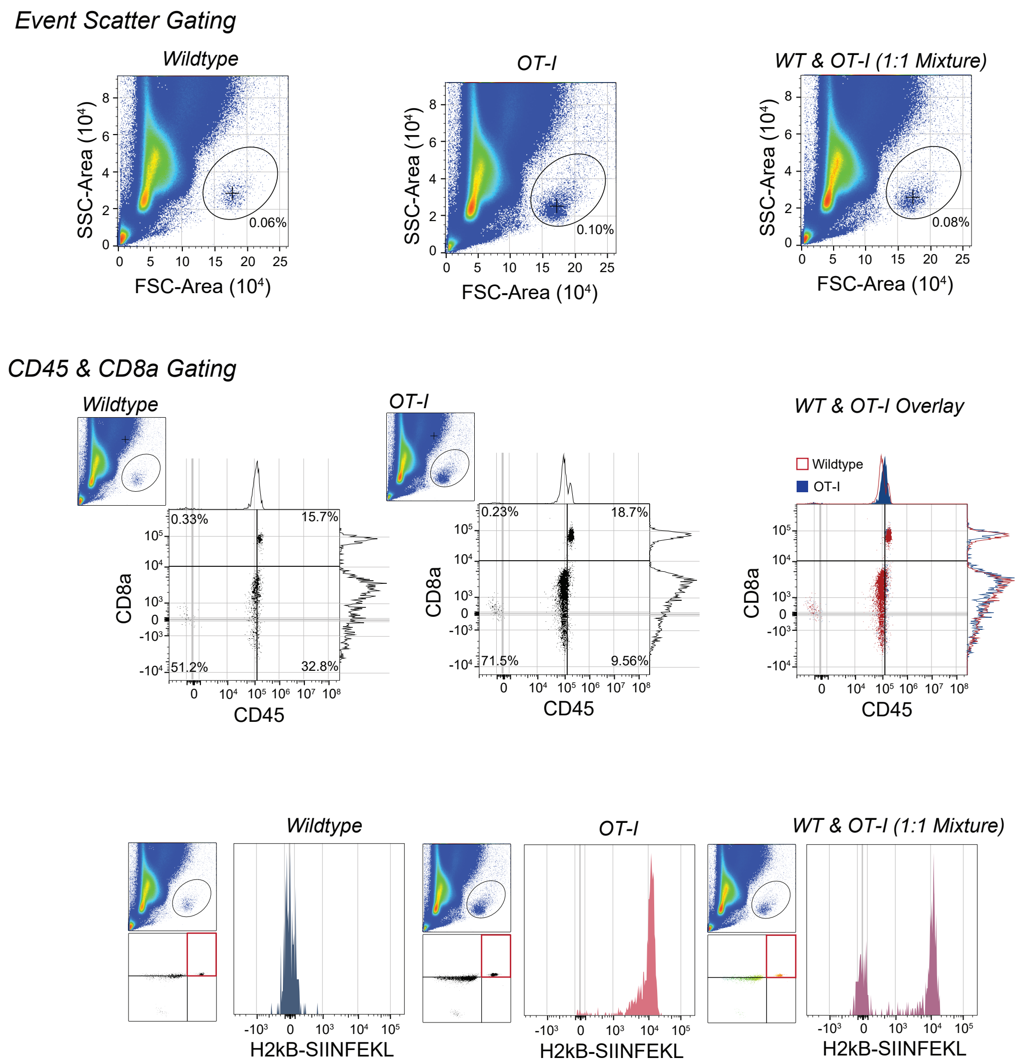
Event Scatter Gating
Wildtype
OT-I
WT & OT-I (1:1 Mixture)
SSC-Area (10⁴)
FSC-Area (10⁴)
0.06%
0.10%
0.08%
CD45 & CD8a Gating
Wildtype
OT-I
WT & OT-I Overlay
Wildtype
OT-I
CD8a
CD45
0.33%
15.7%
51.2%
32.8%
0.23%
18.7%
71.5%
9.56%
Wildtype
OT-I
WT & OT-I (1:1 Mixture)
H2kB-SIINFEKL
H2kB-SIINFEKL
H2kB-SIINFEKL

Figure 24. OT-1 validation

OT-1 or wildtype C57BL/6 splenocytes were isolated and processed for flow cytometry. Samples were divided to create a mixed sample to complement the individual samples. Cells were stained with CD8-alpha, CD45, and an MHC Class 1 (H2kb) dextramer specific for SIINFEKL. Events were gated based on scatter and then elevated expression of CD45 and CD8-alpha in tandem. Histograms comparing normalized probe expression are shown.

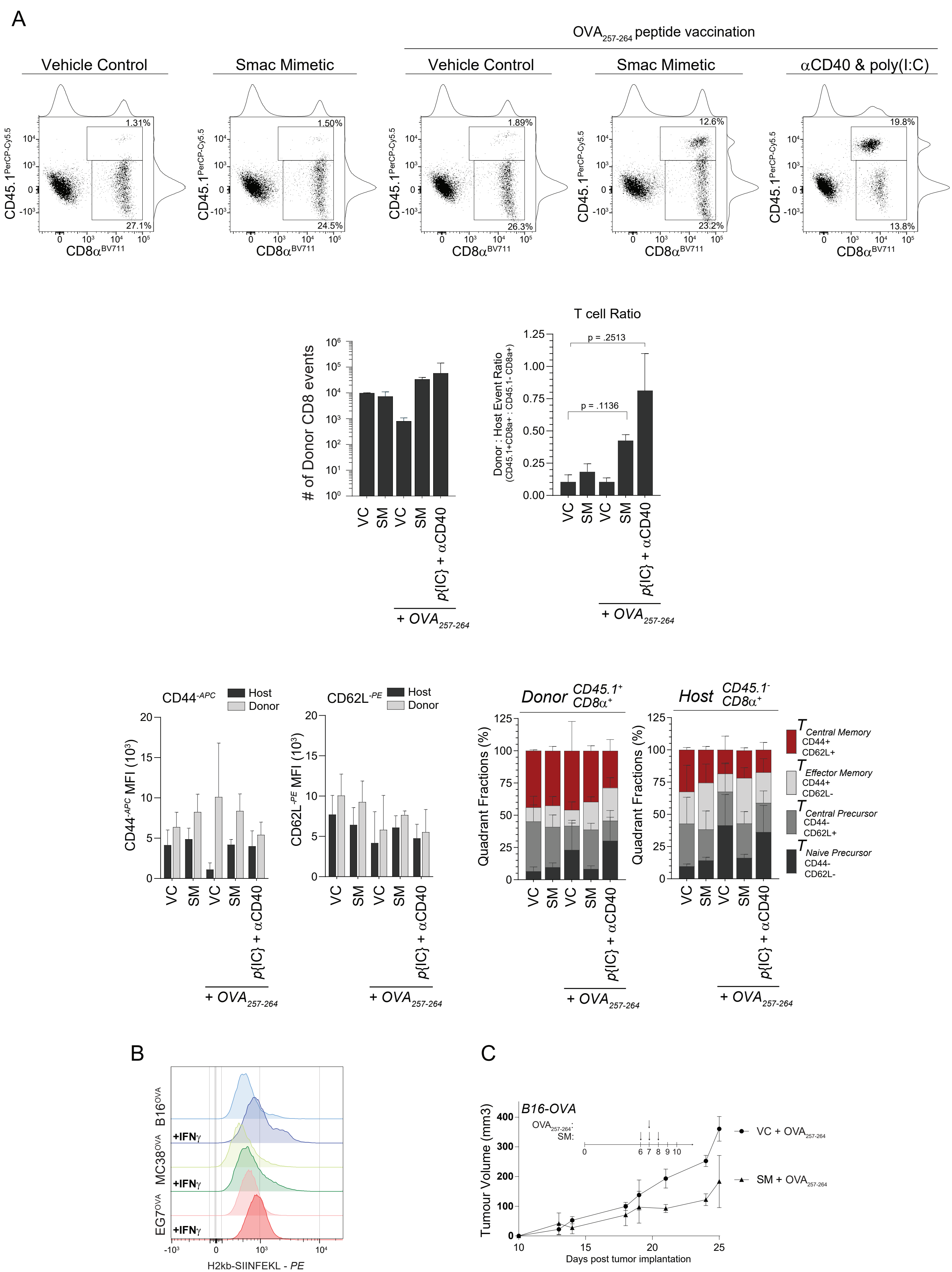
A
OVA257-264 peptide vaccination
Vehicle Control
Smac Mimetic
Vehicle Control
Smac Mimetic
αCD40 & poly(I:C)
CD45.1PerCP-Cy5.5
CD8αBV711
1.31%
27.1%
1.50%
24.5%
1.89%
26.3%
12.6%
23.2%
19.8%
13.8%
T cell Ratio
# of Donor CD8 events
Donor : Host Event Ratio (CD45.1+CD8a+ : CD45.1- CD8a+)
p = .2513
p = .1136
VC
SM
p{IC} + αCD40
+ OVA257-264
CD44-APC
CD62L-PE
Host
Donor
CD44-APC MFI (10³)
CD62L-PE MFI (10³)
Donor CD45.1+ CD8α+
Host CD45.1- CD8α+
Quadrant Fractions (%)
T Central Memory CD44+ CD62L+
T Effector Memory CD44+ CD62L-
T Central Precursor CD44- CD62L+
T Naive Precursor CD44- CD62L-
B
B16OVA
MC38OVA
EG7OVA
+IFNγ
H2kb-SIINFEKL - PE
C
B16-OVA
OVA257-264:
SM:
Tumour Volume (mm3)
Days post tumor implantation
VC + OVA257-264
SM + OVA257-264

Figure 25. SM primes antigen-specific T cells

Donor OT-1 (CD45.1+) T cells were adoptively transferred via tail vein injection into naïve adult recipient mice. A) After 1 day recipient mice were injected with PBS-BSA (1%) or vaccinated with soluble $OVA_{257-264}$ peptide (100ug/100uL) then co-treated with vehicle control (VC, acid buffer) or SM (LCL161, 75mg/kg) by oral gavage, or a cocktail of anti-CD40 (100ug/100uL) and poly I:C (50ug/100uL) intraperitoneally. After an additional 6 days mice were sacrificed and lymph nodes were extracted, processed, and stained for flow cytometry. Events were back-gated as viable (Zombie Green, AF488) and CD3-positive (APC-Cy7), with plots identifying donor T cells (upper gate) and host T cells (lower gate). Events were further sub-gated on CD44 and CD62L to distinguish phenotype. B) Histograms depicting OVA peptide expression among B16-OVA, MC38-OVA, and EG7-OVA in vitro cultured cell lines with or without IFN-y stimulation. C) 8-week-old naïve female C57BL/6 mice were subcutaneously inoculated with 500,000 B16-OVA cells. Mice were intraperitoneally vaccinated with soluble OVA peptide on day 7 post-implantation, with VC or SM (LCL161, 75mg/kg) treatment by oral gavage on days 6-8. Graphed are periodic measurements of subcutaneous tumour outgrowth.

The ratio of adoptively-transferred donor T cells to endogenous T cells was elevated 2-fold or greater for SM and the co-treatment of anti-CD40 and poly(I:C), respectively. Interestingly, SM treatment slightly increased the relative proportion of effector memory cells (CD44+ CD62L-), with marginally fewer cells retaining central memory (CD44+ CD62L+) phenotype. These results provide evidence SM effectively stimulates antigen-specific clonal expansion of an effector T cell response [Dempsey et al., 2019].

To evaluate whether this finding conferred any physiological significance, I cultured cell lines expressing OVA and verified SIINFEKL expression on MHC Class-1 (Figure 25B). I implanted naïve female C57BL/6 mice with B16-OVA cells then vaccinated with OVA-peptide along with oral gavage treatments of VC or SM. Although there was no discernible difference in survival probability (data not shown), SM slightly delayed outgrowth compared to VC (Figure 26C).

I explored the analysis of RNA-sequencing datasets from a publicly available web resource that processes data from nearly 200,000 mouse and human samples [Lachmann et al., 2018]. The top 25 predicted biological functions of BIRC2 (Figure 27A), BIRC3 (Figure 26B), and BIRC4 (Figure 26C), established targets of SMs, were queried and listed in order. BIRC2 and BIRC3, as expected, is associated with alternative NFκB/NIK signaling. Ensuing predictions are central for the genesis of an adaptive immune response, as antigen-processing and regulation of T cell responses dominate the listed processes for BIRC2. BIRC3 similarly is involved in antigen-processing, however, contains additional annotations suggesting critical function in positively regulating the immune response to tumour cells and NK cell immunity. Both lists were completely distinct from BIRC4's predicted functions, as nearly all processes are associated with the metabolism of neurotransmitters.

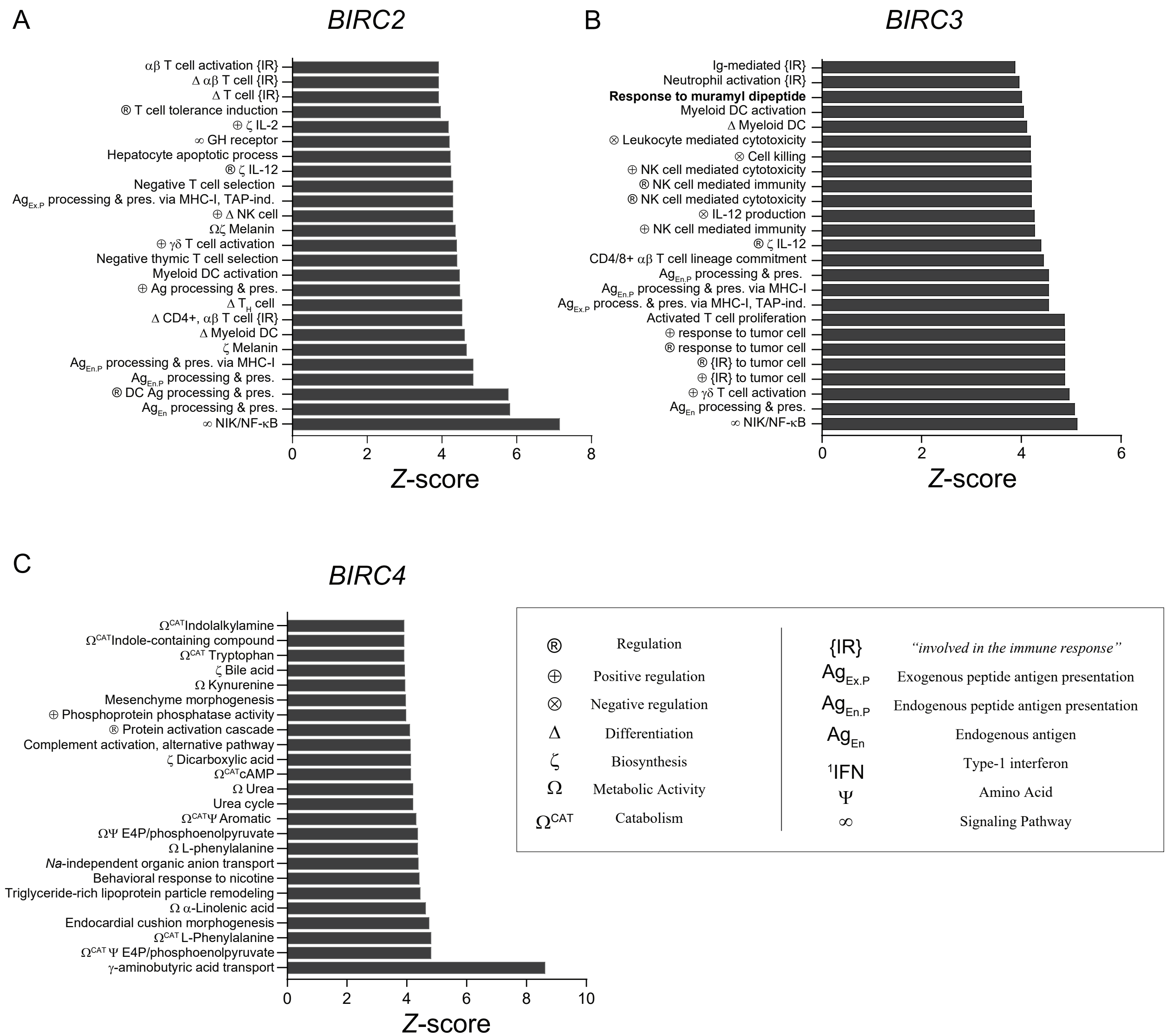
A
BIRC2
αβ T cell activation {IR}
Δ αβ T cell {IR}
Δ T cell {IR}
® T cell tolerance induction
⊕ ζ IL-2
∞ GH receptor
Hepatocyte apoptotic process
® ζ IL-12
Negative T cell selection
Ag Ex.P processing & pres. via MHC-I, TAP-ind.
⊕ Δ NK cell
Ωζ Melanin
⊕ γδ T cell activation
Negative thymic T cell selection
Myeloid DC activation
⊕ Ag processing & pres.
Δ T H cell
Δ CD4+, αβ T cell {IR}
Δ Myeloid DC
ζ Melanin
Ag En.P processing & pres. via MHC-I
Ag En.P processing & pres.
® DC Ag processing & pres.
Ag En processing & pres.
∞ NIK/NF-κB
0 2 4 6 8
Z-score
B
BIRC3
Ig-mediated {IR}
Neutrophil activation {IR}
Response to muramyl dipeptide
Myeloid DC activation
Δ Myeloid DC
⊗ Leukocyte mediated cytotoxicity
⊗ Cell killing
⊕ NK cell mediated cytotoxicity
® NK cell mediated immunity
® NK cell mediated cytotoxicity
⊗ IL-12 production
⊕ NK cell mediated immunity
® ζ IL-12
CD4/8+ αβ T cell lineage commitment
Ag En.P processing & pres.
Ag En.P processing & pres. via MHC-I
Ag Ex.P process. & pres. via MHC-I, TAP-ind.
Activated T cell proliferation
⊕ response to tumor cell
® response to tumor cell
® {IR} to tumor cell
⊕ {IR} to tumor cell
⊕ γδ T cell activation
Ag En processing & pres.
∞ NIK/NF-κB
0 2 4 6
Z-score
C
BIRC4
Ω CAT Indolalkylamine
Ω CAT Indole-containing compound
Ω CAT Tryptophan
ζ Bile acid
Ω Kynurenine
Mesenchyme morphogenesis
⊕ Phosphoprotein phosphatase activity
® Protein activation cascade
Complement activation, alternative pathway
ζ Dicarboxylic acid
Ω CAT cAMP
Ω Urea
Urea cycle
Ω CAT Ψ Aromatic
ΩΨ E4P/phosphoenolpyruvate
Ω L-phenylalanine
Na-independent organic anion transport
Behavioral response to nicotine
Triglyceride-rich lipoprotein particle remodeling
Ω α-Linolenic acid
Endocardial cushion morphogenesis
Ω CAT L-Phenylalanine
Ω CAT Ψ E4P/phosphoenolpyruvate
γ-aminobutyric acid transport
0 2 4 6 8 10
Z-score
® Regulation
⊕ Positive regulation
⊗ Negative regulation
Δ Differentiation
ζ Biosynthesis
Ω Metabolic Activity
Ω CAT Catabolism
{IR} "involved in the immune response"
Ag Ex.P Exogenous peptide antigen presentation
Ag En.P Endogenous peptide antigen presentation
Ag En Endogenous antigen
1 IFN Type-1 interferon
Ψ Amino Acid
∞ Signaling Pathway

Figure 26. BIRC2-4 predicted functional terms

List of gene ontogeny terms generated for genes encoding A) cIAP1 (BIRC2), B) cIAP2 (BIRC3), and C) XIAP (BIRC4) using the ARCHS4 engine for mining publicly available RNA-sequencing data from human and mouse datasets.

3.3 SM and regulatory T cell ablation potentiate anti-cancer immunity

3.3.1 SM in combination with an intratumoural T_{REG}-ablating antibody targeting CTLA-4 cures orthotopic MB49 tumours

I previously demonstrated that the MB49 model is refractory to checkpoint blockade of the PD1-PDL1 axis. Specifically, αPD-1 monotherapy, relative to isotype control antibody treatment, was unable to prolong survival in any of the MB49 tumour-bearing mice tested (Figure 13). I compared intratumoural T CD8 T cell expression of PD-1 following SM treatment. I found SM increased the relative expression of PD-1 in addition to the absolute amount of PD-1-expressing CD8 T cells in the tumour (Figure 27A). Upon combining SM with αPD-1, survival benefit was enhanced significantly, with a greater proportion of animals being cured of disease relative to SM alone (Figure 27B).

I previously demonstrated that the MB49 model is partially responsive to CTLA-4 checkpoint blockade (Figure 14). I compared peripheral T cell expression of CTLA-4 in conjunction with CD86, a cognate ligand, on DCs following treatment with both SM and anti-CTLA-4 (Figure 27C). I found SM and the combination of SM and anti-CTLA-4 reduced the proportion of CD3+ T cells acquired. Within these populations, CTLA-4 was up-regulated to only within the combination-treated cohort. Single-treatment of anti-CTLA-4 and the combination also marginally increased the number of CD11c+ events acquired. Within these populations, CD86 was up-regulated significantly with SM or the combination of SM and anti-CTLA-4. These results indicate T cell activation and egress from the periphery, with resident DCs up-regulating co-stimulatory domains. When combining SM with the Treg-depleting clone of αCTLA-4, I recorded complete eradication of tumours within all test mice with a

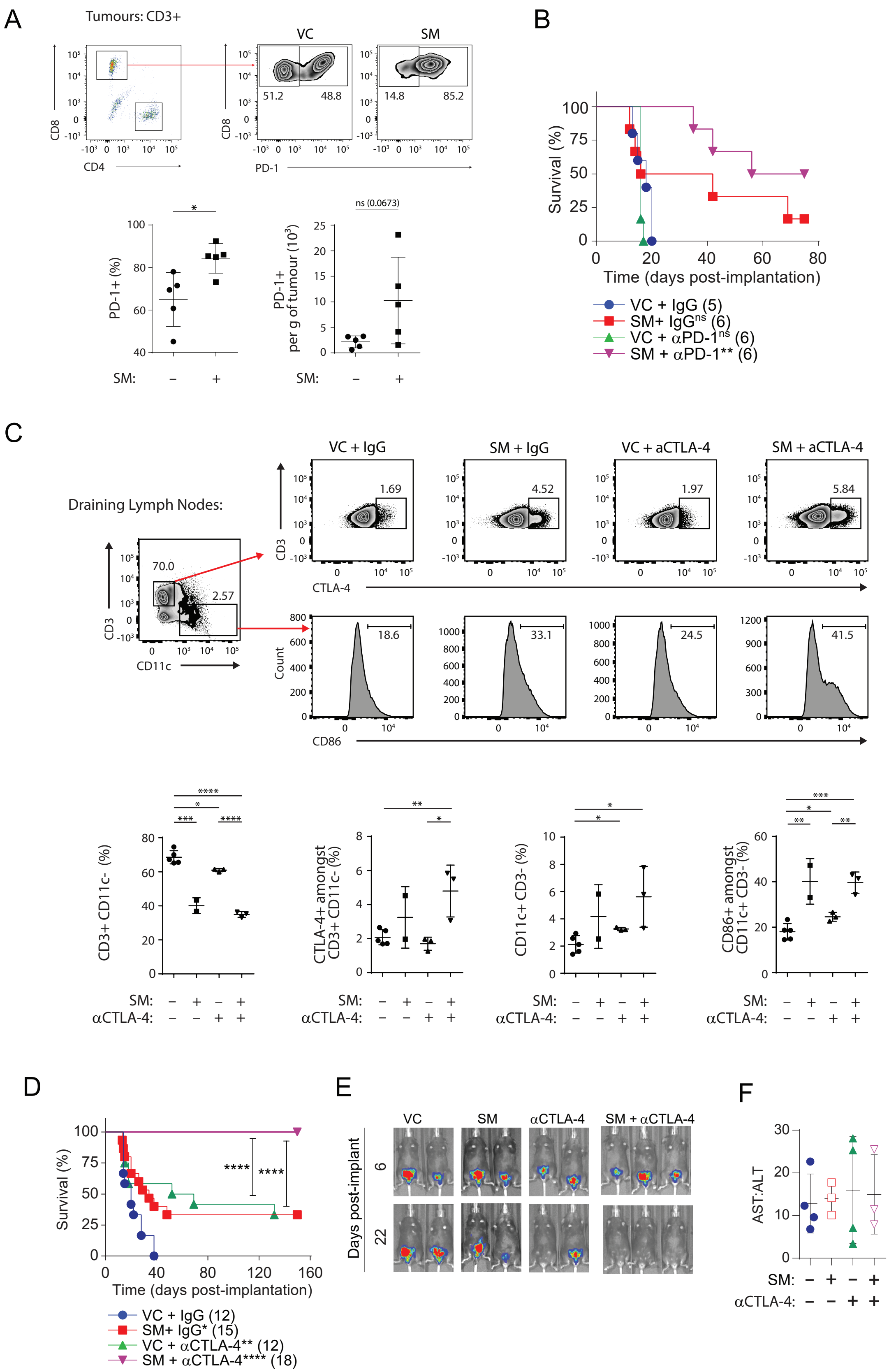
A
Tumours: CD3+
CD8
CD4
VC
SM
51.2
48.8
14.8
85.2
PD-1
PD-1+ (%)
PD-1+ per g of tumour (10³)
ns (0.0673)
SM:
B
Survival (%)
Time (days post-implantation)
VC + IgG (5)
SM+ IgGns (6)
VC + αPD-1ns (6)
SM + αPD-1** (6)
C
Draining Lymph Nodes:
VC + IgG
SM + IgG
VC + aCTLA-4
SM + aCTLA-4
70.0
2.57
CD3
CD11c
1.69
4.52
1.97
5.84
CTLA-4
18.6
33.1
24.5
41.5
Count
CD86
CD3+ CD11c- (%)
CTLA-4+ amongst CD3+ CD11c- (%)
CD11c+ CD3- (%)
CD86+ amongst CD11c+ CD3- (%)
SM:
αCTLA-4:
D
Survival (%)
Time (days post-implantation)
VC + IgG (12)
SM+ IgG* (15)
VC + αCTLA-4** (12)
SM + αCTLA-4**** (18)
E
VC
SM
αCTLA-4
SM + αCTLA-4
Days post-implant
6
22
F
AST:ALT
SM:
αCTLA-4:

Figure 27. The combination of SM and anti-CTLA-4 cures all mice of MB49 bladder tumours

A-F) 25,000 MB49-luc cells were intravesically instilled into the mouse bladder of 8-week-old naïve female C57BL/6 mice. Tumour-bearing mice were treated with A) vehicle control (VC; acid buffer) or Smac mimetic (SM, LCL161, 75mg/kg) by oral gavage on days 8, 10, 15, and 17, and intraperitoneally injected with 250μg of control IgG or anti-PD-1 (RMP1-14 clone) or anti-CTLA-4 (9h10 clone) on days 7, 9, 11, 14, 16, and 18. A) Mice were sacrificed, and tumours resected on day 12. Representative flow plots for viable (BV421, Zombie Violet) intratumoural CD3 (APC-Cy7) + CD8 (BV711) + CD4 (FITC) – events with corresponding PD-1 (BV605) expression. Statistical analysis was performed using an unpaired t test with Welch's correction. **, $p < 0.01$. B, D) Representative Kaplan-Meier survival plots with Mantel-Cox survival curve comparison test. Parentheses indicate number of mice in the treatment group. ***, $p < 0.001$. **, $p < 0.01$. *, $p < 0.05$. C) Mice were sacrificed and draining lymph nodes were resected on day 12. Upper panel depicts representative gating strategy identifying CD3 (APC-Cy7) + events and corresponding CTLA-4 (APC) expression. Lower panel depicts representative gating strategy identifying CD11c (FITC) + events and corresponding CD86 (PE-Cy7) expression. Statistical analysis was performed using ANOVA with Dunnett's multiple comparison test. *, $p < 0.05$. **, $p < 0.01$. ***, $p < 0.001$. ****, $p < 0.0001$. E) Bioluminescent imaging performed on indicated days is shown. Radiance scale: p/sec/cm^2/sr. F) Serum samples were collected, and parallel assays were conducted quantifying aspartate aminotransferase (AST) and alanine aminotransferase (ALT) liver enzyme levels.

significant improvement in survival probability after 150 days post-tumour instillation (Figure 28D, E).

To address treatment-related toxicity, I evaluated mouse serum during the treatment period in tumour-bearing mice for relative differences in liver enzymes. I found no significant changes in the relative amount of aspartate aminotransferase (AST) or alanine transaminase (ALT) levels, or respective ratios among the treatment groups (Figure 27F).

The absence of vestigial bioluminescence alongside long-term survival benefit within the entire test cohort prompted re-inoculation of autologous wildtype or histocompatibility-matched cells to gauge the formation of abscopal immunological memory. MB49 or B16F10 cells were injected in the flanks precisely 150 days following initial orthotopic instillation of MB49. Neither SM monotherapy nor SM in combination with αCTLA-4 yielded palpable tumours following re-challenge with MB49, whereas all mice challenged with B16F10 reached endpoint, as determined by tumour volume (Figure 28A).

The presence of the CD8 compartment is reportedly critical for sustaining anti-tumour benefit following αCTLA-4 monotherapy [Wolchok et al., 2008]. The NK compartment, significant constituents of the innate immune response, is not required to the same degree. Upon co- treatment with SM and αCTLA-4, additional treatment with neutralizing antibodies implicated multiple immune compartments as necessary for the increase in survival probability. Corroborating prior reports, depletion of the CD4 and CD8β compartments abrogated combinatorial survival benefit (Figure 28B, C).

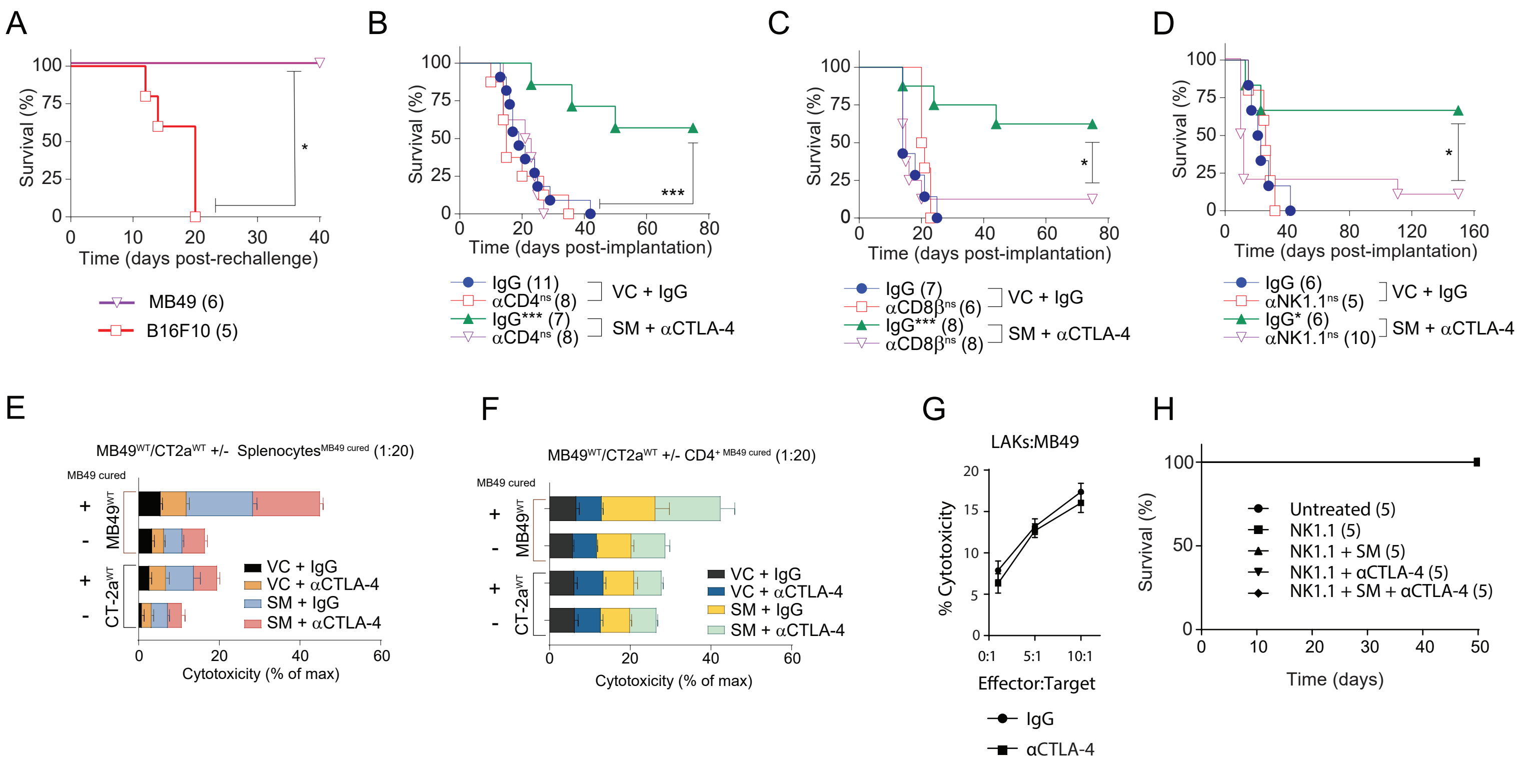

A
B
C
D
E
F
G
H
Survival (%)
Time (days post-rechallenge)
MB49 (6)
B16F10 (5)
Time (days post-implantation)
IgG (11)
αCD4ns (8)
IgG*** (7)
αCD4ns (8)
VC + IgG
SM + αCTLA-4
IgG (7)
αCD8βns (6)
IgG*** (8)
αCD8βns (8)
IgG (6)
αNK1.1ns (5)
IgG* (6)
αNK1.1ns (10)
MB49WT/CT2aWT +/- SplenocytesMB49 cured (1:20)
MB49 cured
MB49WT
CT-2aWT
VC + IgG
VC + αCTLA-4
SM + IgG
SM + αCTLA-4
Cytotoxicity (% of max)
MB49WT/CT2aWT +/- CD4+ MB49 cured (1:20)
LAKs:MB49
% Cytotoxicity
Effector:Target
IgG
αCTLA-4
Untreated (5)
NK1.1 (5)
NK1.1 + SM (5)
NK1.1 + αCTLA-4 (5)
NK1.1 + SM + αCTLA-4 (5)
Time (days)

Figure 28. SM and anti-CTLA-4 generate immune memory with survival benefit dependent on CD4, CD8, and NK cells

A) 150 days following initial MB49 instillation, cured mice were inoculated subcutaneously with 500,000 B16F10 or wildtype MB49 cells. B-D) For cell depletion experiments, tumour-bearing mice vehicle control (VC; acid buffer) or Smac mimetic (SM, LCL161, 75mg/kg) by oral gavage on days 8 and 10, and intraperitoneally injected with 250μg of control IgG or anti-CTLA-4 (9h10 clone) on days 7, 9, and 11. Additional control IgG or E) anti-CD4 (GK1.5 clone), F) anti-CD8-beta (Lyt3.2 clone), or G) anti-NK1.1 (Pk136 clone) by intraperitoneal injection on days 6, 9, and 13. Representative Kaplan-Meier survival plots with Mantel-Cox survival curve comparison test. Parentheses indicate number of mice in the treatment group. ***, $p < 0.001$. **, $p < 0.01$. *, $p < 0.05$. E, F) Splenocytes from naïve or MB49-luc cured mice were either left unpurified or magnetically-isolated CD4 T cells were co-cultured with wildtype MB49 or CT2A cells at 1:20 effector to target ratio. Co-cultures were treated with VC or SM (5μM, LCL161) and IgG or anti-CTLA-4 (1μg/mL, 9h10). Samples were incubated overnight, then supernatants were assayed for LDH release. Stacked bar graphs are displayed. G) LAKs were co-cultured onto MB49 target cells with control IgG or anti-CTLA-4 (9h10, 50ng/mL) for 48 hours, then supernatants were assayed for LDH release. H) Naïve tumour-free mice were treated with SM (LCL161, 75mg/kg) by oral gavage on day 2 and 4, along with intraperitoneal injections of anti-CTLA-4 (9h10, 200μg) on day 1, 3 and 5. Mice were depleted of NK1.1 cells (Pk136, 200μg) by intraperitoneal injection on days 0, 3, and 9. Representative Kaplan-Meier survival plots with Mantel-Cox survival curve comparison test. Parentheses indicate number of mice in the treatment group.

To evaluate immune memory-driven toxicity I isolated splenocytes from naïve or cured mice, then co-cultured raw splenocytes or purified T cells onto wild-type MB49 or histocompatibility-matched CT2A cells. Co-cultures were further treated with VC/SM or IgG/αCTLA-4, then assayed for cytotoxicity by LDH release. I found greater overall toxicity when co-culturing splenocytes or T cells from MB49- cured mice with homologous MB49 cells compared to heterologous CT2A cells (Figure 28E, F). Notably, cured splenocytes elevated cytotoxicity of CT2A cells to a greater proportion than naïve splenocytes onto MB49, suggesting that the cured splenocytes retain a modicum of non-specific cellular toxicity. When comparing T cell co-cultures, I found no significant changes in cytotoxicity between naïve or cured effectors cultured onto heterologous CT2A target cells, irrespective of additional in vitro treatment of SM or αCTLA-4. This remained consistent when comparing with homologous MB49 cells co-cultured with naïve effector T cells. Strikingly, MB49 cells co-cultured with MB49-cured effector T cells only significant elevated toxicity compared to all other treatment groups when further co-treated with SM and αCTLA-4. This suggests the combination treatment may further elevate antigen-specific effector cytotoxicity. Together with SMs enhancing target cell sensitivity to pro-inflammatory cytokines, the overall experiment demonstrates the combination strategy induces a durable T cell-driven anti-cancer functionality.

Surprisingly, antibody-mediated neutralization of the NK compartment abrogated survival benefit, suggesting the combination efficacy was heavily dependent on the presence of NK cells (Figure 28D). I co-cultured effector lymphokine-associated killer (LAK) cells with MB49 cells, treated the heterogenous cells with αCTLA-4 and then quantified lactate dehydrogenase (LDH) release as a measure of target cell cytotoxicity. Although an increasing ratio of effectors to target cells increased cytotoxicity, the inclusion of αCTLA-4 did not selectively enhance cytotoxicity compared to non-specific IgG control antibody (Figure 27G). To dismiss adverse toxicity from the dual treatments, I depleted NK cells in naïve tumour-free mice then treated with SM and/or αCTLA-4. No mice reached endpoint following repeated depletions or treatments (Figure 28H). I inferred NK cells mediate protection from metastases in tumour-bearing mice, however, did not rule out the direct involvement of NK cells in mediating anti-tumour immunity from the combination treatment.

Upon analyzing T cell subsets from the tumours of treated mice, I recorded a decrease in the relative and absolute (per gram of tumour tissue) quantity of CD3+ CD4+ FoxP3+ T_{REGs} in αCTLA-4-treated mice along with an associated increase in the ratio of CD8+ T cells to T_{REGs} (Figure 29A). Although αCTLA-4 potently depleted T_{REGs}, the depletion was incomplete when co-treated with SM. Despite this, the ratio of CD8+ T cells to T_{REGs} was elevated in the combination treatment. Furthermore, neither monotherapy nor the combination retained significant effect on T_{REGs} in both draining lymph nodes or Peyer's Patches, indicative of the precision of 9h10 clone to specifically deplete T_{REGs} in the tumour microenvironment and not the periphery.

To evaluate whether the combination therapy can potentiate de novo tumour-antigen specific immune responses, I instilled mice with MB49-GFP cells and then assessed uptake of tumour-associated GFP from CD11c+ DCs in the tumour microenvironment. Individual treatments of SM or anti-CTLA-4 increased the average number of TILs, however only to a significant degree upon co-treatment. I noted an increase in average tumour antigen uptake following the combination treatment, indicative of antigen spreading (Figure 29D).

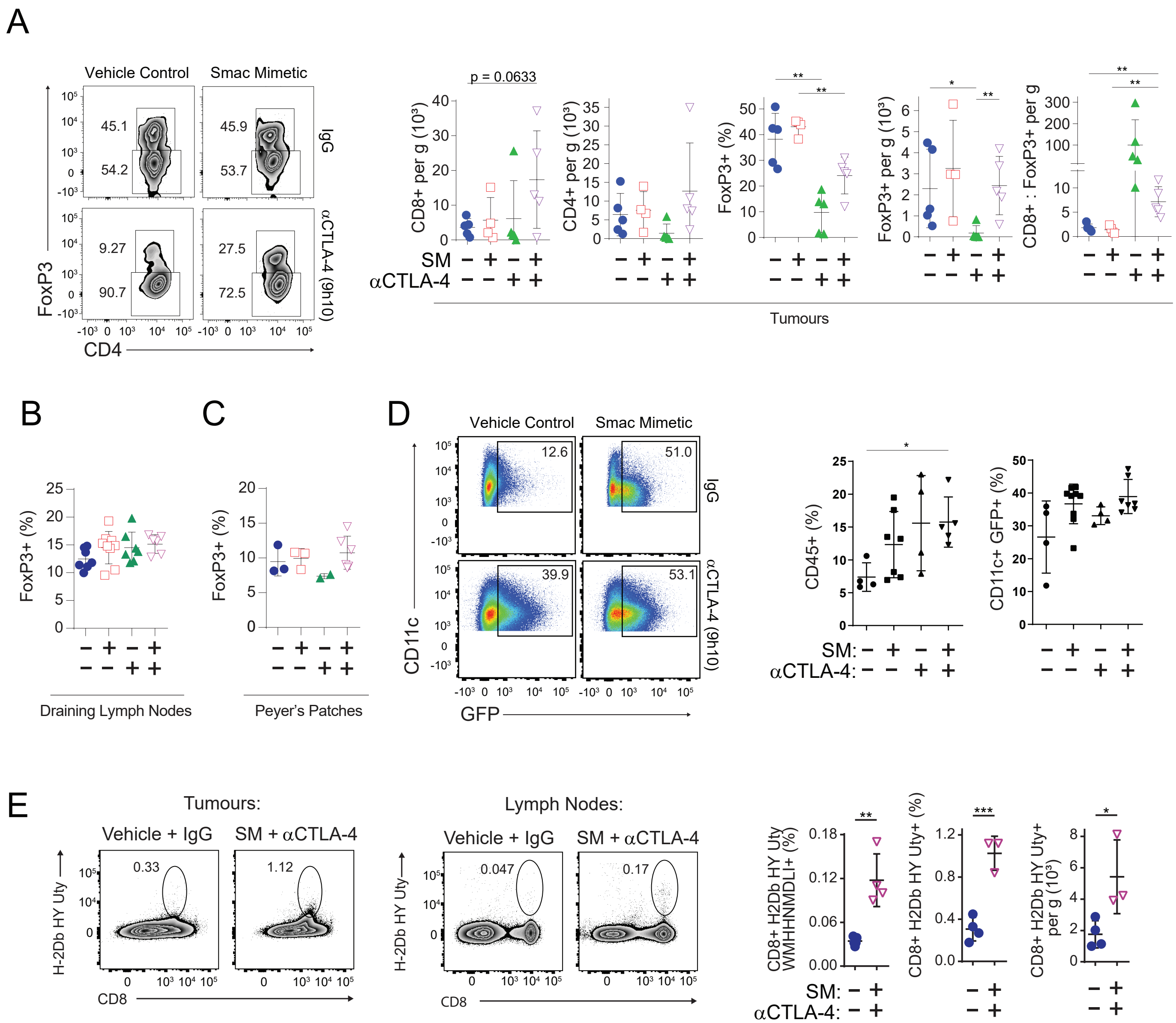
A
Vehicle Control
Smac Mimetic
IgG
αCTLA-4 (9h10)
45.1
54.2
45.9
53.7
9.27
90.7
27.5
72.5
FoxP3
CD4
p = 0.0633
CD8+ per g (10³)
CD4+ per g (10³)
FoxP3+ (%)
FoxP3+ per g (10³)
CD8+ : FoxP3+ per g
SM
αCTLA-4
Tumours
B
FoxP3+ (%)
Draining Lymph Nodes
C
FoxP3+ (%)
Peyer's Patches
D
Vehicle Control
Smac Mimetic
12.6
51.0
39.9
53.1
IgG
αCTLA-4 (9h10)
CD11c
GFP
CD45+ (%)
CD11c+ GFP+ (%)
SM:
αCTLA-4:
E
Tumours:
Vehicle + IgG
SM + αCTLA-4
0.33
1.12
H-2Db HY Uty
CD8
Lymph Nodes:
Vehicle + IgG
SM + αCTLA-4
0.047
0.17
H-2Db HY Uty
CD8
CD8+ H2Db HY Uty WMHHNMDLI+ (%)
CD8+ H2Db HY Uty+ (%)
CD8+ H2Db HY Uty+ per g (10³)
SM:
αCTLA-4:

Figure 29. SM and anti-CTLA-4 combination increases intratumoural CD8 to Treg ratio

25,000 MB49-luc or MB49-GFP cells were intravesically instilled into the mouse bladder of 8-week-old naïve female C57BL/6 mice. Mice were intraperitoneally injected with 250μg of control IgG or anti-CTLA-4 (9h10 clone) on day 8, then treated with vehicle control (VC; acid buffer) or Smac mimetic (SM, LCL161, 75mg/kg) by oral gavage on day 9. Mice were sacrificed on day 10 and A) tumours, B) draining lymph nodes, and C) Peyer's patches were resected for analysis by flow cytometry. Tumour samples were acquired immediately after adding counting beads, enabling absolute quantification of cells per gram of tumour. Plots represent viable CD3+ (APC-Cy7), CD8- (BV711), CD4+ (FITC) events from representative tumour samples. Box inserts discriminate between effector (FoxP3 low, PE) and regulatory (FoxP3 high) CD4 events. D) Plots represent viable (Zombie Violet, BV421) CD45+ (PerCP-Cy5.5) events from representative MB49-GFP tumour samples. Gates discriminate CD11c+ (APC) and GFP+ (PE) events. Statistical analysis was performed using ordinary one-way ANOVA with Tukey's multiple comparisons test. *, $p < 0.05$, **, $p< 0.01$. ***, $p < 0.001$. E) Plots and graphs represent CD8+ (BV711) WMHHNMDLI+ (H-Y peptide, APC) events from MB49-luc tumours. Statistical analysis was performed using unpaired t test with Welch's correction. *, $p < 0.05$, **, $p< 0.01$. ***, $p < 0.001$.

I next utilized an MHC Class I tetramer specific for an endogenous, Y chromosome-linked minor histocompatibility tumour antigen to evaluate the presence of strictly tumour-antigen-specific CD8+ T cells. I found the combination therapy significantly increases the frequency of HY/Uty (WMHHNMDLI)-specific CD8+ T cells in the tumour and draining lymph nodes, as well as the absolute quantity in the tumour (Figure 29E). Collectively, the data indicates the combination therapy fosters a tumour-antigen-specific response by potentiating multiple immune effectors.

3.3.2 Combination therapy requires precise intratumoural T_{REG}-ablation to cure orthotopic MB49 tumours

To substantiate the specificity of αCTLA-4-mediated T_{REG} depletion, I replaced αCTLA-4 with the traditional strategy to ablate $T_{REGs,}$ αCD25. As the alpha chain of the trimeric IL-2 receptor that is responsible for responding to IL-2, CD25 expression is elevated on T_{REGs} relative to conventional CD4 T cells or CD8 T cells [Setiady et al., 2010]. The lack of specificity toward depleting T_{REGs} likely contributed toward the inability of αCD25 to elicit survival benefit as a monotherapy relative to control isotype antibody treatment or enhance survival benefit upon co-treatment with SM [Figure 30A]. I further verified this disparity in surface expression within CD3+ T cell subsets from MB49 tumours [Figure 30B]. Upon treating with αCD25, I recorded selective depletion of CD25-expressing tumour-associated FoxP3+ $T_{REGs,}$ alongside depletion of tumour-associated CD8+CD25+ T cells.

The depletion of T_{REGs} from the tumour microenvironment by αCTLA-4 relieves localized immunosuppression, enabling effector cell activation. Optimal efficacy of αCTLA-4 therapy is reportedly dependent on the Fc gamma receptor 4 (FcγRIV)-mediated binding of tumour-infiltrating lymphocytes (TILs) on T_{REGs}, thereby enabling depletion by antibody-dependent cell-mediated cytotoxicity or phagocytosis (ADCC/ADCP) [Simpson et al., 2013]. I therefore utilized FcγR- deficient mice to determine whether survival efficacy was dependent on the ablation of T_{REGs}. As expected, survival benefit elicited from treating with a T_{REG}-depleting clone of αCTLA-4, along with the relative increase in the ratio of CD8+ T cells to T_{REGs} was abrogated when performed in FcγR-deficient mice (Figure 30C, D). I previously assessed tumour-

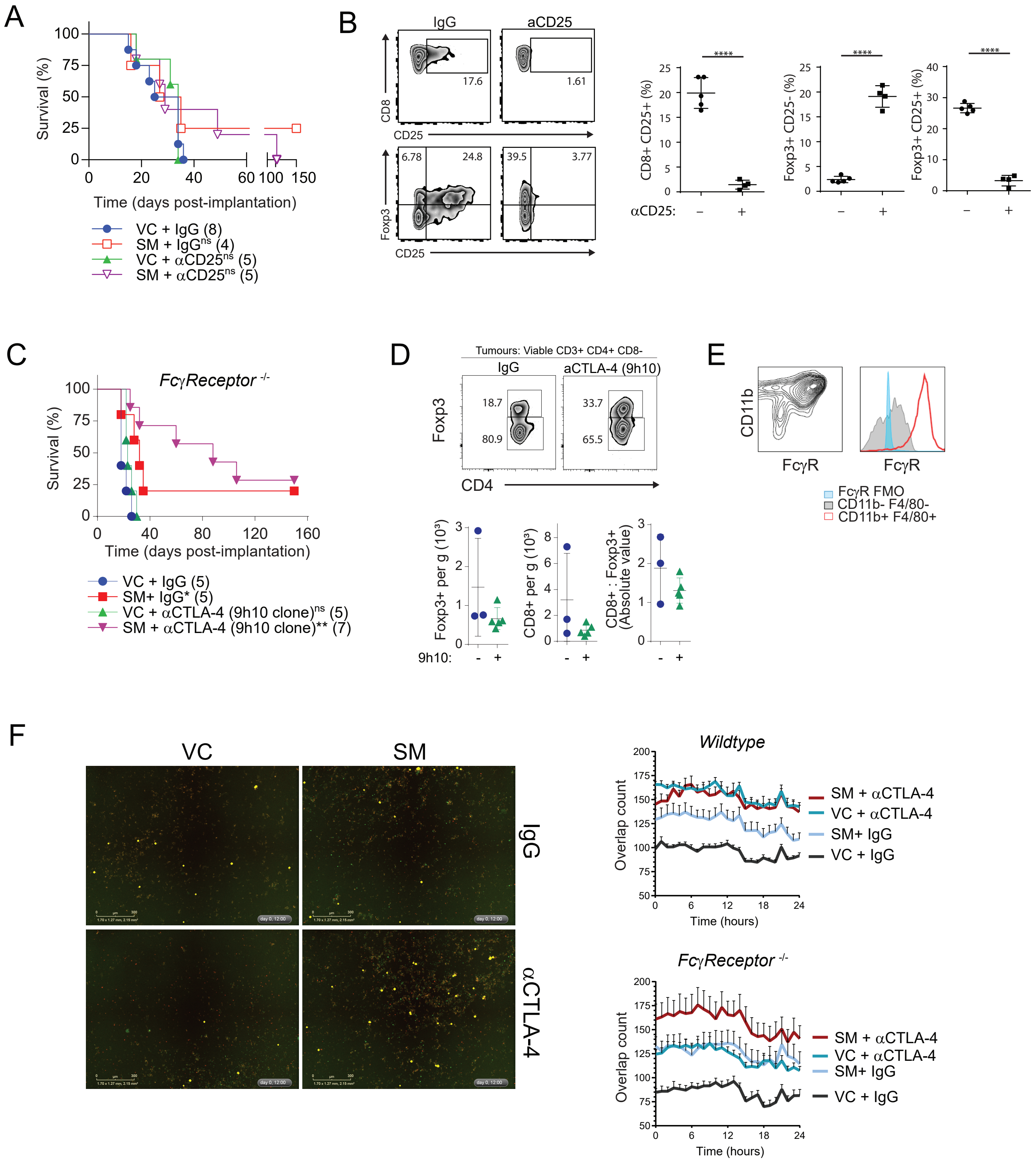
A
Survival (%)
Time (days post-implantation)
VC + IgG (8)
SM + IgG^ns (4)
VC + αCD25^ns (5)
SM + αCD25^ns (5)
B
IgG
aCD25
CD8
CD25
17.6
1.61
Foxp3
6.78
24.8
39.5
3.77
CD8+ CD25+ (%)
Foxp3+ CD25- (%)
Foxp3+ CD25+ (%)
****
αCD25:
C
FcγReceptor -/-
Survival (%)
Time (days post-implantation)
VC + IgG (5)
SM+ IgG* (5)
VC + αCTLA-4 (9h10 clone)^ns (5)
SM + αCTLA-4 (9h10 clone)** (7)
D
Tumours: Viable CD3+ CD4+ CD8-
IgG
aCTLA-4 (9h10)
Foxp3
CD4
18.7
80.9
33.7
65.5
Foxp3+ per g (10³)
CD8+ per g (10³)
CD8+ : Foxp3+ (Absolute value)
9h10:
E
CD11b
FcγR
FcγR FMO
CD11b- F4/80-
CD11b+ F4/80+
F
VC
SM
IgG
αCTLA-4
Wildtype
Overlap count
Time (hours)
SM + αCTLA-4
VC + αCTLA-4
SM+ IgG
VC + IgG
FcγReceptor -/-

Figure 30. Optimal combination efficacy requires precision Fc-dependent Treg depletion

25,000 MB49-luc cells were intravesically instilled into the mouse bladder of 8-week-old naïve or Fc-gamma receptor null (FcyR-/-) female C57BL/6 mice. A) Mice were treated with vehicle control (VC; acid buffer) or Smac mimetic (SM, LCL161, 75mg/kg) by oral gavage on days 8, 10, 15, and 17, and intraperitoneally injected with 250μg of control IgG or anti-CD25 (PC61 clone, 200ug) on days 7, 9, 11, 14, 16, and 18. Representative Kaplan-Meier survival plots with Mantel-Cox survival curve comparison test. Parentheses indicate number of subjects in the treatment group. B) Mice were treated as described in panel A, then sacrificed on day 11. Tumours were resected and processed for analysis by flow cytometry. Box inserts in upper plots represent CD25 (APC)-expression within viable (BV421, Zombie Violet) CD8 (BV711) + events. Lower panels distinguish CD25 expression relative to FoxP3 (PE)-expression. C) FcyR-/- Mice were treated with vehicle control (VC; acid buffer) or Smac mimetic (SM, LCL161, 75mg/kg) by oral gavage on days 8, 10, 15, and 17, and intraperitoneally injected with 250μg of control IgG or anti-CTLA-4 (9h10 clone) on days 7, 9, 11, 14, 16, and 18. Representative Kaplan-Meier survival plots with Mantel-Cox survival curve comparison test. Parentheses indicate number of subjects in the treatment group. **, $p < 0.01$. *, $p < 0.05$. D) Mice were treated as described in panel C, then sacrificed on day 11. Tumours were resected and processed for analysis by flow cytometry. Box inserts within plots distinguish FoxP3 (PE) expression amongst viable (BV421, Zombie Violet), CD3 (APC-Cy7) +, CD4 (FITC) +, CD8 (BV711) - events. E) Untreated MB49-luc tumour was resected and processed for flow cytometry 11 days following instillation. Plot represents CD11b (BV605) expression relative to FcyR. Histogram represents FcyR (PE) expression amongst CD11b and F4/80 (FITC) double positive or double negative populations, along with fluorescence minus one (FMO) control for FcyR antibody. F) Wildtype or FcyR-/- CD11b cells were magnetically isolated and labelled with a pH-sensitive red fluorescent dye, then co-cultured onto induced-regulatory T cells (iTregs) from FoxP3-GFP-DTR mice. Co-cultures were then treated with VC (DMSO) or SM (1μM, LCL161), then co-treated with control IgG or anti-CTLA-4 (9h10, 50ng/mL). Samples were incubated in a time-lapse microscope and imaged hourly. Representative images with quantification of green/red overlap (yellow spots) representing phagocytosis of iTregs by CD11b cells.

infiltrating myeloid cell populations and recorded that SM monotherapy did not reduce the frequency or absolute number of granulocytic precursors, the progenitors constituting FcγRIV-expressing TILs (Figure 18).

I verified Fc-dependent T_{REGs} neutralization by αCTLA-4 using time-lapse microscopy of CD11b-lineage myeloid cells co-cultured with CD4+ induced-T_{REGs} (Figure 30F). Pre-treating effector CD11b cells with a red pH-sensitive fluorescent dye enabled visualization of digested material undergoing lysosomal acidification. I utilized FoxP3-GFP mice for CD4+ isolation to ensure vivid discrimination of endogenously green induced-T_{REGs} from CD11b cells saturated with the red dye. The overlap of these colours, illuminating as a yellow/orange hue, in tandem with phase-contrast overlay, was used to infer instances of ADCP. Interestingly, αCTLA-4 depleted T_{REGs} when co-cultured with wildtype Fc-expressing cells yet was unaffected with the addition of SM. SM alone however, also elevated cell depletion relative to IgG control. Within the Fc-null group, αCTLA-4 was still able to deplete T_{REGs} to a greater degree than IgG, however this did not exceed the depletion achieved from treating with SM alone. The combination of both SM and αCTLA-4 yielded greatest depletion, exceeding either mono-treatment.

3.3.3 SM in combination with systemic T_{REG}-ablation synergize to potentiate T cell immunity and prevent TC-1 tumour establishment

To evaluate whether SM treatment may impact the phenotype of endogenous dendritic cells in a setting devoid of regulatory immune suppression, I treated FoxP3-DTR mice with SM and/or diphtheria toxin (DT) then pooled peripheral lymph nodes after 5 days for flow cytometric analysis. I recorded a significant increase in the proportional and intensity of expression of the endocytic receptor DEC-205 (CD205/Ly-75) upon T_{REG} depletion with SM co-treatment, relative to other treatments (Figure 31A). Given no foreign antigen was introduced, the consistent expression of co-stimulatory CD40 or B7 ligands indicate neither treatment nor the combination instigated self-reactivity, suggesting peripheral tolerance was preserved.

To quantify the presentation of foreign peptide by APCs, magnetically-isolated splenic CD11c+ cells from treated mice were pulsed ex vivo with dose-escalating SIINFEKL peptide for 2 hours. Samples were collected then stained with an MHC class 1 (H2kb/kd) antibody with discrete specificity toward SIINFEKL. I found no significant difference amongst vehicle control (VC)/PBS-treated samples compared to SM/PBS (Figure 31B). Interestingly, the inclusion of DT yielded divergent surface expression of the MHC-bound cognate peptide. Independently, DT uniformly diminished MHC-bound peptide expression compared to all other groups at each dosage. Upon combining SM with DT, surface expression of MHC-bound peptide was rescued, with marginal improvement compared to VC/PBS and SM/PBS at the highest dosage.

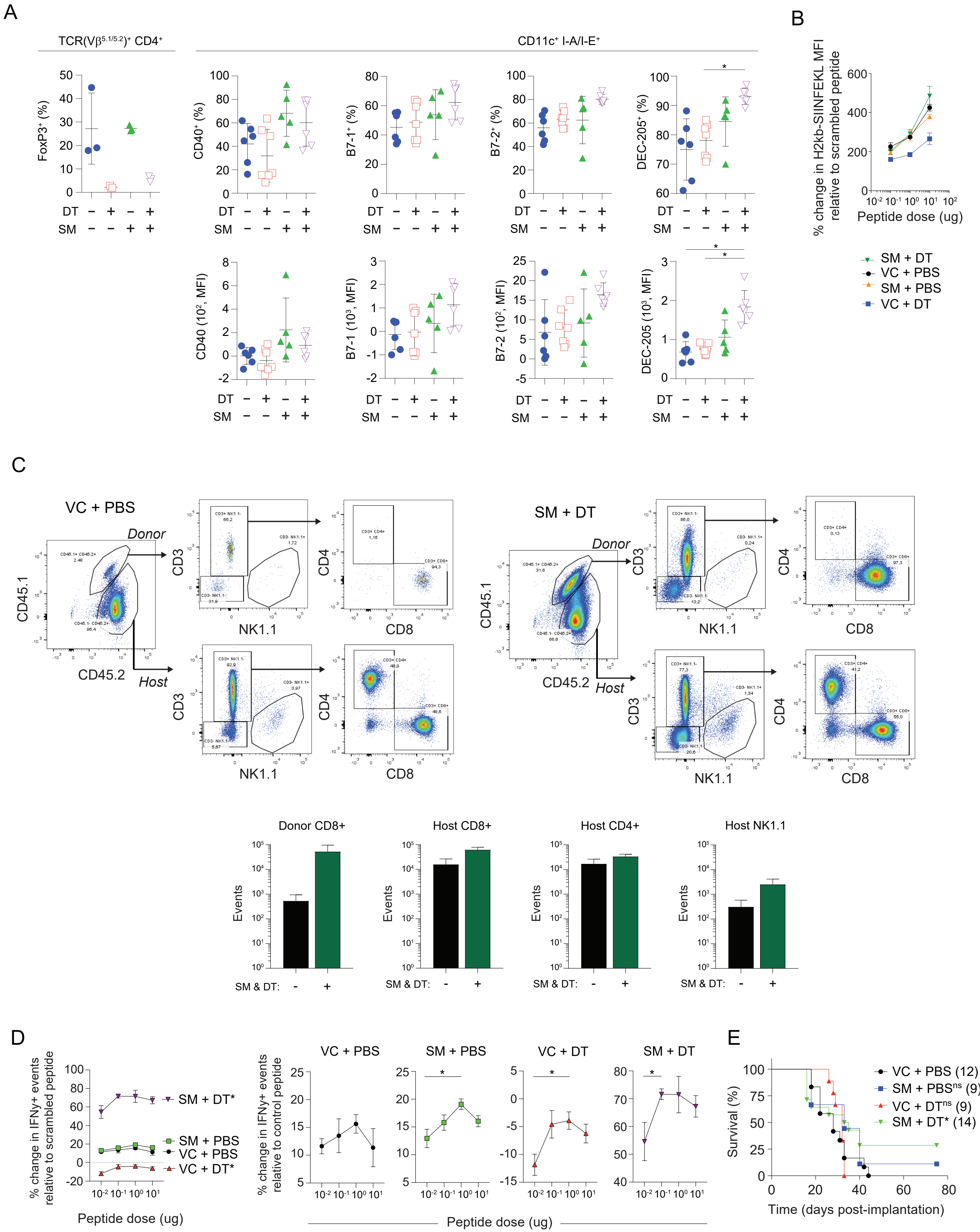

A
TCR(Vβ5.1/5.2)+ CD4+
CD11c+ I-A/I-E+
FoxP3+ (%)
CD40+ (%)
B7-1+ (%)
B7-2+ (%)
DEC-205+ (%)
CD40 (10², MFI)
B7-1 (10³, MFI)
B7-2 (10², MFI)
DEC-205 (10³, MFI)
DT
SM
B
% change in H2kb-SIINFEKL MFI relative to scrambled peptide
Peptide dose (ug)
SM + DT
VC + PBS
SM + PBS
VC + DT
C
VC + PBS
SM + DT
Donor
Host
CD45.1
CD45.2
CD3
NK1.1
CD4
CD8
Donor CD8+
Host CD8+
Host CD4+
Host NK1.1
Events
SM & DT:
D
% change in IFNy+ events relative to scrambled peptide
SM + DT*
SM + PBS
VC + PBS
VC + DT*
Peptide dose (ug)
% change in IFNy+ events relative to control peptide
VC + PBS
SM + PBS
VC + DT
SM + DT
Peptide dose (ug)
E
Survival (%)
VC + PBS (12)
SM + PBSns (9)
VC + DTns (9)
SM + DT* (14)
Time (days post-implantation)

Figure 31. SM treatment and Treg depletion increase antigen sensitivity and enhance prophylactic anti-cancer vaccination

A, B) Naïve 8-week-old FoxP3-DTR mice were injected with PBS or diphtheria toxin (DT, 1ug) intraperitoneally, and treated with SM (LCL161, 75mg/kg) by oral gavage on consecutive days (day 0 and 1). A) On day 3 mice were sacrificed and lymph nodes were isolated, pooled, and processed for flow cytometry. Left panel quantifies proportion of viable (Zombie Violet, BV421) regulatory (FoxP3, PE) T (TCRvB-5.1/5.2, PE-Cy7; FITC, FITC) cells. Right panel separately quantifies proportion and median fluorescence intensity (MFI) of CD40 (PE), B7-1 (CD80, PE-Cy5), B7-2 (CD86, BV786), and DEC-205 (PE-Cy7) amongst viable (Zombie Violet, BV421) CD11c (FITC) I-A/I-E (MHC class 2, BV605) cells. Statistical analysis was performed using ordinary one-way ANOVA with Tukey's multiple comparisons test. *, $p < 0.05$. B) On day 3 mice were sacrificed and CD11c cells were magnetically isolated from spleens. Cells were pulsed with scrambled or dose-escalating SIINFEKL peptide then incubated for 4 hours prior to staining with an H2kb-SIINFEKL-specific fluorescent antibody (PE). Cells were acquired by flow cytometry and MFI was quantified. Results were normalized as a percent change in MFI relative to control scrambled peptide. C) 1e6 magnetically-isolated OT-I CD8+ T cells were adoptively transferred into naïve 8-week-old FoxP3-DTR mice (day 0). Mice were intraperitoneally vaccinated with soluble OVA peptide (SIINFEKL, 100ug), injected with PBS or diphtheria toxin (DT, 1ug) intraperitoneally, and treated with SM (LCL161, 75mg/kg) by oral gavage on consecutive days (day 0 and 1). On day 5 mice were sacrificed and lymph nodes were isolated, pooled, and processed for flow cytometry. Plots represent donor and host immune cells (CD45.1, PerCPCy5.5; CD45.2, FITC) were further sub-gated to identify CD3 (APC-Cy7)-expressing T cells from NK1.1 (PE-Cy5) cells, with final gating distinguishing events as CD4 (AF700) or CD8 (BV786). Graphs represent event quantification. D, E) Naïve 8-week-old FoxP3-DTR mice were intraperitoneally vaccinated with E7 peptide (RAHYNIVTF, 50ug) on day 0, then injected with PBS or diphtheria toxin (DT, 1ug) intraperitoneally, and treated with SM (LCL161, 75mg/kg) by oral gavage on consecutive days (day 0 and 1). D) On day 5 Mice were sacrificed and CD8+ cells were magnetically isolated. CD8+ cells were then co-cultured with feeder APCs (magnetically isolated CD11c cells from naïve mouse spleens) and pulsed with E7 or scrambled (YHVNTAIFR) peptide for 6 hours prior to flow cytometric analysis. Relative change in IFNy (AF647) expression amongst CD8 (BV711) events was quantified and graphed. Statistical analysis was performed using ordinary one-way ANOVA with Tukey's multiple comparisons test. *, $p < 0.05$. E) On day 6 Mice were subcutaneously implanted with 100,000 TC-1 cells in the flank. Representative Kaplan-Meier survival plots with Mantel-Cox survival curve comparison test. Parentheses indicate number of Mice in the treatment group. *, $p < 0.05$.

Upon adoptive transfer of OT-1 T cells into FoxP3 recipient mice, I inoculated mice with soluble OVA peptide (SIINFEKL). Concurrent treatments of DT and SM were administered, then repeated the following day. I recorded a 2-log fold increase in the overall donor CD8+ event count (Figure 31C). As expected, there was no discernible fluctuation within host T cell compartments. Notably, a minor increase in NK1.1-expressing events was recorded.

I proceeded with validating the functional significance of these findings to gauge translational efficacy. I opted to incorporate the HPV-related oncoprotein-expressing lung epithelial mouse tumour model, an established pre-clinical system to evaluate vaccination-specific T cell responses against E6/E7 antigens. To examine T cell antigen sensitivity, bulk CD8 T cells from E7 vaccinated and SM/DT treated FoxP3-DTR mice spleens were magnetically-isolated then co-cultured with naïve feeder CD11c+-isolated APCs. Samples were pulsed with scrambled or dose-escalating homologous peptide, then collected to quantify relative change of IFNγ expression by flow cytometry [Figure 31D]. DT in isolation uniformly diminished IFNγ expression, corroborating the decrease in peptide presentation from prior experimentation with ovalbumin peptide. Furthermore, SM alone did not significantly alter IFNγ expression, yet the combination of SM and DT drastically enhanced expression irrespective of dosages. This suggests SM, upon systemic ablation of T_{REGs}, yields a hyper-responsive CD8 T cell cohort with possibly variable antigen specificity.

I sought functional significance supporting SM-treatment enhancing vaccination sensitivity, with or without additional depletion of T_{REGs}. Following E7 peptide vaccination with simultaneous combination treatment of SM and/or DT in FoxP3-DTR mice, I subcutaneously inoculated syngeneic TC-1 cells into the flanks of all mice. I recorded consistent outgrowth among all mice treated with VC/PBS, and VC/DT. Promisingly, SM treatment prevented outgrowth in a small, albeit statistically insignificant cohort. Upon concurrent treatment of SM with DT, I recorded complete rejection of the graft in most of the mice alongside statistically significant improvement in survival probability (Figure 31E). These results demonstrate functional significance supporting an enhanced immune response upon SM co-treatment with T_{REG} ablation.

4.0 DISCUSSION

4.1 Overview

Our lab is focused toward incorporating combination platforms to demonstrate synergy with other therapeutic modalities in hopes of successfully advocating for the use of SMs in human patient trials. To my surprise, SM generated durable cures in MB49 as a stand-alone therapy. Despite the success of these experiments, my focus was shifted firmly toward combining SM with anti-CTLA-4 given the superior survival benefit generated along with the prevalence of anti-CTLA-4 in ongoing clinical trials. This strategy reflects the practical landscape of clinical trials, wherein combining an experimental therapeutic with a more established, proven pharmaceutical modality is much more likely to enable approval by regulatory bodies than if the experimental drug was tested on its own. Furthermore, the prevalence and success of ICIs in clinical trials requires stand-alone experimental drugs to surpass the perceived benefit of these ICIs.

When advocating for the use of an experimental pharmaceutical agent in clinical practice, one approach is to elucidate its potential mechanisms of action. This involves understanding how the agent interacts with biological systems to produce its therapeutic effects. Deciphering the precise function of an agent is critical for generating hypotheses about the agent's potential uses and efficacy, both required for designing successful experiments and clinical trials. By exploring the immunomodulatory effects of SM in a tumour-free setting, I have created a foundation for future studies to evaluate novel combinatorial platforms for the treatment of cancer. In addition, the results supporting SM mediating cross-priming indicates SMs may be effective vaccine adjuvants. This may further be extended to the applicability of SM as a pre-clinical tool for manipulating in vitro systems, thereby accelerating, or enhancing the production of cells used in adoptive cell therapies, for example.

4.2 Evaluating MB49 sensitivity to selected therapeutic intervention

The preferential lysis of cancer cells by infectious agents is a fundamental component of oncolytic remedies, including BCG. Tumour necrosis factor (TNF), originally discovered within necrotic neoplasms, is an acute-phase stress molecule implicated in signal transduction promoting cell death or survival. Notably, clinical administration of recombinant TNF is currently restricted to isolated limb perfusion, as systemic dissemination elicits toxic shock [Aderka et al., 1998]. Anecdotally accepted to enforce BCG's localized anti-tumour cytotoxicity [Redelman-Sidi et al., 2014], the polarizing phenomenon elicited by TNF signalling is firmly established as principally dependent on intracellular cIAP1/2 levels [Mahoney et al., 2008]. The ablation of cIAP1/2, following SM treatment for example, precludes receptor inducible kinase 1 (RIPK1) poly-ubiquitination, thereby diverting otherwise pro-inflammatory signalling towards cell death. The prevalence of specific molecular components enables the formation of complexes that determine the variety of ensuing cell death cascades [Lacasse, 2015]. SM has shown to sensitize cancer cells to cell death following treatment with TNF-alpha or IFN-beta in vitro [Beug et al., 2014]. Furthermore, SM has been demonstrated to reverse resistance to TRAIL within human UCC cell lines [Metwalli et al., 2010]. Another study found SM sensitizing human UCC cell lines to gemcitabine and cisplatin in vitro [Lee et al., 2013]. My results demonstrated that BCG and TNF-alpha may enable growth or attrition of various UCC cell lines when administered alone in vitro (Figure 6). The addition of SM following TNF-alpha treatment, however, diminished the viability of specific cell lines, namely MB49.

I opted to utilize the MB49 cell line for ensuant in vitro experiments, as this cell line was used for in vivo modelling. Notably, I piloted intravesical instillation of MBT2 cells within

C3H mice, however failed to verify tumour outgrowth within multiple cohorts (data not shown). Apart from MB49, the MBT2 model is the other prevalent syngeneic model used to model UCC. I attributed the failure of the pilot studies because of immunological rejection of the graft by the host. This has been proposed elsewhere, as MBT2 cells have been found to be contaminated with a type-C retrovirus [De Boer et al., 2000].

I found MB49 cells resistant to various doses of BCG with or without SM, yet susceptible to the combination of SM and TNF-alpha (Figure 6-9). The sensitivity of the combination was transient, as the cells inevitably rebounded and continued to proliferate in vitro. Notably, neutrophils are acute responders to immune stimulation and produce copious amounts of inflammatory cytokines at the site of infection. A previous study found BCG-stimulated neutrophils enable the secretion of TNF-alpha, TRAIL, and FasL [Jinesh et al., 2012]. This study found that the addition of SM facilitated RT4 human cancer cell line attrition through TNF-alpha, but not TRAIL or FasL.

Another promising therapeutic strategy is the use of engineered oncolytic viruses. The selective replication of viruses within cancer cells enables protracted infection and thereby oncolysis. I found that oncolytic VSVd51 successfully diminished the viability and increased the cytotoxicity of MB49 cells (Figure 10). Diminished cell expansion following viral infection is sustained for the duration of the analysis, whereas cells treated with recombinant TNF in combination with SM eventually revert toward expansion akin to the PBS-treated assay cohort. This discrepancy reflects the brief effects of synthetic chemical modalities utilized in isolation, analogous to standard chemotherapy treatment. The use of engineered oncolytic viruses thus presents an additional strategy that may be used to generate anti-cancer efficacy against MB49. The effectiveness of VSVd51 encoding TNF transgenes coupled with the potency of the SM+TNF-alpha combination rationalizes the use of oncolytic viruses with simultaneous SM treatment. This avenue has been explored extensively by the lab in previous studies [Beug et al., 2014; Beug et al., 2018]. Collectively, these experiments rationalized adopting a variety of therapeutic strategies, either clinically approved or non-approved, in combination with SM to treat MB49 in vivo.

In line with other reports, live-culture or lyophilized BCG failed to increase survival probability of MB49-bearing mice following multiple instillations in vivo (Figure 12) [Mangsbo et al., 2008; Andrade et al., 2010]. This resistance is a significant factor responsible for the prevalence of this model in preclinical studies, as improving response to BCG-resistant cases is a prevailing focus of UCC research. Notably, the non-specific debulking of tumour cells is likely responsible for the increase in survival probability found in select mice [Iqbal & Hussain, 2014].

Blockade of the PD1-PDL1 axis by use of ICIs has been granted approval for the treatment of advanced non-resectable UCC [Ning et al., 2017]. I found that blockade of either PD-1 or PD-L1 by use of monoclonal antibodies failed to generate any increase in survival benefit (Figure 13). Monoclonal antibody blockade of CTLA-4, however, increased survival benefit in approximately half of the mice treated (Figure 14). This finding has been replicated elsewhere within mice bearing subcutaneous MB49 [Shi et al., 2016].

Notably, the aggressive nature of the orthotopic model coupled with the small size of the primary tumours created technical obstacles for the downstream analysis of the tumours. The tendency for the mice to be healthy without showing any visual symptoms representing sickness or distress, yet classified as endpoint on successive days, suggests MB49-bearing mice generally succumbed due to obstruction of the urinary tract, thereby compromising the function of an essential organ. This would often occur without tumours growing very large. The small tumour sizes would often lead to cell yields that would be far below the threshold required for downstream assays, thereby requiring greater number of animals in experimental cohorts to generate data that could be compared with statistical analysis. This practice, albeit necessary for generating data, may inadvertently enable the analysis of non-responding mice. Specifically, the treatments generated durable cures rapidly to the point wherein resected tumours would be too small to process for analysis. To compensate for this technical obstacle, for ex vivo cytotoxicity assays I utilized splenocytes from cured mice and further treated them following isolation, instead of incorporating tumour-infiltrating CTLs from prior-treated tumour-bearing mice.

Our lab has previously failed to record an increase in survival benefit in immunocompetent and orthotopic mouse models of intracranial glioblastoma (CT-2A, GL261 cell lines) [Beug et al., 2017], systemic multiple myeloma (MPC-11) [Beug et al., 2017], adrenal neuroblastoma (NXS2, N2A) [unpublished results], and mammary carcinoma (EMT6) [Beug et al., 2014] following oral gavage SM treatment. These studies focused on incorporating combination strategies to elicit survival benefit. I found that oral gavage SM treatment alone successfully eradicates orthotopic MB49 and significantly prolongs survival probability (Figure 15). This model may therefore be utilized to evaluate pivotal questions in molecular biology that remain outstanding. For example, it is prudent to explore whether SM treatment discretely requires engagement of apoptotic or necroptotic machinery in the tumour itself or the host to confer survival benefit.

A significant benefit of immune-stimulating therapies is the ability to instill immunological memory of the initial allograft following tumour clearance. This confers a translational benefit wherein an immune response may be recalled upon reintroduction of the malignancy, a common recurrence following conventional chemotherapeutic- or radiotherapeutic- intervention. This protective recall response protects the host from recurrent disease without the administration of additional treatments. I recorded durable protection of MB49-cured mice from additional inoculations of MB49 distal to the bladder, thereby demonstrating abscopal immunity to MB49 (Figure 15).

Immune memory recall manifests from the clonal expansion of tumour-specific cytotoxic T cells. Antibody-mediated depletion of the CD4 and CD8-beta compartments simultaneously with SM treatment completely abrogated survival benefit, firmly implicating T helper and cytolytic immune compartments as necessary for anti-cancer efficacy of SM treatment (Figure 16). Notably, the depletion of these pivotal compartments alters the development of the evolving tumour. Upon verification of antibody-mediated depletion of requisite compartments in the tumour microenvironment, I recorded differing proportions of T and NK cells (Figure 17). The lack of double-positive events was expected as this occurs during early development of T cells [Parel et al., 2004]. The presence of double-negative events was less pronounced within spleen samples, and considerably less within tumour samples, where double-negative events were detected in sizeable amounts. This may have been an artifact of the consistent gating strategy maintained for the analysis of all samples, despite the use of an alternative clone for depletion (GK1.5) compared to detection (RM4-5). Notably, double negative T cells have been documented in cancer tissues, however the function of these cells has not been elucidated [Okamura et al., 2020]. Recent reports suggest these cells may retain anti-tumour functionality, however more studies are required to substantiate these claims [Li et al., 2020]. Despite the dispensability of NK1.1-expressing cells, the role of NKT cells may have been overlooked in this study, as the general gating strategy may have excluded their detection. Specifically, the presence of two distinct populations as visualized with the contour plots within CD3+NKp46- tumour samples (Figure 17A, B) suggest NKT cells are enriched in the tumours compared to secondary lymphoid structures.

As the generation of an adaptive immune response to neoplasm requires the orderly processing and presentation of tumour antigens by specialized immune cells, I evaluated the phenotypes of intratumoural DCs following treatments. I recorded a consistent increase in the absolute quantity of CD11c+ DCs in the tumour microenvironment, with a corresponding increase among sub-gated CD40+ CD86+ and DEC-205+ events (Figure 18A). This data provides evidence supporting pronounced DC activation in the tumour microenvironment.

The trafficking of tumour-associated materials was verified using the MB49-GFP cell line, wherein I report robust uptake of GFP by DCs in the peripheral lymph nodes of orthotopic tumour-bearing mice (Figure 19). Notably, the differences between tumour samples may result from tumour cells losing expression of GFP, or overall intensity being diminished, as the tumour develops within the host [DuPage et al., 2012]. Collectively, these results suggest SM treatment promotes tumour-specific antigen trafficking or spreading.

The presentation of tumour-antigen by APCs in the peripheral lymph nodes is required to effectively form clonally-expanded tumour-specific CTLs that may eventually be trafficked back into the tumour microenvironment and initiate tumour-specific cytotoxicity (Figure 4). As this process requires the coordinated activity of multiple immune cells, I explored the effects SMs would retain on cell types needed for generating an antigenic anti-tumour response.

4.3 Evaluating DC/T cell modulation by SM

The rationale supporting SM treatment enabling antigen presentation was formulated based upon prior reports establishing NIK stabilization in regulating the cross presentation of soluble antigen by dendritic cells [Lind et al., 2008]. This, in tandem with constitutive proteasomal degradation of NIK by cIAP2 [Zarnegar et al., 2008], would suggest IAP antagonism by SMs would promote cross-presentation, thereby priming of T cells. Notably, a study evaluating SM-induced effects on T cell biology reported SM enhanced co-stimulation in vitro [Dougan et al., 2011]. Collectively, I hypothesized SM treatment would augment NIK-dependent cross-presentation within dendritic cells, further engaging cognate T cells toward clonal expansion.

My initial experimentation revealed SM treatment altering the number of isolated CD11c cells in a dose-dependent manner (Figure 20), whereas bulk immature BMDCs expanded with dose-escalating SM (Figure 21). The latter effects were distinct from other established stimulatory or inhibitory treatments tested, suggesting a distinct functional population may have been selectively propagated with SM treatment. Indeed, SM treatment retained a greater proportion of Zbtb46+ cells from BMDCs in vitro (Figure 22A). Furthermore, the pronounced co-expression of NIK with CD11c (Figure 22B) underscores the relevance of NIK signaling within DCs. Upon evaluating CD4 T cells in vitro, I found SM treatment enhanced viability, and promoted a type-1 helper pro-inflammatory phenotype. Notably, the stability of these lineages depends on constitutive cross-talk amongst a variety of host cells. The dynamic expression of the IAPs within different subclassifications of immune cells complicates evaluation of the discrete effects SM treatment has on the overall immune response. Although I attempted to breed NIK-knockout alymphoplasia mice for the purpose of discretely parsing the necessity of a functioning NIK molecule, I was unsuccessful with breeding these mice.

This prevented investigation of SM's effects on specifically DCs or T cells, using cell-intrinsic NIK-knockout samples.

To evaluate the collective impact of SM treatment on stimulating a T cell response specific for a foreign antigen, I transplanted antigen-restricted T cells into naïve mice then vaccinated with the cognate peptide. SM treatment successfully expanded the pool of antigen-specific T cells, effectively priming the T cell response toward the model antigen (Figure 25A). This experiment isolates the 3rd step within the cancer immunity cycle (Figure 4), evaluating priming by SM-mediated immunological modulation in a discrete and tumour-free setting. I further tested the physiological relevance of this response by challenging mice with melanoma cells engineered to express the model antigen, then vaccinating against the antigen with SM co-treatment (Figure 25C). Determining whether this response is a manifestation of IAP antagonism within T cells and/or DCs remains to be evaluated. The translational application of this finding also requires further exploration, as T cell priming is imperative for the clearance of specific viruses [Nobs et al., 2016].

The purported pleiotropy of cIAP1/2 within critical components of the adaptive immune system (Figure 26) coupled with their regulation of life or death signaling suggests these non-redundant IAPs may execute an evolutionarily-conserved mechanism essential for survival. Indeed, the prevalence of IAP family members as cytoplasmic counterparts to transmembrane TNFSFR members provides evidence supporting the involvement of the IAPs in enabling diverse immune responses [Beug et al., 2012].

4.4 Testing and evaluating SM in combination with anti-CTLA-4 ICB

Checkpoint blockade is an emerging anticancer platform that has promoted durable long-term survival in patients bearing advanced disease. Despite its success, many patients are resistant to specific ICIs. My work demonstrates anti-PD-1 or anti-CTLA-4 treatment enhancing survival benefit within MB49-bearing mice upon combining with SM (Figure 27). I found SM treatment up-regulated PD-1 on intratumoural CD8 T cells, suggesting a greater proportion of T cells are primed for anti-PD-1 treatment (Figure 27A). Similarly, SM and CTLA-4 blockade increased the expression of CTLA-4 on CD3+ T cells and CD86 on CD11c DCs in the peripheral lymph nodes (Figure 27C). The increase in expression of the target receptors of PD-1 and CTLA-4 ICB suggests SM treatment upregulates the signaling axes these treatments enact on. The complete eradication of tumours with the novel combination of SM and anti-CTLA-4 (Figure 27D, E) prompted further evaluation aimed at exploring the mechanism responsible for enhanced survival benefit.

Re-challenge experiments evaluating tumour-specific immune memory (Figure 28A) verified the combination therapy engaged components of the adaptive immune response, reiterating the previous experiments evaluating SM mono-therapy. Tumour regression following CTLA-4 blockade has been evaluated extensively and has been firmly established to enable its effects by engaging T cells [Chambers et al., 1997]. I found the combination of SM and anti-CTLA-4 was dependent on the presence of CD4, CD8, and NK cells (Figure 28B-D).

I opted to utilize splenocytes and purified T cells from cured mice for functional analyses as the small tumour sizes following treatments prevented isolation of sufficient number of effector cells. I utilized CT2A cells as control target cells given their similar sensitivity to the combination of SM and TNF in vitro [Beug et al., 2017]. Notably, cured splenocytes elicited greater cytotoxicity of heterologous CT2A cells than naïve splenocytes co-cultured onto MB49 cells. The non-specific cytotoxicity from splenocyte co-cultures onto heterologous cells is inferred given elevated toxicity when further treated with SM. Furthermore, this may be a result of differential intrinsic sensitivity between cell lines to pro-inflammatory cytokines, such as TNF, thereby increasing susceptibility for target cells to undergo cell death. The increase in target cell death upon further treating cured T cells and MB49 co-culture with SM in combination with αCTLA-4 suggests the dual treatment strategy potentiates T cell-mediated cytotoxicity of MB49 cells. This implicates the combination as promoters of cancer cell cytotoxicity in the tumour microenvironment.

The necessity of NK cells was a surprise, as this compartment was not required to sustain survival benefit with SM monotreatment in my prior experiments (Figure 16) and has not been highlighted as a significant factor with αCTLA-4 treatment in the literature thus far. Indeed, αCTLA-4 did not increase LAK-mediated cytotoxicity onto MB49 target cells (Figure 28G). I administered the treatments with NK depletion in a tumour-free setting, which failed to generate any lethal toxicity (Figure 28H), negating the possibility of drug-induced adverse reaction. Given the aggressive infiltration of adjacent organs by MB49 cells, coupled with NK activity reportedly associated with preventing the formation of metastasis [Isaacson, 2019], I surmised NK cells were crucial to restraining ectopic growth.

The ratio of CD8+ T cells to FoxP3+ T_{REGs} in the tumour microenvironment strongly correlate neoadjuvant chemotherapy response among invasive urothelial carcinoma cancer patients [Baras et al., 2016], therefore representing a superior estimate of objective response compared to the densities of either CD8+ T cells or FoxP3+ T_{REGs}. The 9h10 clone of αCTLA-

4 has been previously identified to potently deplete intratumoural Tregs. I verified this within the MB49 model as αCTLA-4 treatment almost completely abrogated TREG-levels in the tumour but not the draining lymph nodes or Peyer's Patches (Figure 29A-C). Despite additional SM treatment slightly mitigating the complete ablation of TREGs in the tumours, I recorded a significant increase in the ratio of CD8 T cells to FoxP3+ TREGs within the tumour microenvironment following the combination treatment of SM and αCTLA-4. Although the combination treatment did not potentiate tumour antigen spreading (Figure 29D), I was able to verify an increase in tumour-specific T CD8+ T cells in the draining lymph nodes and the tumour microenvironment (Figure 29E).

The potent depletion of TREGs by αCTLA-4 prompted evaluation of alternative forms of TREG depletion to verify whether this was the prevailing mechanism required for the increased survival benefit upon combining with SM. Targeting CD25 (alpha chain of the IL-2 receptor) is considered the traditional strategy to neutralize TREGs and has been evaluated clinically using an engineered fusion protein combining IL-2 and DT (denileukin diftitox, Ontak) [Litzinger et al., 2007] and a monoclonal antibody (daclizumab, Zinbryta) [Rech and Vonderheide, 2009]. Monotreatment with αCD25 failed to elicit any survival benefit (Figure 30A). Furthermore, SM and αCD25 co-treatment did not enhance survival benefit compared to SM alone. I found αCD25 treatment selectively depleted intratumoural FoxP3+ TREGs that expressed CD25, but spared FoxP3+ cells that did not express CD25 (Figure 30B). The treatment also depleted intratumoural CD25-expressing CD8 T cells. These findings reiterate the lack of specificity and precision of αCD25 as a TREG-depleting agent [McNeil et al., 2007].

The Fc-portion of αCTLA-4 enables the antibody to bind Fc receptors without interfering with its ability to bind its target, CTLA-4. This enables CTLA-4-expressing cells to be brought within proximity to Fc-expressing cells. This enables Fc-expressing cells to elicit an effector response wherein target TREGs are phagocytosed (ADCP) or exposed to cytotoxic elements (ADCC) [Smyth et al., 2014]. I utilized Fc-receptor deficient mice to evaluate whether the increase in survival benefit with the combination of SM and αCTLA-4 was dependent on the TREG-depleting capability of αCTLA-4. Upon repeating the combination treatment survival study with Fc-receptor deficient mice I recorded no significant difference in survival benefit between SM alone and the combination of SM and αCTLA-4 (Figure 30C). I verified that the 9h10 clone of αCTLA-4 was unable to deplete intratumoural TREGs nor increase the ratio of intratumoural CD8 T cells to FoxP3+ TREGs within Fc-deficient hosts (Figure 30D). Collectively, these results suggest that the combination treatment yielded optimal survival benefit upon intratumoral TREG depletion. I simulated the depletion of TREGs in vitro using Fc-expressing CD11b effector cells and target FoxP3-GFP cells (Figure 30E). I was surprised to find SM enhancing target cell phagocytosis; however, these effects could not be parsed as a manifestation of IAP antagonism within the target or effector cells. Further experimentation into the effects of SM treatment discretely on TREGs was attempted, however the general plasticity of CD4 T cells alongside transient and unstable expression of FoxP3 in vitro proved a major obstacle for the propagation of TREGs (data not shown) [Kanamori et al., 2016]. Elevated attrition with the combination of SM and αCTLA-4 suggests TREG ADCP may be pronounced in vivo, however additional experimentation is required to verify this.

Lastly, I chose to evaluate whether depletion of TREGs and SM treatment would promote an immunological phenotype conducive to generating a de novo antigenic immune response. I found SM and DT treatments upregulated endocytic marker DEC-205 on DCs (Figure 31A). Notably, T_{REG} depletion has been evaluated in combination with anti-cancer vaccination [Jacobs et al., 2010], as T_{REG}-mediated immunosuppression has long been implicated in restraining the efficacy of DC-based immunotherapies [Van Gulijk et al., 2017]. The homeostatic feedback between these two subsets, T_{REGs} and DCs, suggests that depleting T_{REGs} without stimulating DCs would render DCs in a suboptimal state unable to promote an effective antigenic response [Darrasse-Jèze et al., 2009]. Indeed, DT treatment alone yielded diminished expression of surface bound peptide following vaccination (Figure 31B). This was rescued with SM treatment, as the combination restored antigen expression similar to the control treatment. I further verified T_{REG} depletion did not abate SM-mediated cross-priming of OT-1 T cells, and in fact increased cell yield 2-log fold (Figure 31C) compared to 1-log fold increase with SM alone in an earlier experiment (Figure 25A). As expected, DT diminished antigen sensitivity ex vivo, however this was rescued and enhanced with SM co-treatment (Figure 31D). This suggests that SM treatment may stimulate DCs and/or T cells and compensate for any mitigating factors restraining effector cells following T_{REG} depletion. I established functional significance to this by prophylactically vaccinating against a tumour antigen and co-treating with SM and DT (Figure 31E). The combination treatment prevented outgrowth of solid tumours, thereby suggesting a potent tumour antigen-specific response was generated capable of rejecting the graft.

5.0 CONCLUSION

I demonstrated SM monotherapy generates durable cures in murine orthotopic MB49 urothelial carcinoma refractory to established immunotherapies. I further demonstrate significant potential for clinical translation, assessing anti-tumour efficacy in the MB49 model upon combining with prevailing immunotherapies, then treating an analogous model to further test clinical translatability. Optimal anti-tumour efficacy from cytotoxic T lymphocyte-associated protein 4 (CTLA-4, 9h10 clone) blockade requires both CD8 effector co-stimulation and Fc receptor-dependent depletion of immunosuppressive T_{REGs} [Simpson et al., 2013; Vargas et al., 2018]. Within the MB49 model, I report cures in 100% of test subjects upon combining SM simultaneously with a T_{REG}-depleting monoclonal antibody specific for CTLA-4. Collectively, the data establishes T_{REG}-depletion as the primary mechanism of action responsible for enhanced survival benefit in MB49 tumour-bearing mice upon co-treating SM with αCTLA-4.

I explored a possible cellular mechanism of action by evaluating SMs effects on DCs and T cells, compartments essential for generating an antigenic response and prominent targets of emerging immunotherapies, in a tumour-free setting. I found SM stimulated expansion of DCs, along with antigen-specific cross-priming using the OT-1 transgenic TCR model system.

I also evaluate SM in a physiological setting void of regulatory suppression, thereby emulating the necessary mechanism enabling optimal CTLA-4 blockade efficacy. I demonstrated functional significance, as SM treatment with concurrent ablation of T_{REGs} using a transgenic mouse expressing the diphtheria toxin receptor at the FoxP3 locus (FoxP3-DTR) alongside concurrent prophylactic vaccination for human papilloma virus (HPV) E7 peptide successfully prevented the outgrowth of subcutaneous lung epithelial TC-1 tumours. Taken together, I discovered SM treatment enhances anti-cancer vaccination potency, generating antigen-specific protection upon dysregulation of immune tolerance.

6.0 REFERENCES

Aderka, D., Sorkine, P., Abu-Abid, S., Lev, D., Setton, A., Cope, A. P., ... & Klausner, J. (1998). Shedding kinetics of soluble tumor necrosis factor (TNF) receptors after systemic TNF leaking during isolated limb perfusion. Relevance to the pathophysiology of septic shock. *The Journal of clinical investigation*, *101*(3), 650-659.

Aggarwal, B. B. (2003). Signalling pathways of the TNF superfamily: a double-edged sword. *Nature reviews immunology*, *3*(9), 745-756.

Ahmed, S. R., Petersen, E., Patel, R., & Migden, M. R. (2019). Cemiplimab-rwlc as first and only treatment for advanced cutaneous squamous cell carcinoma. *Expert review of clinical pharmacology*, *12*(10), 947-951.

Akbar, A. N., Vukmanovic-Stejic, M., Taams, L. S., & Macallan, D. C. (2007). The dynamic co-evolution of memory and regulatory CD4+ T cells in the periphery. *Nature Reviews Immunology*, *7*(3), 231-237.

Akutsu, M., Dikic, I., & Bremm, A. (2016). Ubiquitin chain diversity at a glance. *Journal of cell science*, *129*(5), 875-880.

Allan, D. C., & Phillips, J. C. (2017). Why ubiquitin has not evolved. *International journal of molecular sciences*, *18*(9), 1995.

Alvaro, T., Lejeune, M., Salvadó, M. T., Bosch, R., García, J. F., Jaén, J., ... & Piris, M. A. (2005). Outcome in Hodgkin's lymphoma can be predicted from the presence of accompanying cytotoxic and regulatory T cells. *Clinical Cancer Research*, *11*(4), 1467-1473.

Andrade, P. M., Chade, D. C., Borra, R. C., Nascimento, I. P., Villanova, F. E., Leite, L. C., ... & Srougi, M. (2010, September). The therapeutic potential of recombinant BCG expressing the antigen S1PT in the intravesical treatment of bladder cancer. In *Urologic Oncology: Seminars and Original Investigations* (Vol. 28, No. 5, pp. 520-525). Elsevier.

Asao, H., Okuyama, C., Kumaki, S., Ishii, N., Tsuchiya, S., Foster, D., & Sugamura, K. (2001). Cutting edge: the common γ-chain is an indispensable subunit of the IL-21 receptor complex. *The Journal of Immunology*, *167*(1), 1-5.

Aspatwar, A., Gong, W., Wang, S., Wu, X., & Parkkila, S. (2021). Tuberculosis vaccine BCG: the magical effect of the old vaccine in the fight against the COVID-19 pandemic. *International Reviews of Immunology*, 1-14.

Baaten, B. J., Li, C. R., Deiro, M. F., Lin, M. M., Linton, P. J., & Bradley, L. M. (2010). CD44 regulates survival and memory development in Th1 cells. *Immunity*, *32*(1), 104-115.

Badoual, C., Hans, S., Rodriguez, J., Peyrard, S., Klein, C., Agueznay, N. E. H., ... & Tartour, E. (2006). Prognostic value of tumor-infiltrating CD4+ T-cell subpopulations in head and neck cancers. *Clinical cancer research*, *12*(2), 465-472.

Bai, L., Smith, D. C., & Wang, S. (2014). Small-molecule SMAC mimetics as new cancer therapeutics. *Pharmacology & therapeutics*, *144*(1), 82-95.

Baras, A. S., Drake, C., Liu, J. J., Gandhi, N., Kates, M., Hoque, M. O., ... & Bivalacqua, T. J. (2016). The ratio of CD8 to Treg tumor-infiltrating lymphocytes is associated with response to cisplatin-based neoadjuvant chemotherapy in patients with muscle invasive urothelial carcinoma of the bladder. *Oncoimmunology*, *5*(5), e1134412.

Barrett, P. N., Mundt, W., Kistner, O., & Howard, M. K. (2009). Vero cell platform in vaccine production: moving towards cell culture-based viral vaccines. *Expert review of vaccines*, *8*(5), 607-618.

Ben Mkaddem, S., Benhamou, M., & Monteiro, R. C. (2019). Understanding Fc receptor involvement in inflammatory diseases: from mechanisms to new therapeutic tools. *Frontiers in immunology*, *10*, 811.

Bellmunt, J., De Wit, R., Vaughn, D. J., Fradet, Y., Lee, J. L., Fong, L., ... & Bajorin, D. F. (2017). Pembrolizumab as second-line therapy for advanced urothelial carcinoma. *New England Journal of Medicine*, *376*(11), 1015-1026.

Beug, S. T., Cheung, H. H., LaCasse, E. C., & Korneluk, R. G. (2012). Modulation of immune signalling by inhibitors of apoptosis. *Trends in immunology*, *33*(11), 535-545.

Beug, S. T., LaCasse, E. C., & Korneluk, R. G. (2014). Smac mimetics combined with innate immune stimuli create the perfect cytokine storm to kill tumor cells. *Oncoimmunology*, *3*(4), e28541.

Beug, S. T., Tang, V. A., LaCasse, E. C., Cheung, H. H., Beauregard, C. E., Brun, J., ... & Korneluk, R. G. (2014). Smac mimetics and innate immune stimuli synergize to promote tumor death. *Nature biotechnology*, *32*(2), 182-190.

Beug, S. T., Conrad, D. P., Alain, T., Korneluk, R. G., & Lacasse, E. C. (2015). Combinatorial cancer immunotherapy strategies with proapoptotic small-molecule IAP antagonists. *International Journal of Developmental Biology*, *59*(1-2-3), 141-147.

Beug, S. T., Beauregard, C. E., Healy, C., Sanda, T., St-Jean, M., Chabot, J., ... & Korneluk, R. G. (2017). Smac mimetics synergize with immune checkpoint inhibitors to promote tumour immunity against glioblastoma. *Nature communications*, *8*(1), 1-15.

Beug, S. T., Pichette, S. J., St-Jean, M., Holbrook, J., Walker, D. E., LaCasse, E. C., & Korneluk, R. G. (2018). Combination of IAP antagonists and TNF-α-armed oncolytic viruses induce tumor vascular shutdown and tumor regression. *Molecular Therapy-Oncolytics*, *10*, 28-39.

Birnberg, T., Bar-On, L., Sapoznikov, A., Caton, M. L., Cervantes-Barragán, L., Makia, D., ... & Jung, S. (2008). Lack of conventional dendritic cells is compatible with normal development and T cell homeostasis, but causes myeloid proliferative syndrome. *Immunity*, *29*(6), 986-997.

Boyerinas, B., Jochems, C., Fantini, M., Heery, C. R., Gulley, J. L., Tsang, K. Y., & Schlom, J. (2015). Antibody-dependent cellular cytotoxicity activity of a novel anti–PD-L1 antibody avelumab (MSB0010718C) on human tumor cells. *Cancer immunology research*, *3*(10), 1148-1157.

Bratton, S. B., Lewis, J., Butterworth, M., Duckett, C. S., & Cohen, G. M. (2002). XIAP inhibition of caspase-3 preserves its association with the Apaf-1 apoptosome and prevents CD95-and Bax-induced apoptosis. *Cell Death & Differentiation*, *9*(9), 881-892.

Cai, J., Lin, Y., Zhang, H., Liang, J., Tan, Y., Cavenee, W. K., & Yan, G. (2017). Selective replication of oncolytic virus M1 results in a bystander killing effect that is potentiated by Smac mimetics. *Proceedings of the National Academy of Sciences*, *114*(26), 6812-6817.

Campbell, G. R., To, R. K., Zhang, G., & Spector, S. A. (2020). SMAC mimetics induce autophagy-dependent apoptosis of HIV-1-infected macrophages. *Cell death & disease*, *11*(7), 1-14.

Carswell, E., Old, L. J., Kassel, R., Green, S., Fiore, N., & Williamson, B. (1975). An endotoxin-induced serum factor that causes necrosis of tumors. *Proceedings of the National Academy of Sciences*, *72*(9), 3666-3670.

Ceramil, A., & Beutler, B. (1988). The role of cachectin/TNF in endotoxic shock and cachexia. *Immunology today*, *9*(1), 28-31.

Cetraro, P., Plaza-Diaz, J., MacKenzie, A., & Abadía-Molina, F. (2022). A Review of the Current Impact of Inhibitors of Apoptosis Proteins and Their Repression in Cancer. *Cancers*, *14*(7), 1671.

Chai, J., Du, C., Wu, J. W., Kyin, S., Wang, X., & Shi, Y. (2000). Structural and biochemical basis of apoptotic activation by Smac/DIABLO. *Nature*, *406*(6798), 855-862.

Chai, J., Shiozaki, E., Srinivasula, S. M., Wu, Q., Dataa, P., Alnemri, E. S., & Shi, Y. (2001). Structural basis of caspase-7 inhibition by XIAP. *Cell*, *104*(5), 769-780.

Chambers, C. A., Sullivan, T. J., & Allison, J. P. (1997). Lymphoproliferation in CTLA-4–deficient mice is mediated by costimulation-dependent activation of CD4+ T cells. *Immunity*, *7*(6), 885-895.

Chang, Y. C., & Cheung, C. H. A. (2021). An Updated Review of Smac Mimetics, LCL161, Birinapant, and GDC-0152 in Cancer Treatment. *Applied Sciences*, *11*(1), 335.

Chen, C., Rowell, E. A., Thomas, R. M., Hancock, W. W., & Wells, A. D. (2006). Transcriptional regulation by Foxp3 is associated with direct promoter occupancy and modulation of histone acetylation. *Journal of Biological Chemistry*, *281*(48), 36828-36834.

Chen, F., Zhang, G., Cao, Y., Hessner, M. J., & See, W. A. (2009). MB49 murine urothelial carcinoma: molecular and phenotypic comparison to human cell lines as a model of the direct tumor response to bacillus Calmette-Guerin. *The Journal of urology*, *182*(6), 2932-2937.

Chen, D. S., & Mellman, I. (2013). Oncology meets immunology: the cancer-immunity cycle. *immunity*, *39*(1), 1-10.

Cheung, H. H., Plenchette, S., Kern, C. J., Mahoney, D. J., & Korneluk, R. G. (2008). The RING domain of cIAP1 mediates the degradation of RING-bearing inhibitor of apoptosis proteins by distinct pathways. *Molecular biology of the cell*, *19*(7), 2729-2740.

Chesi, M., Mirza, N. N., Garbitt, V. M., Sharik, M. E., Dueck, A. C., Asmann, Y. W., ... & Bergsagel, P. L. (2016). IAP antagonists induce anti-tumor immunity in multiple myeloma. *Nature medicine*, *22*(12), 1411-1420.

Choi, Y. E., Butterworth, M., Malladi, S., Duckett, C. S., Cohen, G. M., & Bratton, S. B. (2009). The E3 ubiquitin ligase cIAP1 binds and ubiquitinates caspase-3 and-7 via unique mechanisms at distinct steps in their processing. *Journal of Biological Chemistry*, *284*(19), 12772-12782.

Collette, Y., Gilles, A., Pontarotti, P., & Olive, D. (2003). A co-evolution perspective of the TNFSF and TNFRSF families in the immune system. *Trends in immunology*, *24*(7), 387-394.

Dai, Z., Zhu, W. G., Morrison, C. D., Brena, R. M., Smiraglia, D. J., Raval, A., ... & Plass, C. (2003). A comprehensive search for DNA amplification in lung cancer identifies inhibitors of apoptosis cIAP1 and cIAP2 as candidate oncogenes. *Human molecular genetics*, *12*(7), 791-801.

Dannull, J., Su, Z., Rizzieri, D., Yang, B. K., Coleman, D., Yancey, D., ... & Vieweg, J. (2005). Enhancement of vaccine-mediated antitumor immunity in cancer patients after depletion of regulatory T cells. *The Journal of clinical investigation*, *115*(12), 3623-3633.

Darding, M., & Meier, P. (2012). IAPs: guardians of RIPK1. *Cell Death & Differentiation*, *19*(1), 58-66.

Darrasse-Jèze, G., Deroubaix, S., Mouquet, H., Victora, G. D., Eisenreich, T., Yao, K. H., ... & Nussenzweig, M. C. (2009). Feedback control of regulatory T cell homeostasis by dendritic cells in vivo. *Journal of Experimental Medicine*, *206*(9), 1853-1862.

Darvin, P., Toor, S. M., Sasidharan Nair, V., & Elkord, E. (2018). Immune checkpoint inhibitors: recent progress and potential biomarkers. *Experimental & molecular medicine*, *50*(12), 1-11.

De Boer, E. C., Teppema, J. S., Sterenberg, P. A., & De Jong, W. H. (2000). Retrovirus type C in the mouse bladder carcinoma cell line MBT-2. *The Journal of urology*, *163*(6), 1999-2001.

De Sousa Linhares, A., Leitner, J., Grabmeier-Pfistershammer, K., & Steinberger, P. (2018). Not all immune checkpoints are created equal. *Frontiers in immunology*, *9*, 1909.

Dempsey, L. A. (2019). cDC1 cross-priming. *Nature immunology*, *20*(1), 1-1.

Dobson, C. C., Naing, T., Beug, S. T., Faye, M. D., Chabot, J., St-Jean, M., ... & Holcik, M. (2017). Oncolytic virus synergizes with Smac mimetic compounds to induce rhabdomyosarcoma cell death in a syngeneic murine model. *Oncotarget*, *8*(2), 3495.

Domínguez, P. M., & Ardavín, C. (2010). Differentiation and function of mouse monocyte-derived dendritic cells in steady state and inflammation. *Immunological reviews*, *234*(1), 90-104.

Dougan, S. K., & Dougan, M. (2018). Regulation of innate and adaptive antitumor immunity by IAP antagonists. *Immunotherapy*, *10*(9), 787-796.

Dougan, M., Dougan, S., Slisz, J., Firestone, B., Vanneman, M., Draganov, D., ... & Dranoff, G. (2010). IAP inhibitors enhance co-stimulation to promote tumor immunity. *Journal of Experimental Medicine*, *207*(10), 2195-2206.

Doyle, A. M., Mullen, A. C., Villarino, A. V., Hutchins, A. S., High, F. A., Lee, H. W., ... & Reiner, S. L. (2001). Induction of cytotoxic T lymphocyte antigen 4 (CTLA-4) restricts clonal expansion of helper T cells. *The Journal of experimental medicine*, *194*(7), 893-902.

Du, C., Fang, M., Li, Y., Li, L., & Wang, X. (2000). Smac, a mitochondrial protein that promotes cytochrome c–dependent caspase activation by eliminating IAP inhibition. *Cell*, *102*(1), 33-42.

Dunn, G. P., Bruce, A. T., Ikeda, H., Old, L. J., & Schreiber, R. D. (2002). Cancer immunoediting: from immunosurveillance to tumor escape. *Nature immunology*, *3*(11), 991-998.

DuPage, M., Mazumdar, C., Schmidt, L. M., Cheung, A. F., & Jacks, T. (2012). Expression of tumour-specific antigens underlies cancer immunoediting. *Nature*, *482*(7385), 405-409.

Elgueta, R., Benson, M. J., De Vries, V. C., Wasiuk, A., Guo, Y., & Noelle, R. J. (2009). Molecular mechanism and function of CD40/CD40L engagement in the immune system. *Immunological reviews*, *229*(1), 152-172.

Erdurak, K., Dundar, P. E., Ozyurt, B. C., Negri, E., La Vecchia, C., & Tay, Z. (2014). Smoking, occupation, history of selected diseases and bladder cancer risk in Manisa, Turkey. *European journal of cancer prevention*, *23*(1), 58-61.

Esteso, G., Aguiló, N., Julián, E., Ashiru, O., Ho, M., Martín, C., & Valés-Gómez, M. (2021). Natural Killer Anti-Tumor Activity Can Be Achieved by In Vitro Incubation With Heat-Killed BCG. *Frontiers in immunology*, 17.

Esuvaranathan, K., Alexandroff, A. B., McIntyre, M., Jackson, A. M., Prescott, S., Chisholm, G. D., & James, K. (1995). Interleukin-6 production by bladder tumors is upregulated by BCG immunotherapy. *The Journal of urology*, *154*(2), 572-575.

Fan, Ting-Jun, Li-Hui Han, Ri-Shan Cong, and Jin Liang. "Caspase family proteases and apoptosis." *Acta biochimica et biophysica Sinica* 37, no. 11 (2005): 719-727.

Fischer, K., Tognarelli, S., Roesler, S., Boedicker, C., Schubert, R., Steinle, A., ... & Ullrich, E. (2017). The Smac mimetic BV6 improves NK cell-mediated killing of rhabdomyosarcoma cells by simultaneously targeting tumor and effector cells. *Frontiers in immunology*, *8*, 202.

Fontenot, J. D., Gavin, M. A., & Rudensky, A. Y. (2003). Foxp3 programs the development and function of CD4+ CD25+ regulatory T cells. *Nature immunology*, *4*(4), 330-336.

Freedman, N. D., Silverman, D. T., Hollenbeck, A. R., Schatzkin, A., & Abnet, C. C. (2011). Association between smoking and risk of bladder cancer among men and women. *Jama*, *306*(7), 737-745.

Friedline, R. H., Brown, D. S., Nguyen, H., Kornfeld, H., Lee, J., Zhang, Y., ... & Chambers, C. A. (2009). CD4+ regulatory T cells require CTLA-4 for the maintenance of systemic tolerance. *Journal of Experimental Medicine*, *206*(2), 421-434.

Fulda, S. (2015). Promises and challenges of Smac mimetics as cancer therapeutics. *Clinical Cancer Research*, *21*(22), 5030-5036.

Galkina, E., Florey, O., Zarbock, A., Smith, B. R., Preece, G., Lawrence, M. B., ... & Ager, A. (2007). T lymphocyte rolling and recruitment into peripheral lymph nodes is regulated by a saturable density of L-selectin (CD62L). *European journal of immunology*, *37*(5), 1243-1253.

Gardam, S., Turner, V. M., Anderton, H., Limaye, S., Basten, A., Koentgen, F., ... & Brink, R. (2011). Deletion of cIAP1 and cIAP2 in murine B lymphocytes constitutively activates cell survival pathways and inactivates the germinal center response. *Blood, The Journal of the American Society of Hematology*, *117*(15), 4041-4051.

Gardner, A., de Mingo Pulido, Á., & Ruffell, B. (2020). Dendritic cells and their role in immunotherapy. *Frontiers in Immunology*, *11*, 924.

Gerosa, F., Gobbi, A., Zorzi, P., Burg, S., Briere, F., Carra, G., & Trinchieri, G. (2005). The reciprocal interaction of NK cells with plasmacytoid or myeloid dendritic cells profoundly affects innate resistance functions. *The Journal of Immunology*, *174*(2), 727-734.

Giri, J. G., Ahdieh, M., Eisenman, J., Shanebeck, K., Grabstein, K., Kumaki, S., ... & Anderson, D. (1994). Utilization of the beta and gamma chains of the IL-2 receptor by the novel cytokine IL-15. *The EMBO journal*, *13*(12), 2822-2830

Golay, J., & Taylor, R. P. (2020). The role of complement in the mechanism of action of therapeutic anti-cancer mAbs. *Antibodies*, *9*(4), 58.

Griesenauer, R. H., & Kinch, M. S. (2017). An overview of FDA-approved vaccines & their innovators. *Expert review of vaccines*, *16*(12), 1253-1266.

Günther, J. H., Jurczok, A., Wulf, T., Brandau, S., Deinert, I., Jocham, D., & Böhle, A. (1999). Optimizing syngeneic orthotopic murine bladder cancer (MB49). *Cancer research*, *59*(12), 2834-2837.

Gutiérrez-Martínez, E., Planès, R., Anselmi, G., Reynolds, M., Menezes, S., Adiko, A. C., ... & Guermonprez, P. (2015). Cross-presentation of cell-associated antigens by MHC class I in dendritic cell subsets. *Frontiers in immunology*, *6*, 363.

Gyrd-Hansen, M., & Meier, P. (2010). IAPs: from caspase inhibitors to modulators of NF-κB, inflammation and cancer. *Nature Reviews Cancer*, *10*(8), 561-574.

Hakenberg, O. W. (2017). Nivolumab for the treatment of bladder cancer. *Expert opinion on biological therapy*, *17*(10), 1309-1315.

Heney, N. M., Ahmed, S., Flanagan, M. J., Frable, W., Corder, M. P., Hafermann, M. D., & Hawkins, I. R. (1983). Superficial bladder cancer: progression and recurrence. *The Journal of urology*, *130*(6), 1083-1086.

Hildner, K., Edelson, B. T., Purtha, W. E., Diamond, M., Matsushita, H., Kohyama, M., ... & Murphy, K. M. (2008). Batf3 deficiency reveals a critical role for CD8α+ dendritic cells in cytotoxic T cell immunity. *Science*, *322*(5904), 1097-1100.

Hockenbery, D. (1995). Defining apoptosis. *The American journal of pathology*, *146*(1), 16.

Hodi, F. S., O'Day, S. J., McDermott, D. F., Weber, R. W., Sosman, J. A., Haanen, J. B., ... & Urba, W. J. (2010). Improved survival with ipilimumab in patients with metastatic melanoma. *New England Journal of Medicine*, *363*(8), 711-723.

Hsu, J., Hodgins, J. J., Marathe, M., Nicolai, C. J., Bourgeois-Daigneault, M. C., Trevino, T. N., ... & Ardolino, M. (2018). Contribution of NK cells to immunotherapy mediated by PD-1/PD-L1 blockade. *The Journal of clinical investigation*, *128*(10), 4654-4668.

Huang, A. C., Postow, M. A., Orlowski, R. J., Mick, R., Bengsch, B., Manne, S., ... & Wherry, E. J. (2017). T-cell invigoration to tumour burden ratio associated with anti-PD-1 response. *Nature*, *545*(7652), 60-65.

Huang, Y., Rich, R. L., Myszka, D. G., & Wu, H. (2003). Requirement of both the second and third BIR domains for the relief of X-linked inhibitor of apoptosis protein (XIAP)-mediated caspase inhibition by Smac. *Journal of Biological Chemistry*, *278*(49), 49517-49522.

Hui, E., Cheung, J., Zhu, J., Su, X., Taylor, M. J., Wallweber, H. A., ... & Vale, R. D. (2017). T cell costimulatory receptor CD28 is a primary target for PD-1–mediated inhibition. *Science*, *355*(6332), 1428-1433.

Isaacson, B., & Mandelboim, O. (2019). Natural killer cells control metastasis via structural editing of primary tumors in mice. *Cancer Immunology, Immunotherapy*, *68*(10), 1721-1724.

Iqbal, N. T., & Hussain, R. (2014). Non-specific immunity of BCG vaccine: a perspective of BCG immunotherapy. *Trials in Vaccinology*, *3*, 143-149.

Jacobs, J. F., Punt, C. J., Lesterhuis, W. J., Sutmuller, R. P., Brouwer, H. M. L. H., Scharenborg, N. M., ... & Adema, G. J. (2010). Dendritic cell vaccination in combination with anti-CD25 monoclonal antibody treatment: a phase I/II study in metastatic melanoma patients. *Clinical Cancer Research*, *16*(20), 5067-5078.

Jason, J., & Larned, J. (1997). Single-cell cytokine profiles in normal humans: comparison of flow cytometric reagents and stimulation protocols. *Journal of immunological methods*, *207*(1), 13-22.

Jiang, C., & Lin, X. (2012). Regulation of NF-κB by the CARD proteins. *Immunological reviews*, *246*(1), 141-153.

Jiang, Y., Li, Y., & Zhu, B. (2015). T-cell exhaustion in the tumor microenvironment. *Cell death & disease*, *6*(6), e1792-e1792.

Jinesh G, G., Chunduru, S., & Kamat, A. M. (2012). Smac mimetic enables the anticancer action of BCG-stimulated neutrophils through TNF-α but not through TRAIL and FasL. *Journal of leukocyte biology*, *92*(1), 233-244.

Kamat, A. M., Flaig, T. W., Grossman, H. B., Konety, B., Lamm, D., O'donnell, M. A., ... & Taylor, J. A. (2015). Consensus statement on best practice management regarding the use of intravesical immunotherapy with BCG for bladder cancer. *Nature Reviews Urology*, *12*(4), 225-235.

Kamat, A. M., Hahn, N. M., Efstathiou, J. A., Lerner, S. P., Malmström, P. U., Choi, W., ... & Kassouf, W. (2016). Bladder cancer. *The Lancet*, *388*(10061), 2796-2810.

Kanamori, M., Nakatsukasa, H., Okada, M., Lu, Q., & Yoshimura, A. (2016). Induced regulatory T cells: their development, stability, and applications. *Trends in immunology*, *37*(11), 803-811.

Kavoussi, L. R., Brown, E. J., Ritchey, J. K., & Ratliff, T. L. (1990). Fibronectin-mediated Calmette-Guerin bacillus attachment to murine bladder mucosa. Requirement for the expression of an antitumor response. *The Journal of clinical investigation*, *85*(1), 62-67.

Keats, J. J., Fonseca, R., Chesi, M., Schop, R., Baker, A., Chng, W. J., ... & Bergsagel, P. L. (2007). Promiscuous mutations activate the noncanonical NF-κB pathway in multiple myeloma. *Cancer cell*, *12*(2), 131-144.

Kidd, P. (2003). Th1/Th2 balance: the hypothesis, its limitations, and implications for health and disease. *Alternative medicine review*, *8*(3), 223-246.

Kim, D. S., Dastidar, H., Zhang, C., Zemp, F. J., Lau, K., Ernst, M., ... & Mahoney, D. J. (2017). Smac mimetics and oncolytic viruses synergize in driving anticancer T-cell responses through complementary mechanisms. *Nature communications*, *8*(1), 1-13.

Kim, J. M., Rasmussen, J. P., & Rudensky, A. Y. (2007). Regulatory T cells prevent catastrophic autoimmunity throughout the lifespan of mice. *Nature immunology*, *8*(2), 191-197.

Kimura, Y., Takeshita, T., Kondo, M., Ishii, N., Nakamura, M., Van Snick, J., & Sugamura, K. (1995). Sharing of the IL-2 receptor γ chain with the functional IL-9 receptor complex. *International immunology*, *7*(1), 115-120.

Kondo, M., Takeshita, T., Ishii, N., Nakamura, M., Watanabe, S., Arai, K. I., & Sugamura, K. (1993). Sharing of the interleukin-2 (IL-2) receptor γ chain between receptors for IL-2 and IL-4. *Science*, *262*(5141), 1874-1877.

Kondo, M., Takeshita, T., Higuchi, M., Nakamura, M., Sudo, T., Nishikawa, S. L., & Sugamura, K. (1994). Functional participation of the IL-2 receptor γ chain in IL-7 receptor complexes. *Science*, *263*(5152), 1453-1454.

Krummel, M. F., & Allison, J. P. (1995). CD28 and CTLA-4 have opposing effects on the response of T cells to stimulation. *Journal of Experimental Medicine*, *182*(2), 459-465.

LaCasse, E. C. (2013). Pulling the plug on a cancer cell by eliminating XIAP with AEG35156. *Cancer letters*, *332*(2), 215-224.

Lachmann, A., Torre, D., Keenan, A. B., Jagodnik, K. M., Lee, H. J., Wang, L., ... & Ma'ayan, A. (2018). Massive mining of publicly available RNA-seq data from human and mouse. *Nature communications*, *9*(1), 1-10.

Lee, E. K., Jinesh G, G., Laing, N. M., Choi, W., McConkey, D. J., & Kamat, A. M. (2013). A Smac mimetic augments the response of urothelial cancer cells to gemcitabine and cisplatin. *Cancer biology & therapy*, *14*(9), 812-822.

Lenschow, D. J., Walunas, T. L., & Bluestone, J. A. (1996). CD28/B7 system of T cell costimulation. *Annual review of immunology*, *14*(1), 233-258.

Li, Y., Dong, K., Fan, X., Xie, J., Wang, M., Fu, S., & Li, Q. (2020). DNT cell-based immunotherapy: progress and applications. *Journal of Cancer*, *11*(13), 3717.

Liao, W., Lin, J. X., & Leonard, W. J. (2011). IL-2 family cytokines: new insights into the complex roles of IL-2 as a broad regulator of T helper cell differentiation. *Current opinion in immunology*, *23*(5), 598-604.

Lind, E. F., Ahonen, C. L., Wasiuk, A., Kosaka, Y., Becher, B., Bennett, K. A., & Noelle, R. J. (2008). Dendritic cells require the NF-κB2 pathway for cross-presentation of soluble antigens. *The Journal of Immunology*, *181*(1), 354-363.

Liotta, F., Gacci, M., Frosali, F., Querci, V., Vittori, G., Lapini, A., ... & Annunziato, F. (2011). Frequency of regulatory T cells in peripheral blood and in tumour-infiltrating lymphocytes correlates with poor prognosis in renal cell carcinoma. *BJU International-British Journal of Urology*, *107*(9), 1500.

Lim, T. S., Chew, V., Sieow, J. L., Goh, S., Yeong, J. P. S., Soon, A. L., & Ricciardi-Castagnoli, P. (2016). PD-1 expression on dendritic cells suppresses CD8+ T cell function and antitumor immunity. *Oncoimmunology*, *5*(3), e1085146.

Litzinger, M. T., Fernando, R., Curiel, T. J., Grosenbach, D. W., Schlom, J., & Palena, C. (2007). IL-2 immunotoxin denileukin diftitox reduces regulatory T cells and enhances vaccine-mediated T-cell immunity. *Blood, The Journal of the American Society of Hematology*, *110*(9), 3192-3201.

Lou, Y., Liu, C., Kim, G. J., Liu, Y. J., Hwu, P., & Wang, G. (2007). Plasmacytoid dendritic cells synergize with myeloid dendritic cells in the induction of antigen-specific antitumor immune responses. *The Journal of Immunology*, *178*(3), 1534-1541.

Lueck, S. C., Russ, A. C., Botzenhardt, U., Schlenk, R. F., Zobel, K., Deshayes, K., ... & Bullinger, L. (2016). Smac mimetic induces cell death in a large proportion of primary acute myeloid leukemia samples, which correlates with defined molecular markers. *Oncotarget*, *7*(31), 49539.

Ma, O., Cai, W. W., Zender, L., Dayaram, T., Shen, J., Herron, A. J., ... & Donehower, L. A. (2009). MMP13, Birc2 (cIAP1), and Birc3 (cIAP2), amplified on chromosome 9, collaborate with p53 deficiency in mouse osteosarcoma progression. *Cancer research*, *69*(6), 2559-2567.

Mace, P. D., Shirley, S., & Day, C. L. (2010). Assembling the building blocks: structure and function of inhibitor of apoptosis proteins. *Cell Death & Differentiation*, *17*(1), 46-53.

Martin, F., Ladoire, S., Mignot, G., Apetoh, L., & Ghiringhelli, F. (2010). Human FOXP3 and cancer. *Oncogene*, *29*(29), 4121-4129.

Mahoney, D. J., Cheung, H. H., Mrad, R. L., Plenchette, S., Simard, C., Enwere, E., ... & Korneluk, R. G. (2008). Both cIAP1 and cIAP2 regulate TNFα-mediated NF-κB activation. *Proceedings of the National Academy of Sciences*, *105*(33), 11778-11783.

Mangsbo, S. M., Ninalga, C., Essand, M., Loskog, A., & Tötterman, T. H. (2008). CpG therapy is superior to BCG in an orthotopic bladder cancer model and generates CD4+ T-cell immunity. *Journal of immunotherapy*, *31*(1), 34-42.

Mangsbo, S. M., Sandin, L. C., Anger, K., Korman, A. J., Loskog, A., & Tötterman, T. H. (2010). Enhanced tumor eradication by combining CTLA-4 or PD-1 blockade with CpG therapy. *Journal of immunotherapy*, *33*(3), 225-235.

Matsuzawa, A., Tseng, P. H., Vallabhapurapu, S., Luo, J. L., Zhang, W., Wang, H., ... & Karin, M. (2008). Essential cytoplasmic translocation of a cytokine receptor–assembled signaling complex. *Science*, *321*(5889), 663-668.

McComb, S., Cheung, H. H., Korneluk, R. G., Wang, S., Krishnan, L., & Sad, S. (2012). cIAP1 and cIAP2 limit macrophage necroptosis by inhibiting Rip1 and Rip3 activation. *Cell Death & Differentiation*, *19*(11), 1791-1801.

McGregor, B. A., Campbell, M. T., Xie, W., Siefker-Radtke, A. O., Shah, A. Y., Venkatesan, A. M., ... & Choueiri, T. K. (2019). Phase II study of nivolumab and ipilimumab for advanced bladder cancer of variant histologies (BCVH).

McIlwain, D. R., Berger, T., & Mak, T. W. (2013). Caspase functions in cell death and disease. *Cold Spring Harbor perspectives in biology*, *5*(4), a008656.

McLellan, A. D., Terbeck, G., Mengling, T., Starling, G. C., Kiener, P. A., Gold, R., ... & Kämpgen, E. (2000). Differential susceptibility to CD95 (Apo-1/Fas) and MHC class II-induced apoptosis during murine dendritic cell development. *Cell Death & Differentiation*, *7*(10), 933-938.

McNeill, A., Spittle, E., & Bäckström, B. T. (2007). Partial depletion of CD69low-expressing natural regulatory T cells with the anti-CD25 monoclonal antibody PC61. *Scandinavian journal of immunology*, *65*(1), 63-69.

Metwalli, A. R., Khanbolooki, S., Jinesh, G., Sundi, D., Shah, J. B., Shrader, M., ... & Kamat, A. M. (2010). Smac mimetic reverses resistance to TRAIL and chemotherapy in human urothelial cancer cells. *Cancer biology & therapy*, *10*(9), 885-892.

Metz, A., Ciglia, E., & Gohlke, H. (2012). Modulating protein-protein interactions: from structural determinants of binding to druggability prediction to application. *Current pharmaceutical design*, *18*(30), 4630-4647.

Miller, A. M., Lundberg, K., Özenci, V., Banham, A. H., Hellström, M., Egevad, L., & Pisa, P. (2006). CD4+ CD25high T cells are enriched in the tumor and peripheral blood of prostate cancer patients. *The Journal of Immunology*, *177*(10), 7398-7405.

Milstein, C., & Cuello, A. C. (1983). Hybrid hybridomas and their use in immunohistochemistry. *Nature*, *305*(5934), 537-540.

Mizutani, Y., Katsuoka, Y., & Bonavida, B. (2010). Prognostic significance of second mitochondria-derived activator of caspase (Smac/DIABLO) expression in bladder cancer and target for therapy. *International journal of oncology*, *37*(2), 503-508.

Mocellin, S., & Nitti, D. (2013). CTLA-4 blockade and the renaissance of cancer immunotherapy. *Biochimica et Biophysica Acta (BBA)-Reviews on Cancer*, *1836*(2), 187-196.

Morales, A., Eidinger, D., & Bruce, A. W. (1976). Intracavitary Bacillus Calmette-Guerin in the treatment of superficial bladder tumors. *The Journal of urology*, *116*(2), 180-182.

Morales, A. (1980). Treatment of carcinoma in situ of the bladder with BCG. *Cancer Immunology, Immunotherapy*, *9*(1-2), 69-72.

Morón-Calvente, V., Romero-Pinedo, S., Toribio-Castelló, S., Plaza-Díaz, J., Abadía-Molina, A. C., Rojas-Barros, D. I., ... & Abadía-Molina, F. (2018). Inhibitor of apoptosis proteins, NAIP, cIAP1 and cIAP2 expression during macrophage differentiation and M1/M2 polarization. *PloS one*, *13*(3), e0193643.

Mudde, A. C. A., Booth, C., & Marsh, R. A. (2021). Evolution of our Understanding of XIAP Deficiency. *Frontiers in Pediatrics*, *9*, 557.

Murray, S. E., Ligman, B., Burton, A., & Kearney, C. (2020). The effect of SMAC mimetics on human T cell activation.

Nadella, V., Mohanty, A., Sharma, L., Yellaboina, S., Mollenkopf, H. J., Mazumdar, V. B., ... & Prakash, H. (2018). Inhibitors of apoptosis protein antagonists (Smac mimetic compounds) control polarization of macrophages during microbial challenge and sterile inflammatory responses. *Frontiers in immunology*, *8*, 1792.

Nam, S., Lee, A., Lim, J., & Lim, J. S. (2019). Analysis of the expression and regulation of PD-1 protein on the surface of myeloid-derived suppressor cells (MDSCs). *Biomolecules & therapeutics*, *27*(1), 63.

Nandi, D., Gross, J. A., & Allison, J. P. (1994). CD28-mediated costimulation is necessary for optimal proliferation of murine NK cells. *The Journal of Immunology*, *152*(7), 3361-3369.

Ning, Y. M., Suzman, D., Maher, V. E., Zhang, L., Tang, S., Ricks, T., ... & Pazdur, R. (2017). FDA approval summary: atezolizumab for the treatment of patients with progressive advanced urothelial carcinoma after platinum-containing chemotherapy. *The oncologist*, *22*(6), 743-749.

Nobs, S. P., Schneider, C., Heer, A. K., Huotari, J., Helenius, A., & Kopf, M. (2016). PI3Kγ is critical for dendritic cell-mediated CD8+ T cell priming and viral clearance during influenza virus infection. *PLOS pathogens*, *12*(3), e1005508.

Nocentini, G., & Riccardi, C. (2005). GITR: a multifaceted regulator of immunity belonging to the tumor necrosis factor receptor superfamily. *European journal of immunology*, *35*(4), 1016-1022.

Okamura, K., Nagayama, S., Tate, T., Kiyotani, K., & Nakamura, Y. (2020). The potential target of double negative T cells in cancer immunotherapy.

Okazaki, T., Chikuma, S., Iwai, Y., Fagarasan, S., & Honjo, T. (2013). A rheostat for immune responses: the unique properties of PD-1 and their advantages for clinical application. *Nature immunology*, *14*(12), 1212-1218.

Old, L. J., Clarke, D. A., & Benacerraf, B. (1959). Effect of Bacillus Calmette-Guerin infection on transplanted tumours in the mouse. *Nature*, *184*(4682), 291-292.

Pardoll, D. M. (2012). The blockade of immune checkpoints in cancer immunotherapy. *Nature Reviews Cancer*, *12*(4), 252-264.

Parel, Y., & Chizzolini, C. (2004). CD4+ CD8+ double positive (DP) T cells in health and disease. *Autoimmunity reviews*, *3*(3), 215-220.

Pearl, R. (1928). On the Pathological Relations Between Cancer and Tuberculosis. *Proceedings of the Society for Experimental Biology and Medicine*, *26*(1), 73-75.

Peggs, K. S., Quezada, S. A., Chambers, C. A., Korman, A. J., & Allison, J. P. (2009). Blockade of CTLA-4 on both effector and regulatory T cell compartments contributes to the antitumor activity of anti–CTLA-4 antibodies. *Journal of Experimental Medicine*, *206*(8), 1717-1725.

Peltzer, N., Darding, M., & Walczak, H. (2016). Holding RIPK1 on the ubiquitin leash in TNFR1 signaling. *Trends in cell biology*, *26*(6), 445-461.

Petersen, S. L., Wang, L., Yalcin-Chin, A., Li, L., Peyton, M., Minna, J., ... & Wang, X. (2007). Autocrine TNFα signaling renders human cancer cells susceptible to Smac-mimetic-induced apoptosis. *Cancer cell*, *12*(5), 445-456.

Pham, L. V., Fu, L., Tamayo, A. T., Bueso-Ramos, C., Drakos, E., Vega, F., ... & Ford, R. J. (2011). Constitutive BR3 receptor signaling in diffuse, large B-cell lymphomas stabilizes nuclear factor-κB–inducing kinase while activating both canonical and alternative nuclear factor-κB pathways. *Blood, The Journal of the American Society of Hematology*, *117*(1), 200-210.

Poirier, A. E., Ruan, Y., Walter, S. D., Franco, E. L., Villeneuve, P. J., King, W. D., ... & ComPARe Study Team. (2019). The future burden of cancer in Canada: Long-term cancer incidence projections 2013–2042. *Cancer epidemiology*, *59*, 199-207.

Powles, T., Park, S. H., Voog, E., Caserta, C., Valderrama, B. P., Gurney, H., ... & Grivas, P. (2020). Avelumab maintenance therapy for advanced or metastatic urothelial carcinoma. *New England Journal of Medicine*, *383*(13), 1218-1230.

Ratliff, T. L., Gillen, D., & Catalona, W. J. (1987). Requirement of a thymus dependent immune response for BCG-mediated antitumor activity. *The Journal of urology*, *137*(1), 155-158.

Raulf, N., El-Attar, R., Kulms, D., Lecis, D., Delia, D., Walczak, H., ... & Tavassoli, M. (2014). Differential response of head and neck cancer cell lines to TRAIL or Smac mimetics is associated with the cellular levels and activity of caspase-8 and caspase-10. *British journal of cancer*, *111*(10), 1955-1964.

Rech, A. J., & Vonderheide, R. H. (2009). Clinical use of anti-CD25 antibody daclizumab to enhance immune responses to tumor antigen vaccination by targeting regulatory T cells. *Annals of the New York Academy of Sciences*, *1174*(1), 99-106.

Redelman-Sidi, G., Iyer, G., Solit, D. B., & Glickman, M. S. (2013). Oncogenic activation of Pak1-dependent pathway of macropinocytosis determines BCG entry into bladder cancer cells. *Cancer research*, *73*(3), 1156-1167.

Redelman-Sidi, G., Glickman, M. S., & Bochner, B. H. (2014). The mechanism of action of BCG therapy for bladder cancer—a current perspective. *Nature Reviews Urology*, *11*(3), 153-162.

Richter, B. W., Mir, S. S., Eiben, L. J., Lewis, J., Reffey, S. B., Frattini, A., ... & Duckett, C. S. (2001). Molecular cloning of ILP-2, a novel member of the inhibitor of apoptosis protein family. *Molecular and cellular biology*, *21*(13), 4292-4301.

Richters, A., Aben, K. K., & Kiemeney, L. A. (2020). The global burden of urinary bladder cancer: an update. *World journal of urology*, *38*(8), 1895-1904.

Riedl, S. J., Renatus, M., Schwarzenbacher, R., Zhou, Q., Sun, C., Fesik, S. W., ... & Salvesen, G. S. (2001). Structural basis for the inhibition of caspase-3 by XIAP. *Cell*, *104*(5), 791-800.

Rosenberg, S. A., & Restifo, N. P. (2015). Adoptive cell transfer as personalized immunotherapy for human cancer. *Science*, *348*(6230), 62-68.

Samson, A. L., Zhang, Y., Geoghegan, N. D., Gavin, X. J., Davies, K. A., Mlodzianoski, M. J., ... & Murphy, J. M. (2020). MLKL trafficking and accumulation at the plasma membrane control the kinetics and threshold for necroptosis. *Nature communications*, *11*(1), 1-17.

Sánchez-Paulete, A. R., Cueto, F. J., Martínez-López, M., Labiano, S., Morales-Kastresana, A., Rodríguez-Ruiz, M. E., ... & Melero, I. (2016). Cancer immunotherapy with immunomodulatory anti-CD137 and anti–PD-1 monoclonal antibodies requires BATF3-dependent dendritic cells. *Cancer discovery*, *6*(1), 71-79.

Sanli, O., Dobruch, J., Knowles, M. A., Burger, M., Alemozaffar, M., Nielsen, M. E., & Lotan, Y. (2017). Bladder cancer. *Nature reviews Disease primers*, *3*(1), 1-19.

Sarkis, A. S., Bajorin, D. F., Reuter, V. E., Herr, H. W., Netto, G., Zhang, Z. F., ... & Scher, H. I. (1995). Prognostic value of p53 nuclear overexpression in patients with invasive bladder cancer treated with neoadjuvant MVAC. *Journal of clinical oncology*, *13*(6), 1384-1390.

Satpathy, A. T., Kc, W., Albring, J. C., Edelson, B. T., Kretzer, N. M., Bhattacharya, D., ... & Murphy, K. M. (2012). Zbtb46 expression distinguishes classical dendritic cells and their committed progenitors from other immune lineages. *Journal of Experimental Medicine*, *209*(6), 1135-1152.

Schmid, P., Adams, S., Rugo, H. S., Schneeweiss, A., Barrios, C. H., Iwata, H., ... & Emens, L. A. (2018). Atezolizumab and nab-paclitaxel in advanced triple-negative breast cancer. *New England Journal of Medicine*, *379*(22), 2108-2121.

Schumacher, T. N., & Schreiber, R. D. (2015). Neoantigens in cancer immunotherapy. *Science*, *348*(6230), 69-74.

Scott, F. L., Denault, J. B., Riedl, S. J., Shin, H., Renatus, M., & Salvesen, G. S. (2005). XIAP inhibits caspase-3 and-7 using two binding sites: evolutionarily conserved mechanism of IAPs. *The EMBO journal*, *24*(3), 645-655.

Segura, E., & Amigorena, S. (2014). Cross-presentation by human dendritic cell subsets. *Immunology letters*, *158*(1-2), 73-78.

Setiady, Y. Y., Coccia, J. A., & Park, P. U. (2010). In vivo depletion of CD4+ FOXP3+ Treg cells by the PC61 anti-CD25 monoclonal antibody is mediated by FcγRIII+ phagocytes. *European journal of immunology*, *40*(3), 780-786.

Shi, L. Z., Fu, T., Guan, B., Chen, J., Blando, J. M., Allison, J. P., ... & Sharma, P. (2016). Interdependent IL-7 and IFN-γ signalling in T-cell controls tumour eradication by combined α-CTLA-4+ α-PD-1 therapy. *Nature communications*, *7*(1), 1-12.

Shinkura, R., Kitada, K., Matsuda, F., Tashiro, K., Ikuta, K., Suzuki, M., ... & Honjo, T. (1999). Alymphoplasia is caused by a point mutation in the mouse gene encoding NF-κB-inducing kinase. *Nature genetics*, *22*(1), 74-77.

Shrimpton, R. E., Butler, M., Morel, A. S., Eren, E., Hue, S. S., & Ritter, M. A. (2009). CD205 (DEC-205): a recognition receptor for apoptotic and necrotic self. *Molecular immunology*, *46*(6), 1229-1239.

Sica, A., Schioppa, T., Mantovani, A., & Allavena, P. (2006). Tumour-associated macrophages are a distinct M2 polarised population promoting tumour progression: potential targets of anti-cancer therapy. *European journal of cancer*, *42*(6), 717-727.

Silke, J., & Meier, P. (2013). Inhibitor of apoptosis (IAP) proteins–modulators of cell death and inflammation. *Cold Spring Harbor perspectives in biology*, *5*(2), a008730.

Simpson, T. R., Li, F., Montalvo-Ortiz, W., Sepulveda, M. A., Bergerhoff, K., Arce, F., ... & Quezada, S. A. (2013). Fc-dependent depletion of tumor-infiltrating regulatory T cells co-defines the efficacy of anti–CTLA-4 therapy against melanoma. *Journal of Experimental Medicine*, *210*(9), 1695-1710.

Sittig, S. P., Bakdash, G., Weiden, J., Sköld, A. E., Tel, J., Figdor, C. G., ... & Schreibelt, G. (2016). A comparative study of the T cell stimulatory and polarizing capacity of human primary blood dendritic cell subsets. *Mediators of inflammation*, *2016*.

Smyth, M. J., Ngiow, S. F., & Teng, M. W. (2014). Targeting regulatory T cells in tumor immunotherapy. *Immunology and cell biology*, *92*(6), 473.

Socinski, M. A., Jotte, R. M., Cappuzzo, F., Orlandi, F., Stroyakovskiy, D., Nogami, N., ... & Reck, M. (2018). Atezolizumab for first-line treatment of metastatic nonsquamous NSCLC. *New England Journal of Medicine*, *378*(24), 2288-2301.

Soltes, G., Muller, E., & D'Aversa, T. G. (2011). Ubiquitin, ubiquitination, and proteasomal degradation in the eukaryotic cell: a review. *Bios*, *82*(3), 64-71.

Soumelis, V., & Liu, Y. J. (2006). From plasmacytoid to dendritic cell: morphological and functional switches during plasmacytoid pre-dendritic cell differentiation. *European journal of immunology*, *36*(9), 2286-2292.

Srinivasula, S. M., Hegde, R., Saleh, A., Datta, P., Shiozaki, E., Chai, J., ... & Alnemri, E. S. (2001). A conserved XIAP-interaction motif in caspase-9 and Smac/DIABLO regulates caspase activity and apoptosis. *Nature*, *410*(6824), 112-116.

Srinivasula, S. M., & Ashwell, J. D. (2008). IAPs: what's in a name?. *Molecular cell*, *30*(2), 123-135.

Steinman, R. M. (1991). The dendritic cell system and its role in immunogenicity. *Annual review of immunology*, *9*(1), 271-296.

Stojdl, D. F., Lichty, B., Knowles, S., Marius, R., Atkins, H., Sonenberg, N., & Bell, J. C. (2000). Exploiting tumor-specific defects in the interferon pathway with a previously unknown oncolytic virus. *Nature medicine*, *6*(7), 821-825.

Stucci, S., Palmirotta, R., Passarelli, A., Silvestris, E., Argentiero, A., Lanotte, L., ... & Silvestris, F. (2017). Immune-related adverse events during anticancer immunotherapy: Pathogenesis and management. *Oncology letters*, *14*(5), 5671-5680.

Sung, H., Ferlay, J., Siegel, R. L., Laversanne, M., Soerjomataram, I., Jemal, A., & Bray, F. (2021). Global cancer statistics 2020: GLOBOCAN estimates of incidence and mortality worldwide for 36 cancers in 185 countries. *CA: a cancer journal for clinicians*, *71*(3), 209-249.

Tanaka, H., Tanaka, J., Kjaergaard, J., & Shu, S. (2002). Depletion of CD4+ CD25+ regulatory cells augments the generation of specific immune T cells in tumor-draining lymph nodes. *Journal of Immunotherapy*, *25*(3), 207-217.

Taniguchi, K., Koga, S., Nishikido, M., Yamashita, S., Sakuragi, T., Kanetake, H., & Saito, Y. (1999). Systemic immune response after intravesical instillation of bacille Calmette–Guerin (BCG) for superficial bladder cancer. *Clinical & Experimental Immunology*, *115*(1), 131-135.

Thibult, M. L., Mamessier, E., Gertner-Dardenne, J., Pastor, S., Just-Landi, S., Xerri, L., ... & Olive, D. (2013). PD-1 is a novel regulator of human B-cell activation. *International immunology*, *25*(2), 129-137.

Thornton, A. M., & Shevach, E. M. (1998). CD4+ CD25+ immunoregulatory T cells suppress polyclonal T cell activation in vitro by inhibiting interleukin 2 production. *The Journal of experimental medicine*, *188*(2), 287-296.

Trevejo, J. M., Marino, M. W., Philpott, N., Josien, R., Richards, E. C., Elkon, K. B., & Falck-Pedersen, E. (2001). TNF-α-dependent maturation of local dendritic cells is critical for activating the adaptive immune response to virus infection. *Proceedings of the National Academy of Sciences*, *98*(21), 12162-12167.

Tsuchiya, Y., Nakabayashi, O., & Nakano, H. (2015). FLIP the Switch: Regulation of Apoptosis and Necroptosis by cFLIP. *International journal of molecular sciences*, *16*(12), 30321-30341.

Tuosto, L., & Acuto, O. (1998). CD28 affects the earliest signaling events generated by TCR engagement. *European journal of immunology*, *28*(7), 2131-2142.

Twomey, J. D., & Zhang, B. (2021). Cancer immunotherapy update: FDA-approved checkpoint inhibitors and companion diagnostics. *The AAPS Journal*, *23*(2), 1-11.

Van Gulijk, M., Dammeijer, F., Aerts, J. G., & Vroman, H. (2018). Combination strategies to optimize efficacy of dendritic cell-based immunotherapy. *Frontiers in immunology*, 2759.

Van Themsche, C., Chaudhry, P., Leblanc, V., Parent, S., & Asselin, E. (2010). XIAP gene expression and function is regulated by autocrine and paracrine TGF-β signaling. *Molecular cancer*, *9*(1), 1-12.

Vargas, F. A., Furness, A. J., Litchfield, K., Joshi, K., Rosenthal, R., Ghorani, E., ... & Veeriah, R. (2018). Fc effector function contributes to the activity of human anti-CTLA-4 antibodies. *Cancer cell*, *33*(4), 649-663.

Vignali, D. A., Collison, L. W., & Workman, C. J. (2008). How regulatory T cells work. *Nature reviews immunology*, *8*(7), 523-532.

Williams, M. A., Holmes, B. J., Sun, J. C., & Bevan, M. J. (2006). Developing and maintaining protective CD8+ memory T cells. *Immunological reviews*, *211*(1), 146-153.

Wills, S., Hochmuth, L. K., Bauer Jr, K. S., & Deshmukh, R. (2019). Durvalumab: a newly approved checkpoint inhibitor for the treatment of urothelial carcinoma. *Current Problems in Cancer*, *43*(3), 181-194.

Wolchok, J. D., & Saenger, Y. (2008). The mechanism of anti-CTLA-4 activity and the negative regulation of T-cell activation. *The oncologist*, *13*, 2-9.

Wolchok, J. D., Kluger, H., Callahan, M. K., Postow, M. A., Rizvi, N. A., Lesokhin, A. M., ... & Sznol, M. (2013). Nivolumab plus ipilimumab in advanced melanoma. *N Engl J Med*, *369*, 122-133.

Woo, E. Y., Chu, C. S., Goletz, T. J., Schlienger, K., Yeh, H., Coukos, G., ... & June, C. H. (2001). Regulatory CD4+ CD25+ T cells in tumors from patients with early-stage non-small cell lung cancer and late-stage ovarian cancer. *Cancer research*, *61*(12), 4766-4772.

Xu, L., Xu, W., Qiu, S., & Xiong, S. (2010). Enrichment of CCR6+ Foxp3+ regulatory T cells in the tumor mass correlates with impaired CD8+ T cell function and poor prognosis of breast cancer. *Clinical immunology*, *135*(3), 466-475.

Yi, M., Jiao, D., Xu, H., Liu, Q., Zhao, W., Han, X., & Wu, K. (2018). Biomarkers for predicting efficacy of PD-1/PD-L1 inhibitors. *Molecular cancer*, *17*(1), 1-14.

Yokosuka, T., Kobayashi, W., Takamatsu, M., Sakata-Sogawa, K., Zeng, H., Hashimoto-Tane, A., ... & Saito, T. (2010). Spatiotemporal basis of CTLA-4 costimulatory molecule-mediated negative regulation of T cell activation. *Immunity*, *33*(3), 326-339.

Zarnegar, B. J., Wang, Y., Mahoney, D. J., Dempsey, P. W., Cheung, H. H., He, J., ... & Cheng, G. (2008). Noncanonical NF-κB activation requires coordinated assembly of a regulatory complex of the adaptors cIAP1, cIAP2, TRAF2 and TRAF3 and the kinase NIK. *Nature immunology*, *9*(12), 1371-1378.

Zhang, Y. E., Khoo, H. E., & Esuvaranathan, K. (1999). Effects of bacillus Calmette-Guerin and interferon alpha-2B on cytokine production in human bladder cancer cell lines. *The Journal of urology*, *161*(3), 977-983.

Zhang, D., Goldberg, M. V., & Chiu, M. L. (2016). Fc engineering approaches to enhance the agonism and effector functions of an anti-OX40 antibody. *Journal of Biological Chemistry*, *291*(53), 27134-27146.

Zheng, Y., Josefowicz, S. Z., Kas, A., Chu, T. T., Gavin, M. A., & Rudensky, A. Y. (2007). Genome-wide analysis of Foxp3 target genes in developing and mature regulatory T cells. *Nature*, *445*(7130), 936-940.